AD-A162 154 MICROWAVE AND INFRARED ABSORPTION PROPERTIES OF ATMOSPHERIC SPECIES WITH.. (U) LOWELL UNIV MA CENTER FOR ATMOSPHERIC RESEARCH R R GAMACHE JUL 85 ULRF-428/CAR 1/2

UNCLASSIFIED AFGL-TR-85-0168 F19628-82-K-0043 F/G 7/4 NL

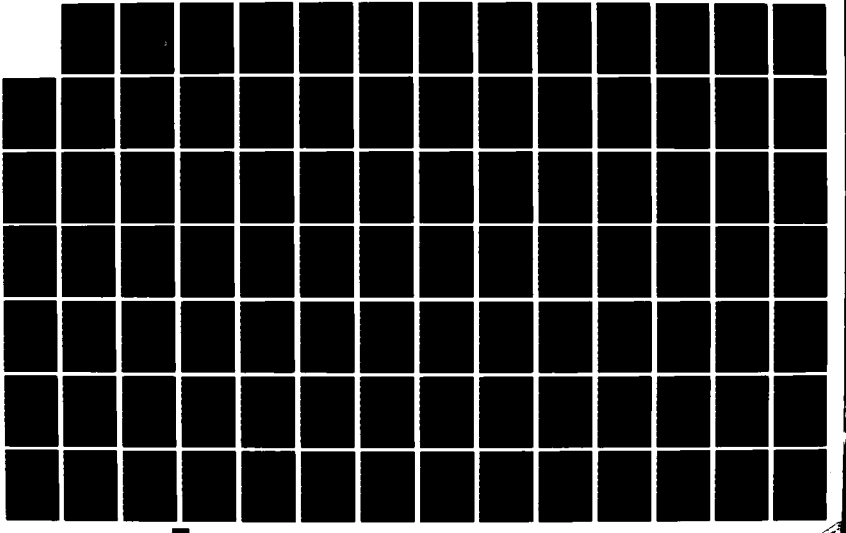

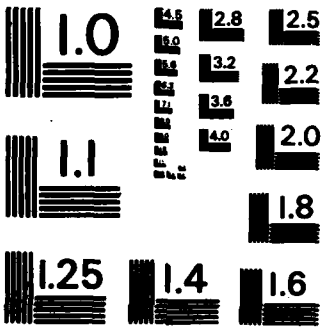

MICROCOPY RESOLUTION TEST CHART
NATIONAL BUREAU OF STANDARDS - 1963 - A

(12)

AFGL-TR-85-0168

MICROWAVE AND INFRARED ABSORPTION PROPERTIES OF ATMOSPHERIC SPECIES WITH SPECIAL EMPHASIS ON LINE WIDTHS AND SHIFTS

Robert R. Gamache

University of Lowell
Center for Atmospheric Research
450 Aiken Street
Lowell, Massachusetts 01854

July 1985

Final Report

April 29, 1982 to July 29, 1985

Approve for public release; distribution unlimited.

AIR FORCE GEOPHYSICS LABORATORY
AIR FORCE SYSTEMS COMMAND
UNITED STATES AIR FORCE
HANSCOM AFB, MASSACHUSETTS 01731

This technical report has been reviewed and is approved for publication.

LAURENCE S. ROTHMAN
Contract Manager

BERTRAM D. SCHURIN
Branch Chief

FOR THE COMMANDER

JOHN S. GARING
Division Director

This report has been reviewed by the ESD Public Affairs Office (PA) and is releasable to the National Technical Information Service (NTIS).

Qualified requestors may obtain additional copies from the Defense Technical Information Center. All others should apply to the National Technical Information Service.

If your address has changed, or if you wish to be removed from the mailing list, or if the addressee is no longer employed by your organization, please notify AFGL/DAA, Hanscom AFB, MA 01731. This will assist us in maintaining a current mailing list.

UNCLASSIFIED

SECURITY CLASSIFICATION OF THIS PAGE (When Data Entered)

REPORT DOCUMENTATION PAGE	READ INSTRUCTIONS BEFORE COMPLETING FORM
1. REPORT NUMBER: AFGL-TR-85-0168	2. GOVT ACCESSION NO.: AD-A162154
	3. RECIPIENT'S CATALOG NUMBER:
4. TITLE (and Subtitle): MICROWAVE AND INFRARED ABSORPTION PROPERTIES OF ATMOSPHERIC SPECIES WITH SPECIAL EMPHASIS ON LINE WIDTHS AND SHIFTS	5. TYPE OF REPORT & PERIOD COVERED: Final April 29,1982-July 29, 1985
	6. PERFORMING ORG. REPORT NUMBER: ULRF-428/CAR
7. AUTHOR(s): Robert R. Gamache	8. CONTRACT OR GRANT NUMBER(s): F19628-82-K-0043
9. PERFORMING ORGANIZATION NAME AND ADDRESS: University of Lowell, Center for Atmospheric Research, 450 Aiken Street, Lowell, Massachusetts 01854	10. PROGRAM ELEMENT, PROJECT, TASK AREA & WORK UNIT NUMBERS: 61102F 2310G1AZ
11. CONTROLLING OFFICE NAME AND ADDRESS: Air Force Geophysics Laboratory Hanscom AFB, MA 01731 Contract Monitor: Laurence S. Rothman (OPI)	12. REPORT DATE: July 1985
	13. NUMBER OF PAGES: 126
14. MONITORING AGENCY NAME & ADDRESS (if different from Controlling Office)	15. SECURITY CLASS. (of this report): Unclassified
	15a. DECLASSIFICATION/DOWNGRADING SCHEDULE

16. DISTRIBUTION STATEMENT (of this Report)

Approved for public release; distribution unlimited.

17. DISTRIBUTION STATEMENT (of the abstract entered in Block 20, if different from Report)

18. SUPPLEMENTARY NOTES

Keywords:

19. KEY WORDS (Continue on reverse side if necessary and identify by block number)

Molecular Spectroscopy,
Atmospheric Optics,
Collision Broadened Halfwidth and Line Shifts
Temperature Dependence of Halfwidth and Shift
Nitrogen, Oxygen, Etc.

20. ABSTRACT (Continue on reverse side if necessary and identify by block number)

In this report the work performed on updating the ~~AFGL~~ HITRAN data base and hot gas atlas is described and the list of data given. Our work on the development of the QFT-ID theory for collision broadened halfwidths of asymmetric rotors, i.e. O_3 and H_2O, is described. A review of second order perturbation schemes to calculate the line shift and width is given with application to H_2O. The temperature dependence of the line shift

DD FORM 1 JAN 73 1473 EDITION OF 1 NOV 65 IS OBSOLETE

UNCLASSIFIED

SECURITY CLASSIFICATION OF THIS PAGE (When Data Entered)

20. ABSTRACT

and halfwidth is formulated and results are presented for the $O_3^{\wedge}-N_2^{\sim}$ and $O_3^{\wedge}-O_2^{\sim}$ systems. → To follow

TABLE OF CONTENTS

LIST OF FIGURES

LIST OF TABLES

LIST OF TABLES (Continued)

1.0 HITRAN DATABASE

Throughout the course of this contract data was received from research groups to add to the HITRAN database for the main[1/] IR absorbers and the trace gas[2/] absorbers of the atmosphere. Before any data is added to either of the atlases it must be studied and its quality determined. This is accomplished by consultation with other colleagues, numerical and graphical analysis of the data and comparison with the data that it is to replace. Most of the procedures are automated so there is little chance of adding typographical errors. Many programs were written and/or customized for the data considered. The ultimate aim of the procedures set up was to handle a large amount of data, perform conversions, rearrange, coalesce, etc. without generating any errors or inconsistencies in the data base.

In Table 1 the data that was added to the atlases by ULCAR is listed along with the source of the data and atlas it was (to be) added to. This represents some two hundred thousand lines of data that were manipulated by the ULCAR programs. Generally the data that is received is not complete, the halfwidths for the individual transitions must be added as well as an internal date code. Sometimes other parameters must be added, e.g. isotope code or parameters rearranged, e.g. put vibration or rotation quantum numbers in AFGL format.

Within the contract period new versions of the Main Gas Atlas and Trace Gas Atlas were released (1982). Publications describing these new versions are given in Appendices B1 and B2. These contained most of the data from Table 1. Part of the data from Table 1 has been added to the in-house atlas and will be released on the next edition. In addition to this some of the data has been copied and stored and will be processed for the next edition of the atlas.

Table 1. HITRAN Data Processed Under Contract

Molecule	Isotope	Bands	Source	Atlas	# Lines
HDO	162	ν_1, $2\nu_2$	R. Toth (JPL)	1982 Main	2,234
HCN	124	Pure Rot.	JPL Catalogue	1982 Trace	45
	134	Pure Rot.	JPL Catalogue	1982 Trace	45
	125	Pure Rot.	JPL Catalogue	1982 Trace	35
H_2O_2	1661	Pure Rot.	JPL Catalogue	1982 Trace	883
N_2O	446	Pure Rot.	JPL Catalogue	1982 Main	61
ClO	56	Pure Rot.	JPL Catalogue	1982 Trace	2,610
	76	Pure Rot.	JPL Catalogue	1982 Trace	2,645
HOCl	165	Pure Rot.	JPL Catalogue	1982 Trace	3,697
	167	Pure Rot.	JPL Catalogue	1982 Trace	673
HNO_3	146	Pure Rot.	JPL Catalogue	1982 Trace	7,259
H_2O	181	Pure Rot.	French Atlas[a]	1982 Main	766
	171	Pure Rot.	French Atlas	1982 Main	672
	181	ν_2 Pure Rot.	French Atlas	1982 Main	202
	161	$2\nu_2$ Pure Rot.	French Atlas	1982 Main	134
	171	ν_2 Pure Rot.	French Atlas	1982 Main	117
	161	ν_1 Pure Rot.	French Atlas	1982 Main	24
	161	ν_3 Pure Rot.	French Atlas	1982 Main	18
	161	$\nu_3 - \nu_1$	French Atlas	1982 Main	1
	161	$\nu_3 - 2\nu_2$	French Atlas	1982 Main	1

a. J.-M. Flaud, C. Camy-Peyret and R. A. Toth, "Parametres des Raies de la Vapeur d'Eau des Micro-ondes a L'Infrarange Moyen," Pergamon Press, 1981.

Table 1. HITRAN Data Processed Under Contract (Continued)

Molecule	Isotope	Bands	Source	Atlas	# Lines
H_2O	161	$3\nu_2 - 2\nu_2$	French Atlas[a]	1982 Main	121
	181	$2\nu_2 - \nu_2$	French Atlas	1982 Main	187
	171	$2\nu_2 - \nu_2$	French Atlas	1982 Main	86
	181	ν_2	French Atlas	1982 Main	852
	171	ν_2	French Atlas	1982 Main	668
	181	$\nu_3 - \nu_1$	French Atlas	1982 Main	16
	161	$3\nu_2 - \nu_2$	French Atlas	1982 Main	313
	181	$2\nu_2$	French Atlas	1982 Main	388
	171	$2\nu_2$	French Atlas	1982 Main	247
	181	$\nu_1 + \nu_2 - \nu_2$	French Atlas	1982 Main	3
	161	$\nu_1 + \nu_2 - \nu_2$	French Atlas	1982 Main	365
	181	ν_1	French Atlas	1982 Main	553
	171	ν_1	French Atlas	1982 Main	387
	161	$2\nu_2 + \nu_3 - 2\nu_2$	French Atlas	1982 Main	49
	181	$\nu_2 + \nu_3 - \nu_2$	French Atlas	1982 Main	101
	171	$\nu_2 + \nu_3 - \nu_2$	French Atlas	1982 Main	34
	161	$\nu_2 + \nu_3 - \nu_2$	French Atlas	1982 Main	527
	181	ν_3	French Atlas	1982 Main	711
	171	ν_3	French Atlas	1982 Main	529
CH_4	211	ν_2, ν_4	L. Brown	1982 Main	2,230
	311	ν_2, ν_4	L. Brown	1982 Main	422

a. J.-M. Flaud, C. Camy-Peyret and R. A. Toth, "Parametres des Raies de la Vapeur d'Eau des Micro-ondes a L'Infrarange Moyen," Pergamon Press, 1981.

Table 1. HITRAN Data Processed Under Contract (Continued)

Molecule	Isotope	Bands	Source	Atlas	# Lines
HDO	162	ν_3, $\nu_1 + \nu_2$, $3\nu_2$	R. Toth	1982 Main	3,113
O_3	666	ν_2, $2\nu_2 - \nu_2$	A. Goldman et al.	1982 Main	10,931
	666	$\nu_2 + \nu_3$, $\nu_1 + \nu_2$	A. Goldman et al.	1982 Main	3,846
	666	ν_1, ν_3	A. Goldman et al.	1982 Main	11,016
	666	$\nu_1 + \nu_3 - \nu_1$, $2\nu_3 - \nu_3$, $\nu_2 + \nu_3 - \nu_2$, $\nu_1 + \nu_2 - \nu_2$	1978 Atlas	1982 Main	5,164
HNO_3	12	11.3 μm	A. Goldman	In-House Trace	24,412
H_2S	-	-	A. Goldman	Storage[b]	661
HCOOH	-	-	A. Goldman	Storage[b]	3,388
O_3	666	$\nu_1 + \nu_2 + \nu_3$	A. Goldman	Storage[b]	1,927
O_3	666	Pure Rot.	JPL Catalogue Rev. 2	Storage[b]	6,471
	666	ν_2 Rot.	JPL Catalogue Rev. 2	Storage	4,337
	666	ν_1 Rot.	JPL Catalogue Rev. 2	Storage	9,459
	668	Pure Rot.	JPL Catalogue Rev. 2	Storage	7,304
	686	Pure Rot.	JPL Catalogue Rev. 2	Storage	3,184
HDO	162	Pure Rot.	JPL Catalogue Rev. 2	Storage[b]	461
SO_2	626	Pure Rot.	JPL Catalogue Rev. 2	Storage[b]	9,622
NO_2	646	Pure Rot.	JPL Catalogue Rev. 2	Storage[b]	6,360
OH	16	Pure Rot.	JPL Catalogue Rev. 2	Storage[b]	299

b. To be added to 1985 atlas in new format.

Table 1. HITRAN Data Processed Under Contract (Continued)

Molecule	Isotope	Bands	Source	Atlas	# Lines
H_2CO	126	Pure Rot.	JPL Catalogue Rev. 2	Storage[b]	611
HOCl	165	Pure Rot.	JPL Catalogue Rev. 2	Storage[b]	3,919
	167	Pure Rot.	JPL Catalogue Rev. 2	Storage	3,923
H_2O_2	1661	Pure Rot.	JPL Catalogue Rev. 2	Storage[b]	883
N_2O	all	all	GEISA Atlas	Storage[b]	15,845
NO_2	all	all	GEISA Atlas	Storage[b]	23,050
C_2H_4	all	all	GEISA Atlas	Storage[b]	203
H_2S	all	all	GEISA Atlas	Storage[b]	4,058
HCOOH	all	all	GEISA Atlas	Storage[b]	3,388

b. To be added to 1985 atlas in new format.

The next edition of the HITRAN database is scheduled to be released in 1985 and will see many new changes. The main gas and trace gas atlases will be incorporated into one and several new molecules will be added. The format of the data has also changed to allow more information to be stored. Under the new scheme the vibrational assignment and isotope codes will be a single integer and correspondence with spectroscopic notation is accomplished through a double array lookup scheme. Each transition will have the uncertainty of the line wavenumber, intensity and halfwidth and references indicated by the same type of lookup scheme. Also, a change to storing the wavenumber of the transition in the same format for all the data will make the data easier to use. The format of the new atlas is given in Table 2. In order to facilitate the use of the new database a user friendly program will be provided that will read the new format, do the necessary lookups, and write or print the desired file in the usual spectroscopic notation.

A program has been written that will convert the 1982 format to the 1985 format. In doing this we have tried to allow for many of the known incorrect format of data on the 1982 tapes.

To ease the conversion and simplify future modifications a new data storage system has been implemented. The two atlases have been combined and twenty files created which are in one transition per record and in ASCII. Thus buffered binary and unpacking are no longer necessary. The twenty files created are small enough to be handled by the editor and used as input interactively. The twenty files, wavenumber ranges and line count are given in Table 3.

These files exist on both the Cyber and Vax systems. The incorporation of AFGL's Vax 11/780 into the data manipulation scheme is recent and was done to take advantage of the Vax's greater storage capacity, to allow us to test programs

Table 2. Record Format of 1985 Atlas

MOL, ISO, σ, S, R, α, α-S, E", n, δ, V', V"

I2, I1, F12.6, 1P2E10.3, 0P2F5.4, F10.4, F4.2, F8.6, 2I3,

Q', Q", SYM, E(3), ref(3)

2(A8, A1), 3I1, 3I2

Table 3. Files for File Management System, Wavenumber Range and Line Count

File	σ_{Low}	σ_{High}	No. Lines
FMS01	0.	99.99	20,386
FMS02	100.0000	599.9996	14,711
FMS03	600.0000	699.9970	18,062
FMS04	700.0010	799.9829	12,787
FMS05	800.0004	884.9998	19,907
FMS06	885.0000	999.9960	17,676
FMS07	1000.0070	1099.9970	13,403
FMS08	1100.0002	1299.9920	19,552
FMS09	1300.0136	1699.9993	17,427
FMS10	1700.0070	1899.9992	13,914
FMS11	1900.0709	2199.9870	13,285
FMS12	2200.0013	2399.9615	14,896
FMS13	2400.0246	2899.9430	15,963
FMS14	2900.0475	3099.9950	13,237
FMS15	3100.0306	3599.9960	17,678
FMS16	3600.0018	3899.9120	13,803
FMS17	3900.0300	4999.6863	12,191
FMS18	5000.0515	6999.9730	13,369
FMS19	7000.0330	10999.200	13,685
FMS20	11000.090	17879.736	5,417

on a 32 bit machine, and to benefit from many additional features present on the Vax. With the communication link between the Cyber and Vax the files can be transferred back and forth between both systems.

One last project performed under this contract dealing with HITRAN data was the generation of an atlas of CO_2 and H_2O to be used at the 1000 - 1200 K range. This was called the Hot Gas Atlas and differs from the Main Gas Atlas in that it only contains two molecules, a much lower strength criteria is applied so many high J transitions are included. For water vapor halfwidths had to be added to the Hot Gas Atlas which contains the isotopes $H_2{}^{16}O$, $H_2{}^{17}O$ and $H_2{}^{18}O$ (note no HDO data is present). The halfwidths added are from two sources: for the 171, 181 and some of the 161 transitions the values are from Davies' optimum combination algorithm.[3] For many of the 161 transitions values were taken from the more rigorous quantum Fourier transform[4] calculations of Gamache and Davies.[5] Many halfwidth values were not available for the high J transitions required by this atlas, for these transitions the extrapolated default values in Table 4 were used. All halfwidth files were put in to mass storage (random access) with the keys being related to the upper and lower state rotational quantum numbers of the transition. No vibrational dependence was considered in this work. The halfwidths were added to the Hot Gas Atlas and the tape delivered to Dr. John Selby of Grumman Aerospace.

Along with this work, Dr. Selby requested an average ratio of self-broadened halfwidth of H_2O for the N_2-broadened value as a function of J". Presently in Fascode[6] an average ratio of 5 is assumed for $\gamma(self)/\gamma(N_2)$. Using the self- and N_2-broadened halfwidths of reference 5, the ratio was formed and then averaged over the number of transitions of a particular J". The results are given in Table 5 which displays a clear J" dependency with the ratio increasing with increasing J".

Table 4. High J" Default Halfwidths for Various Isotopes of Water Vapor

Isotope	Default Halfwidth cm^{-1}/atm	$J"^{a}$
161	0.0086	20
171	0.0084	15
181	0.0082	15
162	0.0086	15

a. J" value after which default value applies.

Table 5. Average Ratio of Self-Broadened Halfwidth to N_2-Broadened Halfwidth for H_2O as a Function of J"

J"	$\gamma(self)/\gamma(N_2)$	No. in Average
1	4.69	2
2	5.01	7
3	5.23	14
4	5.31	21
5	5.27	28
6	5.37	36
7	5.30	42
8	5.22	49
9	5.29	56
10	5.50	64
11	5.62	70
12	5.74	77
13	5.82	84
14	5.76	92
15	5.75	98
16	5.95	105
17	6.14	112
18	6.35	113
19	6.68	106
20	6.58	115

2.0 HALFWIDTH CALCULATIONS FOR O_3 PERTURBED BY N_2, O_2, AIR

One of the main tasks of this work was to produce a database of transition dependent halfwidths for ozone. The intent was to use the ATC[7] or QFT[4] method to generate halfwidths for all unique rotational transitions of ozone on the 1982 main gas atlas. Many programs had to be revived for calculating dipole and quadrupole matrix elements. Because ozone has a relatively small dipole moment the quadrupole-quadrupole interaction was included in the anisotropic potential. This addition has to be made to our existing halfwidth programs.

After months of preparing the programs and performing check runs we were ready to start the ozone calculations. The molecular constants used in the calculations are listed in Table I of Appendix B5 and are referenced therein. These values represent the state-of-the-art at the time of the calculations and in all cases confirmed by several experiments. The results of the ATC and QFT calculations was to produce N_2-broadened halfwidths 16% low and O_2-broadened halfwidths 30% low compared with experiment.[8-11] These results agree with the work of Mandin et al[12] who also used up-to-date constants. They did not agree with the calculations of Tejwani and Yeung[13] (TY) and test calculations using the constants from TY failed to give the same A-type, B-type dependence reported in reference 13.

Many test calculations were performed, Anderson's $S_2(b)_{middle}$ term was included explicitly in the calculations, all avenues in the calculations double checked and the results remained the same, too low.

It was decided to improve the theory rather than scale the results to match experiment. In this vein several suggestions for improving impact theory were made, these are listed in Table 6. The use of velocity integration applies

I: Use theory directly, scale final answers

II: 1) Curved Trajectories

2) Velocity Integration

3) Exponential Cut-Off Criterion

4) Higher Order Multipole Interations

Table 6. Suggestions to Improve Impact Theory

only to ATC theory since QFT contains the velocity average explicitly. The results of the velocity integration for ATC are in Table 7. Two schemes for doing the integration are presented and both give roughly the same values. The effect of velocity integration is to lower the halfwidths an additional 7% thus ATC is now low by 23% (N_2-broadening) compared with experiment.

Another suggestion to improve the theory was to use a cutoff free impact approach. In the usual ATC approach when the impact parameter becomes small the interruption function S(b,v) attains unphysically large values. After much handwaving, the argument is made that once S(b,v) = 1 from that point inward s ≡ 1 and this cutoff point is called b_0. This leads to the formula

$$\gamma(m^{-1}) = \frac{N\bar{v}}{2\pi c} \{\pi b_0^2 + \int_{b_0}^{\infty} 2\pi\ b\ db\ S(b)\} \qquad (1)$$

where N is the perturber density, $\bar{v}$ the mean relative thermal velocity and S(b) the interruption function. Several authors have succeeded in eliminating the cutoff point from the theory. Murphy and Boggs[14] developed a method that used an exponential expansion of the collision matrix elements for all values of b. Cattani[15] combined the Murphy-Boggs expansion with the ATC formalism. Salesky and Korff[16] have given the first rigorous derivation of the cutoff free theory. In their formalism they use a linked-cluster expansion theorem for degenerate states to obtain a form for the interruption function in which the dependence on the interaction potential is exponential. Independently Robert and Bonamy[17] have developed a similar formulation although a derivation is not given in their work.

In the method the perturbation operator is given by

$$\phi_{if} = n\ \bar{v}\ \sigma_2 = n\ \bar{v}\ (\sigma_R + i\ \sigma_i) \qquad (2)$$

ν_3 Transitions	V = 10528	V = 25528	V = 40528	$\overline{V}$ = 59528	V = 70528	V = 85528	V = 100528	$\overline{\gamma}(v)$
2 1 1 3 1 2	.02148	.04352	.05715	.07206	.07999	.09029	.10034	.06640
5 3 3 5 3 2	.01906	.03393	.04891	.06761	.07751	.08980	.10105	.06255
11 2 10 12 2 11	.01637	.03400	.05148	.06970	.07862	.08969	.09998	.06283
19 3 17 18 3 16	.01653	.03256	.04724	.06634	.07649	.08903	.10032	.06122
25 3 23 26 3 24	.01750	.03136	.04699	.06569	.07554	.08806	.09957	.06067
27 5 23 28 5 24	.01712	.03263	.04600	.06192	.07116	.08351	.09519	.05822

ν_3 Transitions	$\gamma_{\overline{v}}$	$\overline{\gamma}^a$	$\frac{\gamma(\overline{v})-\overline{\gamma}(v)}{\overline{\gamma}_{\overline{v}}} \times 100$	$\gamma_{sum}{}^b$	$\frac{\gamma(\overline{v})-\gamma_{sum}}{\gamma_{\overline{v}}} \times 100$
2 1 1 3 1 2	.07206	.06640	7.85	.06717	6.79
5 3 3 5 3 2	.06761	.06255	7.48	.06269	7.28
11 2 10 12 2 11	.06970	.06283	9.86	.06380	8.46
19 3 17 18 3 16	.06634	.06122	7.72	.06149	7.32
25 3 23 26 3 24	.06569	.06067	7.64	.06082	7.42
27 5 23 28 5 24	.06192	.05822	5.98	.05820	6.01

[a]Average individual values

[b]Result of velocity integration

Table 7. Effects of Velocity Integration and Velocity Averaging on the Halfwidth for 6 ν_3 Transitions of Ozone

where

$$\sigma_2 = \int_0^\infty 2\pi b \, db \, S(b). \tag{3}$$

The interruption function given in eq. (3) is derived via the linked cluster theorem and is given by

$$S(b) = 1 - \exp\{- i\Delta_i + i\Delta_f - s_{2i}^{outer} - s_{2f}^{outer} - s_2^{middle} + \ldots \text{higher order interactions}\}, \tag{4}$$

where Δ_i and Δ_f are the first order phase shifts in the usual ATC theory and the s_{2i}^{outer}, s_{2f}^{outer}, s_2^{middle} are the usual second order terms from ATC theory. So we see that in this theory the interruption function is given as 1 minus the exponential of the phase shifts and interruption functions (small f(k)) from conventional ATC theory. In this formulation S(b) is well behaved at all values of the impact parameter so no cutoff procedure is needed, eq. (3) is simply integrated from 0 to ∞.

For our problem we can write eq. (4) as

$$S(b) = 1 - \exp\{- i\Delta^{dq} - i\Delta^{qq} - s_{outer}^{dq} - s_{outer}^{qq} - s_{middle}^{qq}\}, \tag{5}$$

where Δ^{dq} is the total shift (imaginary part of the interruption function evaluated by f(k) functions) due to the dipole-quadrupole (d-q) interaction Δ^{qq} is the total shift due to the quadrupole-quadrupole (q-q) interaction, and s_{outer}^{dq}, s_{outer}^{qq} and s_{middle}^{qq} are the real part of the interruption function evaluated by f(k) resonance functions for the d-q and q-q outer terms and the q-q middle terms. If we group real and imaginary terms together we get

$$s(b) = 1 - \exp\{- i\Delta - s\} \tag{6}$$

which can be rewritten as

$$S(b) = 1 - \cos\Delta \exp(-s) + i \sin\Delta \exp(- s). \tag{7}$$

The pressure induced shift and pressure broadened line width for the linked cluster approach can be written as

$$\Delta\omega(cm^{-1}/atm) = \frac{n\,\bar{v}}{2\pi c} \sum_{J_2} \rho_{J_2} \int_0^\infty \sin(\Delta)\, \exp(-s)\, 2\pi b\, db \qquad (8)$$

and

$$\gamma(cm^{-1}/atm) = \frac{n\,\bar{v}}{2\pi c} \sum_{J_2} \rho_{J_2} \int_0^\infty [1 - \cos(\Delta)\, \exp(-s)]\, 2\pi b\, db. \qquad (9)$$

In general we expect the halfwidth calculated using eq. (9) to be somewhat smaller than the corresponding value from ATC or QFT theory. This is easily understood by viewing Figure 1 in which the interruption functions from the ATC and linked-cluster (L-C) approaches are plotted vs. the impact parameter. The ATC curve comes in from large b smoothly to a point where S(b) = 1 where it is cut off and assumed equal to one from the cutoff point to zero. The L-C curve, however, is continuous from zero to infinity and smoothly goes from 1 at the origin to zero at infinity.

Test calculations were performed on ten ν_3 transitions via the linked-cluster theorem approach. In the exponential conventional ATC interruption functions are used and in Table 8 the results are compared with ATC results. Also present in the table are the calculated line shifts. As expected the linked-cluster approach gives halfwidths smaller than the usual ATC results. The most striking feature of the table is the fluctuation of the shift for the various methods. If shift measurements were available for this system we could better evaluate the methods.

The next attempt to improve the theory was based on the use of approximate trajectories to better represent actual trajectories. The hope here was that more correct dynamics would affect the calculations near the distance of closest

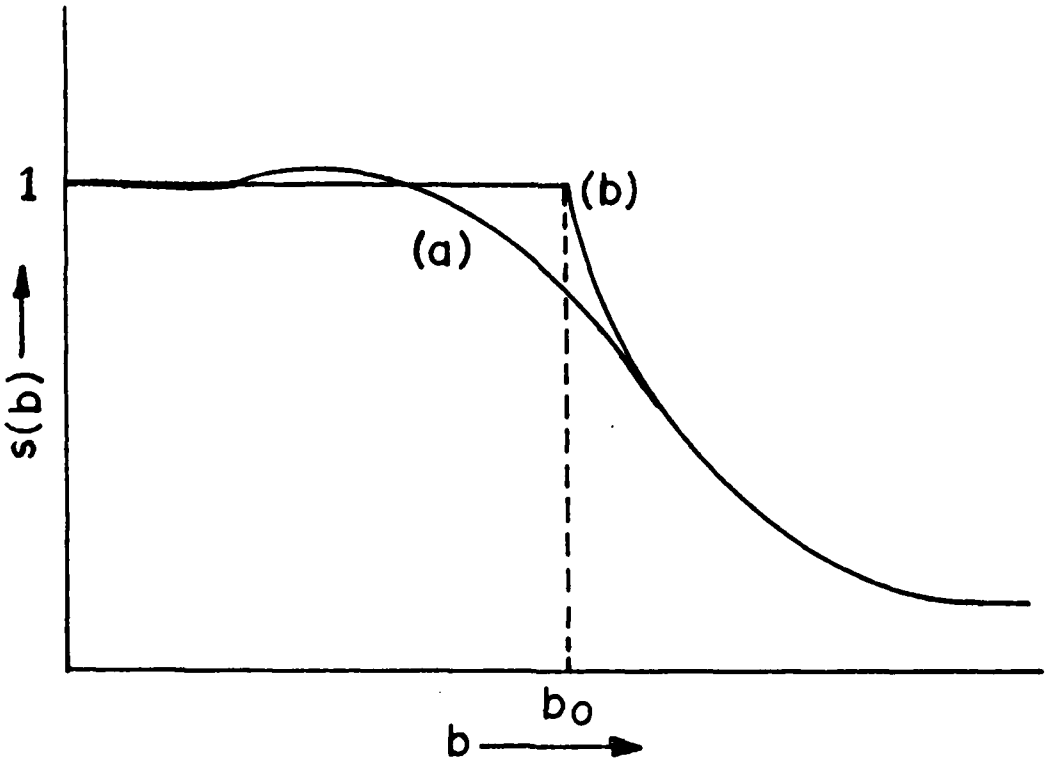

Figure 1. Comparison of Interruption Functions from ATC and Cutoff Free Theory . (a) Cutoff Free Theory (b) ATC Theory

Transition	Conventional			
	Linked Cluster		ATC	
	Width	Shift	Width (%)	Shift
9 4 6 — 10 4 7	.05713	.00774	.05987 (4.6)	.00936 (17.5)
12 7 5 — 13 7 6	.05556	.00760	.05827 (4.7)	.00921 (17.5)
10 4 6 — 11 4 7	.05728	.00785	.05999 (4.5)	.00951 (17.7)
11 2 10 — 12 2 11	.06125	.00686	.06522 (6.1)	.00798 (14.0)
12 4 8 — 13 4 9	.05746	.00804	.06007 (4.3)	.00980 (18.0)
17 9 9 — 18 9 10	.05485	.00759	.05746 (4.5)	.00917 (17.2)
12 0 12 — 13 0 13	.06322	.00606	.06789 (6.9)	.00690 (12.2)
18 9 9 — 19 9 10	.05480	.00765	.05734 (4.4)	.00928 (17.6)
13 4 10 — 14 4 11	.05747	.00810	.00604 (4.3)	.00991 (18.3)

Table 8. Comparison of Linked Cluster Results with Conventional ATC Results. Percent Difference in Brackets (ATC-LC)/ATC, Units are cm^{-1}/atm.

approach, giving more reasonable results. The properties we have been studying arise because of collisions between the molecule in question and some perturbing gas molecule. In order to fully understand these properties the exact dynamics of the molecular motions has to be determined. This is much too difficult to do generally, so approximations must be made. The first assumption made is the so called "impact" approximation thus we are dealing with uncorrelated two-body collisions. Next it is assumed that the kinetic energies are large enough so that classical mechanics can be used to describe the motion of the centers of gravity of the colliding particles. This limits the exchange of energy between kinetic and internal degrees of freedom to a very small fraction of the kinetic energy. In what follows it is assumed the main interaction between the two colliding particles can be described by an isotropic potential, $\phi(r)$, so that the trajectories will be planar.

For the problem of the width or shift of a spectral line one has to consider the time evolution of the perturbation potential $V[r(t), \Omega(t)]$, which is obtained from the coordinates of the centers of gravity of the colliding particles as a function of time. Generally one works with the spectral power density of the perturbation

$$P(\omega) = \left|\int V[r(t), \Omega(t)\, e^{i\omega t}\, dt\right|^2. \qquad (10)$$

From the equations of motion of classical mechanics $r(t)$, $\Omega(t)$ is obtained for each trajectory, labeled by its initial relative velocity v and the impact parameter b. The overall effect of collisions is then obtained by taking a proper average of $p_{bv}(\omega)$ for all possible trajectories. This is given by integrals of the form

$$P(\omega) = A \int 2\pi b\, db \int v^3\, dv\, e^{-\frac{\mu v^2}{2kT}}\, p_{b,v}(\omega), \qquad (11)$$

with A being a normalization factor. Here μ is the reduced mass of the system and kT the thermal energy. Often the correlation function of the perturbation is considered

$$C(\tau) = \langle V[r(t), \Omega(t)]\, V^*[r(t+\tau), \Omega(t+\tau)]\rangle \qquad (12)$$

which is simply the Fourier transform of $P(\omega)$.

With the assumption of an isotropic potential $\phi(r)$, the dynamics of the collision are understood in terms of plane trajectories that are determined by the impact parameter b and the initial relative velocity v (or the total energy of the motion $E = \frac{1}{2}\mu v^2$). The equations of motion are given in polar coordinates as

$$\dot{\theta} = bv/r^2 \qquad (13)$$

$$\dot{r} = v\sqrt{1 - \frac{b^2}{r^2} - \frac{\phi(r)}{E}}. \qquad (14)$$

The distance of closest approach $r_c(b,E)$ is obtained from the equation (which is a statement of conservation of energy)

$$1 - \left(\frac{b^2}{r^2}\right) - \frac{\phi(r)}{E} = 0. \qquad (15)$$

The potential ϕ in general contains both an attractive and a repulsive term and equation (15) may have several solutions. Here only the largest is retained, thereby discarding trajectories corresponding to stable or metastable bound states. In the work we have done and in most other work a Lennard-Jones potential has been chosen

$$\phi(r) = 4\varepsilon\left[\left(\frac{\sigma}{r}\right)^{12} - \left(\frac{\sigma}{r}\right)^{6}\right]. \qquad (16)$$

The above equations can be solved by expanding r and θ in a time series and then doing the integrals numerically. However, most work has been done by approximations to the dynamics.

In the theory of Anderson-Tsao-Curnutte[7] and Davies QFT method[4] straight line trajectories were used, i.e.

$$r(t) = \sqrt{b^2 + v^2t^2};\ \theta(t) = \text{Arc tan } (\frac{vt}{b}). \qquad (17)$$

As we have seen this leads to halfwidths some 25-35% too low. The correction we made was to use bent trajectories determined by the method of Tipping and Herman.[18] The method actually uses linear trajectories with constant velocities chosen to give values of θ and r exact to first order in t, i.e.

$$\bar{r}(t) = \bar{r}_c + \bar{v}_c t \text{ with } \bar{v}_c = \dot{\bar{r}}(t=0) \text{ so that } v_c = r_c\,\dot{\theta}(0) = \frac{bv}{r_c}. \qquad (18)$$

$$\text{Thus } r(t) = \sqrt{r_c^2 + (v_c t)^2} \text{ and } \theta(t) = \text{Arc sin } (v_c t/r_c). \qquad (19)$$

This replaces b,v in eq. (11) with the actual distance of closest approach r_c and the relative velocity v_c determined above.

Bonamy et al[19] along similar lines have incorporated linear trajectories with constant velocity where the velocity is chosen to yield proper time dependence to second order in t

$$\bar{r}(t) = \bar{r}_c + \bar{v}_c' t \qquad \bar{r}_c \text{ perpendicular to } \bar{v}_c' \qquad (20)$$

with

$$r(t) = \sqrt{r_c^2 + (v_c' t)^2},$$

$$v_c' = v_c - \frac{r_c}{\mu}\left(\frac{d\phi}{dr}\right)_{r_c} \qquad (21)$$

and

$$\theta(t) = \text{arc sin } [v_c t/r(t)].$$

Gersten[20] has formulated the problem in terms of actual parabolic trajectories. All three approximations are discussed in the work of Berard and Lallemand.[21]

Both the first-order-in-time (Tipping[18]) and second-order-in-time (Bonamy[19]) trajectory methods were tested along with the first-order-in-time resonance functions in the cutoff free approach. The results for the conventional calculations, first-order-in-time dynamics, second-order-in-time dynamics and cutoff free first-order-in-time dynamics is listed in Table 9. The results of the calculations indicated the QFT calculations with dynamics correct to first-order-in-time give the most acceptable results and this method, henceforth called QFT-ID (Improved Dynamics), was used to generate the transition dependent halfwidths. A complete derivation of the QFT-ID method and comparison with experimentally determined halfwidths is given in Appendix B5. The results of the calculations for the unique rotational transitions of ozone present on the AFGL atlas are in Appendix B6.

Table 9. Comparison of Halfwidths Calculated by Various Theories with Experiment, N_2-Broadening of Ozone

Theory	ave $\frac{\lvert(\gamma_{exp}-\gamma_{theo})\rvert}{\gamma_{exp}} \times 100$
Conventional ATC, QFT	24
First Order in Time ATC	13
First Order in Time QFT	6
Second Order in Time QFT	8
Conventional Cutoff Free Theory	29
First Order in Time Cutoff Free Theory	9

3.0 HALFWIDTH CALCULATIONS FOR H_2O

The success of the QFT-ID calculations on pressure broadening of ozone transitions encouraged us to apply the method to other systems. The programs were developed for ozone (an asymmetric rotor) and should be applicable to other asymmetric rotor molecules. The obvious choice was H_2O for which we have previously done QFT calculations (see Appendix B3). The molecular constants of H_2O used in these calculations are given in Table 10 for the Hamiltonian constants for the ground and ν_2 states and Table 11 for the dipole moment expansion coefficient for the same bands. The QFT-ID scaling factor was adjusted by the same method used for ozone (see Appendix B4), i.e. a fit to four halfwidths of H_2O calculated by velocity averaged ATC method. Note here the transitions chosen posed no cutoff problems which are still a problem for H_2O. The final value was $\alpha = 2.50$ for the QFT-ID method. To test the method fourteen transitions were selected that were experimentally studied and previously studied by the QFT method by Davies and Oli.[22] The results of the comparison are given in Table 12 as one can see the QFT-ID calculations agree with experiment to 7.7% (note this is an average of absolute percent differences thus there is no cancellation) whereas the QFT method gives 12.2, QFT-ID gives roughly 5% better agreement.

The QFT-ID method was later used to generate N_2- and O_2-broadened halfwidths as discussed below.

Table 10. Ground State Hamiltonian Constants for the Ground and ν_2 States of $H_2{}^{16}O$

Constant	Ground State	ν_2 State
h_{000}	0.	1594.7475
h_{100}	1.1899588833 E01	1.1903701 E01
h_{010}	1.5980993262 E01	1.9215062 E01
h_{001}	2.6218069272 E00	2.7778759 E00
h_{200}	-1.2472229831 E-03	-1.3542093 E-03
h_{110}	5.7960538326 E-03	7.9231928 E-03
h_{020}	-3.2529699250 E-02	-5.7970224 E-02
h_{101}	-1.0110281073 E-03	-1.1451653 E-03
h_{011}	-1.2924135019 E-03	-3.8323087 E-03
h_{002}	0.	0.
h_{300}	4.6949813817 E-07	5.0656451 E-07
h_{210}	-2.1187178761 E-06	2.2175297 E-06
h_{120}	-1.6424049553 E-05	-4.6466869 E-05
h_{030}	1.3083972929 E-04	3.6913932 E-04
h_{201}	4.7048756677 E-07	5.7151085 E-07
h_{111}	-9.4533643844 E-07	1.3132987 E-06
h_{021}	2.8398803330 E-05	7.8156063 E-04
h_{102}	0.	0.
h_{012}	0.	0.
h_{003}	0.	0.
h_{040}	-9.4685485615 E-07	-2.4769822 E-05
h_{130}	1.6740040972 E-07	2.2049512 E-08
h_{220}	-3.7603344716 E-08	-1.7451411 E-09
h_{310}	2.0720390182 E-09	0.
h_{050}	7.7093370616 E-09	1.7069358 E-08
h_{140}	-1.5062807928 E-10	-4.3939773 E-09
h_{230}	0.	1.8593616 E-09
h_{320}	0.	0.
h_{060}	-5.9621206910 E-11	-5.1256347 E-11

Table 10 (Continued)

Constant	Ground State	ν_2 State
h_{150}	0.	0.
h_{240}	0.	0.
h_{330}	0.	0.
h_{070}	3.0462960460 E-13	7.4777605 E-14
h_{080}	-8.5116601707 E-16	-3.3050319 E-18
h_{090}	9.7985872525 E-19	7.5951676 E-20
h_{031}	-2.1857012815 E-07	-1.9073085 E-07
h_{121}	3.9741624543 E-09	0.
h_{211}	1.6261468128 E-09	8.5469196 E-10
h_{301}	-5.0801820008 E-12	-1.2063848 E-10
h_{041}	4.6413035022 E-10	7.8925603 E-10

Table 11. Molecular Constants for $H_2{}^{16}O$

Q (Ground State) = 7.715×10^{-24} esu cm^2

(Stogryn and Stogryn definition)

Dipole Moment Expansion Coefficients in I^r Representation

Ground State	PHI(x)	PHI(y)	PHI(z)
μ	-1.85371	0.	0.
X	0.	0.	0.
Y	0.	0.	0.
Z	0.	0.	0.
XX	1.06499 E-04	0.	0.
YY	-3.34247 E-06	0.	0.
ZZ	-4.05110 E-04	0.	0.
XY	0.	8.77629 E-05	0.
YZ	0.	0.	0.
ZX	0.	0.	-5.42499 E-05
ν_2 or (010)			
μ	-1.82059	0.	0.
X	0.	0.	0.
Y	0.	0.	2.269535 E-19
Z	0.	0.	0.
XX	1.06312 E-04	0.	0.
YY	-3.10996 E-06	0.	0.
ZZ	-4.05142 E-04	0.	0.
XY	0.	1.08999 E-06	0.
YZ	0.	0.	0.
ZX	0.	0.	-7.54910 E-05

Table 12. Comparison of QFT, QFT-ID and Exp Halfwidth of H_2)

Transition	QFT[22/] α = 2.79	% Dif.[a]	Exp[b]	% Dif.	QFT-ID α = 2.50
$5_{2\,3} \rightarrow 6_{1\,6}$	0.1005	3.4	0.104 (300K)	9.0	0.09466
$2_{2\,0} \rightarrow 3_{1\,3}$	0.10629	-11.9	0.095	- 4.0	0.09877
		4.2	0.111	11.0	
		4.2	0.111	11.0	
$3_{2\,1} \rightarrow 4_{1\,4}$	0.10443	1.1	0.10556*	7.8	0.09736
$5_{3\,3} \rightarrow 6_{6\,0}$	0.07148	19.6	0.0889*	7.9	0.08187
$5_{3\,2} \rightarrow 6_{1\,6}$	0.07984	20.2	0.100*	17.4	0.08257
$6_{3\,4} \rightarrow 7_{6\,1}$	0.07043	9.4	0.07778*	- 6.1	0.08254
$6_{3\,3} \rightarrow 7_{6\,2}$	0.08464	- 8.8	0.07778*	- 9.7	0.08534
$6_{2\,5} \rightarrow 7_{5\,2}$	0.07132	19.8	0.08889*	4.4	0.08497
$6_{1\,6} \rightarrow 7_{4\,3}$	0.08137	26.7	0.1111*	19.8	0.08934
$7_{3\,5} \rightarrow 8_{6\,2}$	0.06772	12.9	0.07778*	- 4.6	0.081395
$7_{3\,4} \rightarrow 8_{6\,3}$	0.08865	11.4	1.000*	12.3	0.08771
$7_{2\,6} \rightarrow 8_{5\,3}$	0.06551	15.8	0.07778*	- 7.6	0.08369
$7_{1\,7} \rightarrow 8_{4\,4}$	0.08119	8.7	0.08889*	2.9	0.08634
$8_{2\,6} \rightarrow 9_{5\,5}$	0.08081	9.1	0.08889	- 0.3	0.08915
Average Absolute % Dif.		12.2		7.7	

a. % Dif. = $\left(\frac{\text{Exp-Calc}}{\text{Exp}}\right) \times 100$

b. See references within Ref. 22.

* Scaled to nitrogen-broadening, see Ref. 22.

4.0 SECOND ORDER PERTURBATIVE APPROACHES TO COLLISIONAL BROADENING AND PRESSURE SHIFTS

In all of the calculations previously discussed in addition to calculating the halfwidths of transitions the pressure shifts were evaluated as well. The results were not presented or discussed mostly due to the lack of experimental measurements to compare with. For ozone we know of no such measurements, for water there are eight transitions studied by Eng,[23] seven measurements for air perturbing H_2O and two for N_2 as the perturbing gas.

A problem with using halfwidth measurements to test the theories is that some 60 to 85% of the calculated halfwidth comes from a region where the interruption function can not be conveniently summed. The line shift on the other hand does not suffer this malady making it a better gauge to test the theories. One drawback of this is that the experimental measurements are difficult to perform and the quality of the results are in question.

The eight transitions have been studied by the various theories of pressure broadening discussed below. The two general methods of a second order perturbation theory approach, ATC[7] and QFT[4] were used. For each of these, we applied the usual cutoff in the interruption function and also applied the cutoff free theory given by the linked cluster theorem. For each of these two methods, we used classical trajectories and non-linear trajectories (Tipping and Herman model[18]). This gives eight different theoretical approaches to compare with Eng's results. Two of the experimental shifts were in total disagreement with all eight theories and are dropped from this discussion. Our calculations were for N_2 as the perturbing gas. To compare to experiment, Eng's air results were scaled to N_2 values by using the ratio of Δ_{air} to Δ_{N_2} from the

15 1 15 → 16 0 16 transition for which Eng reports an air and N_2 value for the shift. Eng's results are given in Table 13.

In Table 13 the results from the theories are reported. Given in the table is the calculated line shift in (cm^{-1}/atm) and in parenthesis the percent difference from experiment. Several conclusions can be drawn from the table. The first and most important is the comparison of QFT with ATC. We find in all cases the QFT results superior to ATC, this is due in part to the more correct nature of QFT (i.e. fully quantum mechanical, conservation of momentum in collisions, etc.). Looking at the QFT results, we find that for most transitions the more realistic bent trajectories gives an improvement in the results. We note the effect of applying the linked cluster theory to produce a cutoff free theory yields smaller shifts in all cases (just as it yields smaller halfwidths). The conclusion that results from the table is that the QFT method with more realistic trajectories gives the best agreement with experimental shifts. This conclusion was also borne out from our results on halfwidths of ozone.

More recently Dr. J. Johns of the Herzberg Institute of Astrophysics has made available shift results for several lines of the pure rotation spectrum of H_2O. A similar type of analysis was performed testing ten different ways of calculating the shift. The calculations were done and data was exchanged with Dr. Johns during a meeting with him at the 39th Molecular Spectroscopy Symposium at Ohio State University. The results supplied to us are given in Table 14 and the calculations given in Table 15. The overall agreement from any one particular method is not apparent, this is not too surprising due to the sensitivity of shift measurements and calculations. Also after discussions with Dr. Johns it was revealed that the spectra from which the shift values were obtained were uncalibrated and the low pressure lines were low by a <u>few</u> × 10^{-3} cm^{-1}. From further questioning we found it

Table 13. Comparison of Calculated Shifts, Percent Difference with Experiment in Parenthesis

QFT Shifts (cm^{-1}/atm)

Transition	Conventional Method		Linked Cluster Theorem	
	Classical	NLT	Classical	NLT
8 3 5 → 9 4 6	-0.00220 (67)	0.00012 (102)	-0.00100 (85)	0.00005 (101)
6 4 2 → 7 5 3	-0.00555 (20)	-0.00567 (18)	-0.00422 (39)	-0.00293 (58)
6 4 3 → 7 5 2	-0.00571 (16)	-0.00594 (13)	-0.00423 (38)	-0.00395 (42)
5 4 1 → 6 5 2	-0.00617 (24)	-0.00653 (19)	-0.00479 (41)	-0.00427 (47)
5 4 2 → 6 5 1	-0.00625 (23)	-0.00813 (-.3)	-0.00477 (41)	-0.00477 (41)
5 0 5 → 6 3 4	0.01111 (-118)	.00824 (-62)	+0.00876 (-72)	0.00630 (43)
		ATC		
8 3 5 → 9 4 6	0.00070 (111)	0.00145 (122)	0.00086 (113)	0.00113 (117)
6 4 2 → 7 5 3	-0.00319 (54)	-0.00139 (80)	-0.00236 (66)	-0.00122 (82)
6 4 3 → 7 5 2	-0.00309 (55)	-0.00151 (77.8)	-0.00240 (65)	-0.00157 (77)
5 4 1 → 6 5 2	-0.00345 (57)	-0.00187 (77)	-0.00273 (66)	-0.00187 (77)
5 4 2 → 6 5 1	-0.00361 (55)	-0.00213 (74)	-0.00285 (65)	-0.00213 (74)
5 0 5 → 6 3 4	0.00815 (-85)	0.00562 (-28)	0.00691 (-57)	0.00511 (-16)

Transition Upper	Transition Lower	Position cm^{-1} Low Pressure	Position cm^{-1} 500 Ton N_2	$\Delta\nu$ (cm^{-1})
11_{39}	10_{010}	580.533	580.540	+0.007
12_{39}	11_{210}	580.729	580.724	-0.005
9_{64}	8_{35}	581.085	581.088	+0.003
		584.124	584.127	+0.003
12_{58}	11_{29}	584.705	584.723	+0.018
		585.726	585.715	-0.011
9_{54}	8_{27}	591.694	591.705	+0.011
10_{65}	9_{36}	592.051	592.064	+0.013
8_{62}	7_{35}	594.945	594.946	+0.001
12_{49}	11_{110}	600.100	600.111	+0.011
9_{45}	8_{18}	616.070	616.077	+0.007
9_{63}	8_{36}	625.265	625.268	+0.003

[a] NOTE: Measurements from an uncalibrated spectrum

∴ Low pressure lines are low by a few × 10^{-3}

Table 14. H_2O Pressure Shifts, Pure Rotation Spectrum from J. Johns, Herzberg Institute of Astrophysics NRCC, 1984[a]

Theory	$^{10}_{0\ 10} \leftarrow ^{11}_{3\ 9}$	$^{11}_{2\ 10} \leftarrow ^{12}_{3\ 9}$	$^{8}_{3\ 5} \leftarrow ^{9}_{6\ 4}$	$^{8}_{2\ 7} \leftarrow ^{9}_{5\ 4}$	$^{9}_{3\ 6} \leftarrow ^{10}_{6\ 5}$
Conventional QFT (b_{min} - 1.75 × 10^{-8} cm)	-0.00919	-0.02383	-0.00143	0.02302	0.00051
Conventional ATC (b_{min} = 1.75 × 10^{-8} cm)	-0.00777	-0.01426	+0.00150	0.01589	0.00188
QFT-ID (b_{min} = 1.75 × 10^{-8} cm)	-0.01318	-0.02762	+0.00056	0.02308	0.00107
ATC-ID (b_{min} = 1.75 × 10^{-8} cm)	-0.01016	-0.01609	+0.00203	0.01196	0.00199
QFT (2nd order in time)	+0.02743	-0.01203	+0.00004	+0.02033	0.00086
ATC (2nd order in time)	+0.00007	-0.00439	+0.00137	+0.01163	0.00164
Cut-Off Free Theory					
QFT-ID	-0.00862	-0.01205	0.00050	0.00846	0.00076
QFT	-0.00490	-0.01181	-0.00033	0.01424	0.00054
ATC-ID	-0.00704	-0.00789	+0.00169	+0.00735	+0.00179
ATC	-0.00530	-0.00942	0.00157	0.01174	0.00176

Table 15. N_2 Pressure Induced Shifts for H_2O by Several Theoretical Methods

was impossible to numerically fix what a few was without repeating the experiment to give calibrated spectra.

From these discussions it was concluded that the results were probably good for determining the direct of the shift except for the small shift values for which the uncertainty in the low pressure lines makes these shifts of limited value.

4c

5.0 TEMPERATURE DEPENDENCE OF THE HALFWIDTH AND SHIFT N_2- AND O_2-BROADENING OF OZONE

In order to use the halfwidths calculated for ozone for atmospheric applications, the temperature dependence of the halfwidth must be understood as well as the halfwidth at a given temperature. Here we are concerned with the molecule ozone which has a very rich spectrum and is known to play an important role in the temperature regulation of the lower atmosphere, air chemical cycles, and climate and which must be well determined in order to extract information on trace atmospheric constituents in the far IR.[24]

Some experimental results exist for the temperature dependence of the broadening coefficient of ozone, although they are limited. Barbe et al[25] have reported an average temperature exponent of n = 1.3 for six oxygen-broadened lines of ozone. Comont and Monnanteuil[26] have reported the temperature exponent in the range 240-293K for the 96 282.34 MHz line of ozone ($2_{1\,1} \leftarrow 2_{0\,2}$) for self-, N_2, O_2, and air-broadening. More recently Connor and Radford[27] have studied pressure-broadening of the 110.8 GHz line of ozone ($6_{1\,5} \leftarrow 6_{0\,6}$) for the foreign gases N_2 and O_2. Considering a temperature range from 200-300K the temperature exponents for N_2, O_2 and air-broadening were determined.

In the theoretical work of Tejwani and Yeung[13] the halfwidth was calculated via the ATC method at two temperatures for a limited number of transitions to address the temperature dependence. They report an average temperature exponent for A- and B-type transitions of n = 0.68 and 0.73 respectively. The ATC calculations of reference (12) investigate the temperature dependence of several lines. There are large variations in the experimental and theoretical results for the temperature dependence that are not likely due to a variation with rotational quantum numbers and must be explained.

In order to address these questions we have calculated N_2- and O_2-broadened halfwidths over a wide range of temperatures of stratospheric and theoretical interest for a fair number of transitions of ozone. From the results the temperature dependence of the halfwidths have been calculated and are discussed below.

By evaluating the halfwidth at a series of temperatures the variation with temperature can be determined in terms of a particular model. To see this we consider the form of the halfwidth (note, here we work in terms of constant density, not constant pressure) which is the density times the velocity times the optical cross-section, i.e.

$$\gamma(T) = \rho(T) \cdot v(T) \cdot \sigma(T). \tag{22}$$

The temperature dependence of the density ($n_0 \left(\frac{273}{T}\right)$) and the velocity ($(8kT/\pi\mu)^{1/2}$) are known. The temperature dependence of the optical cross-section has been rigorously determined for the case of CO perturbed by Ar or N_2[28] by expanding the optical cross-section in terms of the various interactions involved and studying the temperature dependence of these terms. The usual approach, and the one adopted here, is to take the temperature dependence of the optical cross-section as T to a power m, i.e. $\sigma(T) = T^m \sigma_0$ where σ_0 is independent of temperature. With this approximation and the known dependence of the density and velocity, the halfwidth from equation (22) is considered at two temperatures, T_1 and T_2, and the ratio is taken to give

$$\frac{\gamma(T_1)}{\gamma(T_2)} = \frac{n_0 \ (273/T_1)(8kT_1/\pi\mu)^{1/2} \ T_1^{\,m} \ \sigma_0}{n_0 \ (283/T_2)(8kT_2/\pi\mu)^{1/2} \ T_2^{\,m} \ \sigma_0} = \left(\frac{T_1}{T_2}\right)^{-1/2} \left(\frac{T_1}{T_2}\right)^{m}. \tag{23}$$

By setting $-n = -1/2 + m$ we arrive at the usual formula

$$\gamma(T_1) = \gamma(T_2) \ (T_1/T_2)^{-n}. \tag{24}$$

Thus the temperature dependence of the halfwidth is contained in the value of n. To determine the temperature exponent the halfwidth is evaluated at a number of temperatures and a plot (linear regression) of the set of points $\ln (T_2/T_1)$ vs. $\ln (\gamma(T_1)/\gamma(T_2))$ yields a straight line of slope = n. Furthermore the correlation of the fit of the points to a straight line relates to the validity of the assumed temperature dependence of the optical cross-section, i.e. the closer the correlation coefficient is to |1.| the better the assumption.

By analogous arguments the temperature dependence of the line shift can be evaluated by considering the imaginary part of the optical cross-section, however, here the sign of the cross-section must also be considered, i.e.

$$\Delta(T) = \rho(T)\ v(T)\ S(T)\ \mathrm{Im}\ \sigma(T) \tag{25}$$

where S is the sign of the imaginary part of the cross-section at the temperature T and all other terms have the same meaning as before. The temperature dependence assuming the same form for $\sigma(T)$ as before is given by

$$\frac{\Delta(T_1)}{\Delta(T_2)} = \frac{S(T_1)}{S(T_2)} \cdot \left(\frac{T_1}{T_2}\right)^{-1/2} \cdot \frac{T_1^{\,m}}{T_2^{\,m}} \frac{\sigma}{\sigma} = \frac{S(T_1)}{S(T_2)} \left(\frac{T_1}{T_2}\right)^{-n} . \tag{26}$$

The reason the sign had to be included was in order to take the log of Eq. (26) to give

$$\ln \left\{\frac{S(T_2)\ \Delta(T_1)}{S(T_1)\ \Delta(T_2)}\right\} = -n \ln \left\{\frac{T_1}{T_2}\right\} \tag{27}$$

which is well behaved (i.e. the log of a negative number is not encountered). Note, to use equation (27) we must give the sign of the shift with respect to temperature as well as n.

Caution must be exercised when applying equation (27) to shift results. In particular we have found that when the shift is very small the calculations are sometimes not very accurate and can have incorrect signs, the same is true

for experiment. Applying equation (27) to such results can give meaningless values for the temperature coefficient n, however, this should be reflected in the correlation coefficients. For larger shifts, the more reliable the calculations and experiments, although the magnitude is still in question the signs are usually correct. From the results obtained here, only linear regressions with correlation coefficients greater than 0.95 are retained. As expected the transitions removed by this criterion all had very small values for the line shift.

The nitrogen-broadened calculations were done at a total of seven temperatures. The temperatures are 200.0, 216.6, 245.0, 275.0, 296.0, 350.0 and 500.0 and were partially selected from a temperature profile of the U.S. Standard Atmosphere. The temperature dependence of the halfwidth and shift was evaluated as a function of J" and type of transition (ΔJ, ΔK_a) up to J" = 35. The 125 transitions studies include transitions of stratospheric importance when accurate T-dependence is desired.

The results for the temperature dependence of the halfwidth are in Table 16. Listed are the rotational quantum numbers of the transition, the temperature exponent n and the value of the correlation coefficient to show the validity of equation (24), note here the correlation coefficients are equal to one to three places after the decimal. In Figure 2, the temperature coefficient n is plotted vs. the lower state rotational quantum number, there appears to be no strong dependence in the temperature coefficient on the rotational quantum numbers or on the type of transition. The average n value for the 125 lines was n = 0.77 with a standard deviation of 0.036, the value of n for different transitions fluctuates ±6% about this average value.

The results for the temperature coefficient of the N_2-induced line shift are presented in Table 17. The criterion of the correlation being greater than 0.95 was enforced on

Table 16. Temperature Exponent and Correlation of Fit for O_3 Halfwidths Broadened by N_2 Calculated by QFT-ID Method

Transition						n	r
20	15	5	21	16	6	.75	1.000
27	14	14	28	15	13	.76	1.000
34	13	21	35	14	22	.78	1.000
21	15	7	22	16	6	.75	1.000
28	14	14	29	15	15	.76	1.000
22	15	7	23	16	8	.75	1.000
29	14	16	30	15	15	.76	1.000
23	15	9	24	16	8	.75	1.000
30	14	16	31	15	17	.76	1.000
24	15	9	25	16	10	.75	1.000
31	14	18	32	15	17	.76	1.000
18	16	2	19	17	3	.74	1.000
14	2	12	13	3	11	.76	1.000
2	0	2	2	1	1	.79	1.000
4	0	4	4	1	3	.79	1.000
1	1	1	1	1	0	.78	1.000
2	0	2	2	1	1	.79	1.000
2	0	2	2	2	1	.77	1.000
2	2	0	3	2	1	.75	1.000
3	1	3	4	1	4	.79	1.000
3	1	3	4	3	2	.77	1.000
4	0	4	5	0	5	.79	1.000
5	0	5	6	0	6	.79	1.000
5	1	4	6	1	5	.78	1.000
5	1	5	6	1	6	.78	1.000
5	2	3	6	2	4	.75	1.000
5	2	4	6	2	5	.75	1.000
5	3	3	6	3	4	.75	1.000
5	4	1	6	4	2	.76	1.000
5	4	2	6	4	3	.76	1.000
5	5	0	6	5	1	.79	1.000
5	5	1	6	5	2	.79	1.000
6	1	5	6	3	4	.76	1.000
7	0	7	8	2	6	.77	1.000
7	3	5	8	3	6	.75	1.000
7	7	1	8	8	0	.82	1.000
8	0	8	8	3	5	.77	1.000
8	2	8	8	4	5	.76	1.000
9	2	8	10	4	7	.76	1.000
10	3	7	10	5	6	.77	1.000
11	0	11	11	2	10	.77	1.000
11	0	11	12	0	12	.77	1.000
11	1	10	11	3	9	.76	1.000
11	1	10	12	1	11	.77	1.000
11	1	11	11	3	8	.76	1.000
11	1	11	11	4	8	.77	1.000
11	1	11	12	1	12	.77	1.000
11	2	9	11	4	8	.76	1.000
11	2	9	12	2	10	.76	1.000
11	2	10	11	4	7	.76	1.000
11	2	10	12	2	11	.76	1.000
11	3	8	11	5	7	.77	1.000
11	3	8	12	3	9	.75	1.000
11	3	9	11	5	6	.77	1.000
11	3	9	12	3	10	.75	1.000
11	4	7	12	4	8	.76	1.000
11	4	8	11	6	5	.78	1.000
11	4	8	12	4	9	.76	1.000
11	5	6	12	5	7	.78	1.000
11	5	7	11	7	4	.79	1.000
11	5	7	12	5	8	.78	1.000
11	6	5	12	6	6	.80	1.000
11	6	6	11	8	3	.80	1.000
11	6	6	12	6	7	.80	1.000
11	7	5	11	9	2	.81	1.000

Table 16. (Continued)

Transition						n	r
11	7	5	12	7	6	.81	1.000
11	8	3	12	8	4	.81	1.000
11	8	4	12	8	5	.81	1.000
11	9	2	12	9	3	.81	1.000
11	9	3	12	9	4	.81	1.000
11	10	1	12	10	2	.80	1.000
11	10	2	12	10	3	.80	1.000
11	11	1	12	11	2	.79	1.000
12	0	12	13	2	11	.77	1.000
12	7	5	13	7	6	.80	1.000
12	12	1	13	12	2	.78	1.000
13	0	13	14	0	14	.77	1.000
13	7	7	14	7	8	.80	1.000
13	13	0	14	13	1	.77	1.000
14	0	14	15	0	15	.76	1.000
14	7	7	15	8	8	.80	1.000
15	8	8	16	7	9	.80	1.000
16	5	11	17	7	10	.79	1.000
17	5	13	18	2	16	.78	1.000
18	1	17	18	4	14	.77	1.000
18	12	6	19	14	5	.77	1.000
19	12	7	20	10	10	.79	1.000
20	0	20	20	2	18	.75	1.000
20	1	20	21	1	21	.75	1.000
20	2	18	20	4	17	.77	1.000
20	4	16	20	6	15	.79	1.000
20	6	14	20	8	13	.80	1.000
20	8	12	20	10	11	.80	1.000
20	10	10	20	12	9	.79	1.000
20	12	8	20	13	7	.77	1.000
20	14	6	20	14	7	.76	1.000
20	16	4	20	16	5	.74	1.000
20	18	2	20	18	3	.73	1.000
21	6	16	21	8	13	.80	1.000
21	7	15	21	9	12	.80	1.000
22	12	11	22	12	10	.78	1.000
22	15	7	23	15	8	.75	1.000
23	2	21	23	4	20	.77	1.000
23	10	14	24	11	13	.79	1.000
24	6	18	25	6	19	.80	1.000
25	3	23	26	2	24	.76	1.000
25	20	6	25	20	5	.73	1.000
26	9	18	26	11	15	.79	1.000
26	9	18	27	7	21	.80	1.000
27	8	20	28	7	21	.80	1.000
27	13	15	27	15	12	.76	1.000
28	6	23	28	6	22	.80	1.000
28	6	23	29	4	26	.79	1.000
29	2	28	30	3	27	.76	1.000
29	5	25	29	7	22	.80	1.000
30	8	22	30	10	21	.80	1.000
30	8	22	31	6	25	.80	1.000
32	8	24	32	10	23	.80	1.000
32	9	23	33	9	24	.80	1.000
33	4	30	33	5	29	.79	1.000
33	5	28	34	7	28	.80	1.000
34	0	34	35	0	35	.79	1.000
34	13	21	34	14	20	.77	1.000
35	4	32	35	5	31	.80	1.000

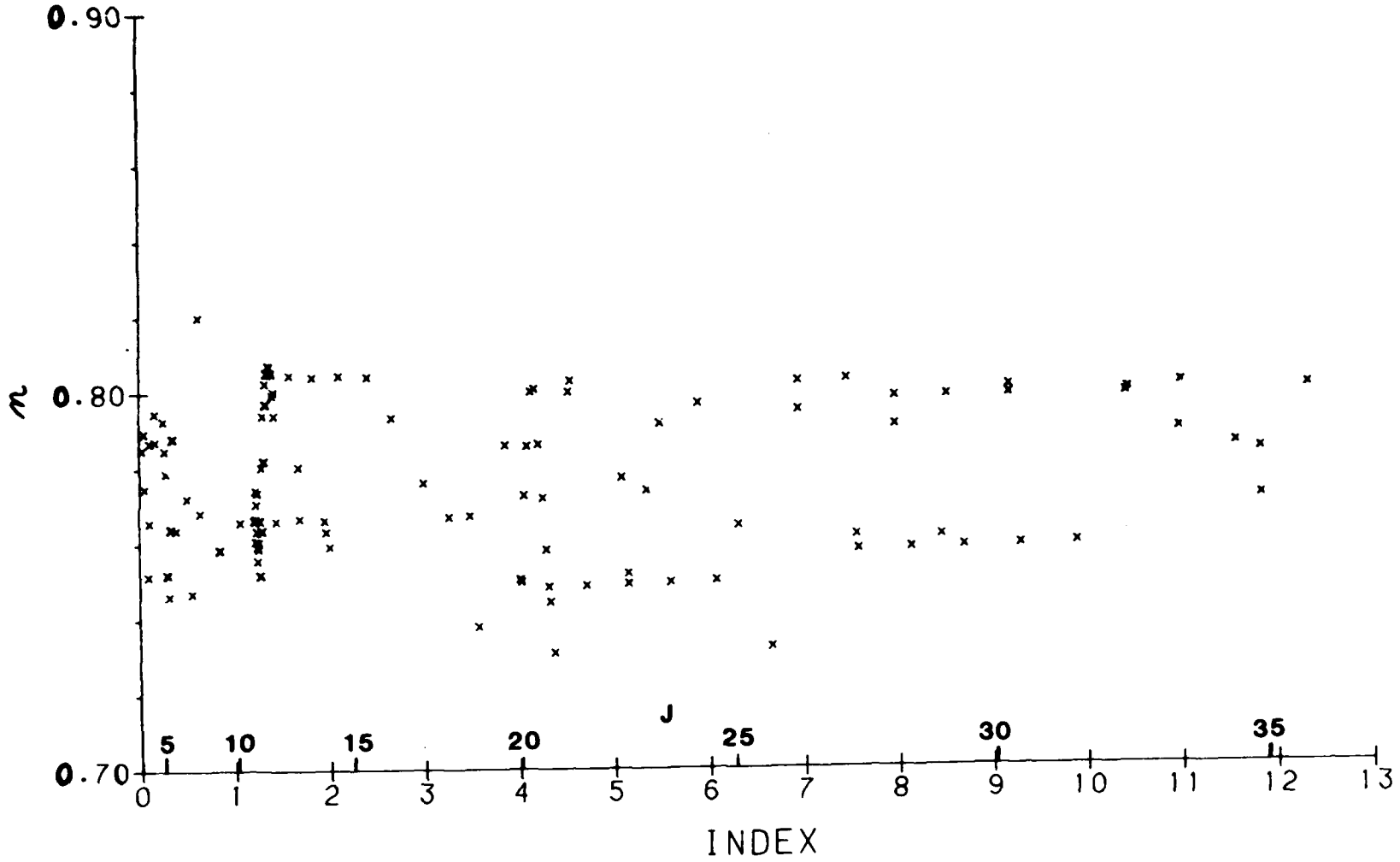

Figure 2. Temperature Exponent vs. Lower State Rotational Quantum State Index ($J"(J" + 1) + K_a" - K_c" + 1$) or $J"$. O_3-N_2 System.

Table 17. Temperature Dependence of the Shift, O_3-N_2 System, QFT-ID Calculations

Transition						n[a]	Δ[b]	T[c]	r[d]
2	0	2	2	1	1	3.66	.00063	-	0.993
4	0	4	4	1	3	2.32	.00071	-	0.999
1	1	1	1	1	0	1.23	.00013	-	1.000
2	0	2	2	2	1	1.93	.00182	-	1.000
2	2	0	3	2	1	0.45	.00009	-	0.978
3	1	3	4	3	2	1.18	.00008	-	0.999
5	0	5	6	0	6	1.55	-.00008	-	0.997
5	1	4	6	1	5	0.58	-.00008	-	0.946
5	4	1	6	4	2	0.92	-.00007	-	0.999
6	1	5	6	3	4	1.20	.00111	-	0.988
7	0	7	8	2	6	1.60	-.00156	-	1.000
8	0	8	8	3	5	1.35	.00174	-	0.999
10	3	7	10	5	6	2.52	-.00042	750	0.964
11	0	11	11	2	10	1.30	-.00101	-	0.999
11	0	11	12	0	12	1.87	-.00004	-	0.999
11	1	10	11	3	9	1.11	-.00076	-	0.984
11	1	10	12	1	11	0.47	-.00004	-	0.997
11	1	11	11	3	8	1.09	.00176	-	0.998
11	1	11	11	4	8	0.94	.00167	-	0.996
11	1	11	12	1	12	1.51	.00002	1000	0.999
11	3	8	11	5	7	2.45	.00038	750	0.965
11	3	9	11	5	6	2.27	-.00035	750	0.961
11	4	8	11	6	5	1.75	-.00052	-	0.988
11	5	7	11	7	4	.99	-.00047	-	0.955
12	0	12	13	2	11	1.25	.00131	-	1.000
13	0	13	14	0	14	2.40	-.00003	-	0.999
16	5	11	17	7	0	1.21	-.00037	-	0.981
20	1	20	21	1	21	1.59	-.00004	-	0.998
20	4	16	20	6	15	1.55	-.00016	-	0.980
20	20	0	20	20	1	1.16	.00017	-	0.977
23	2	21	23	4	20	2.46	.00042	750	0.955
25	3	23	26	2	24	2.79	.00045	-	0.988
28	6	23	29	4	26	2.12	.00020	-	0.995
29	2	28	30	3	27	1.04	.00153	-	0.999
32	9	23	33	9	24	1.07	.00002	500	0.976
35	4	32	35	5	31	1.56	-.00029	-	0.992

a. n = temperature exponent

b. Δ = line shift at 296°K cm^{-1}/atm

c. T = temperature °K at which shift changes sign from sign at 296°K, - indicates sign does not change over the range studied (200° - 1000°K)

d. r = correlation coefficient of fit

the 125 transitions to produce Table 17. Listed are the rotational quantum numbers, the temperature exponent, the line shift at 296°K, the temperature at which the sign changes and the correlation coefficient. One can see the line shift changes more with temperature than the halfwidth and the temperature exponents have much greater spread.

Preliminary O_2-broadening calculations were done using the QFT-ID method, however, cutoff problems occurred due to the small quadrupole moment of O_2. Only ten transitions were studied here in an attempt to compare with experimental measurements.[25,26,29] Because of the cutoff problems, a second set of QFT-ID calculations were performed with a very low cutoff, to do this in the QFT-ID formalism below σ (Lennard-Jones) we use the relationship $b = r_c$. The thought here was that since we are studying the temperature dependence of the optical cross-section in a sense we do not wish to cutoff in the calculation of the cross-section. By allowing the calculations to go unusually low we hoped the form of the cross-section would be correct. The results from these two methods are in Table 18. There is no way to be certain which set is better, even though the low cutoff values agree better with the work of Barbe et al.[25]

To eliminate these cutoff problems, the cluster expansion method (cutoff free theory) was used to study the transition of ozone for O_2-broadening. The interruption functions (optical cross-sections) were the QFT-ID type, where α was scaled to match the experimental value of Connor[27] for the $6_{1\,5} \leftarrow 6_{0\,6}$ transition for column three, the experimental values of Barbe[25] (column two) and the theoretically set set (column one). This yields the following values of α, 4.83, 3.70 and 2.99, respectively. The temperature exponent from these calculations are in Table 19. The agreement with Connor's results[27] improve with the $\alpha = 4.83$ calculations, however, the theoretical value of $\alpha = 2.99$ gives the best agreement with Barbe's value[25] of $X_{O_2} = 1.3$.

Table 18. Preliminary Temperature Exponents for O_3-O_2 System by QFT-ID Method with Different Cutoffs

Transition	Temperature Exponent b_0 = σ(Lennard-Jones) = 3.23 × 10^{-8} cm	Temperature Exponent b_0 = 1.75 × 10^{-8} cm
2 0 2 — 2 1 1	0.81	1.07
26 1 25 — 25 1 24	0.89	1.06
25 5 21 — 24 5 20	0.87	1.10
24 7 17 — 23 7 16	0.92	1.10
25 4 22 — 24 4 21	0.90	1.10
26 0 26 — 25 0 25	1.02	1.02
25 3 23 — 24 3 22	0.91	1.06
5 5 1 — 6 5 2	0.93	1.08
10 3 7 — 10 5 6	0.90	1.07
15 8 8 — 16 7 9	0.81	1.17
average	0.90	1.08

Table 19. Temperature Exponent for O_2-Broadened Ozone from Cutoff Free Theory

Transition	X_{O_2} QFT Scale Factor $\alpha = 2.99$	$\alpha = 3.70$	$\alpha = 4.83$
$^{6}{}_{0\ 6} - {}^{6}{}_{1\ 5}$	0.91	0.81	0.78
$^{4}{}_{0\ 4} - {}^{4}{}_{1\ 3}$	0.91	0.82	0.78
$^{2}{}_{0\ 2} - {}^{2}{}_{1\ 1}$	0.91	0.82	0.78
$^{25}{}_{5\ 21} - {}^{24}{}_{5\ 20}$	0.94	0.82	0.75

To summarize, the agreement between theory and experiment for the broadening coefficients of ozone is quite satisfactory for N_2-broadening; this includes the temperature dependence of the coefficients. For oxygen broadening, the situation is not so good and we comment that there is much more work to be done both theoretically and experimentally.

6.0 HALFWIDTH AND SHIFT CALCULATIONS IN COLLABORATION WITH OTHER SCIENTIFIC GROUPS

There is a need for accurate halfwidths and shifts to aid in reducing atmospheric spectroscopic data. During the course of this contract, many groups have contacted us to request data for particular transitions of H_2O and O_3. Although producing the data requires additional work, giving the data to groups who use it immediately benefits us in that the quality of the data is assessed by laboratory measurements. Below the people who requested the data are listed and the data and its use given.

Dr. Weslie Traub and Dr. Kelly Chance of the Harvard-Smithsonian Astrophysical Observatory in Cambridge, Massachusetts, requested halfwidths for H_2O and O_3 to help reduce balloon spectra. For the requested transitions halfwidths were calculated and supplied to them, these are listed in Table 20.

Dr. Curt Rinsland of NASA at Langley requested halfwidths for ν_2 transitions of O_3 to use to analyze a segment of stratospheric spectra from 779-781 cm^{-1}, the results are given in Table 21.

In Section 4.0 the shift calculations done in collaboration with Dr. John Johns of the Hertzburg Institute of Astrophysics were listed and discussed.

Samuel Gaster, a graduate student of Dr. Charles Townes, from the University of California at Berkeley requested some O_2-broadening of H_2O calculations to compare with his FTS measurements. Because of cutoff problems the calculations had to be done by the linked-cluster theorem program. The results sent to Gaster are listed in Table 22.

H_2O													
Transition						$\gamma(N_2)$	Transition						$\gamma(N_2)$
2	2	1	1	1	0	0.11267	3	3	1	2	2	0	0.10009
6	3	4	6	2	5	.09264	3	3	0	2	2	1	.09977
6	1	5	6	0	6	.10085	6	2	5	5	1	4	.10294
6	4	2	6	3	3	.10061	6	6	0	6	5	1	.07678
6	2	4	5	3	3	.10479	6	6	1	6	5	2	.07601
2	2	1	1	1	1	.11023	4	4	0	5	1	5	.09196
5	1	4	4	2	3	.10688	4	3	1	4	0	4	.10444
5	0	5	4	1	4	.10546	5	4	1	6	1	6	.09159
5	4	1	5	3	2	.09578	4	3	2	3	2	1	.10235
4	4	0	4	3	1	.09000	4	2	2	3	1	3	.11174
5	1	5	4	0	4	.10646	5	3	2	5	0	5	.10389
4	4	1	4	3	2	.09115	5	3	3	4	2	2	.10442
6	2	5	6	1	6	.09477	5	5	0	6	2	5	.08584
5	4	2	5	3	3	.09367	6	3	4	5	2	3	.10558
6	4	3	6	3	4	.09064	4	4	1	3	3	0	.08651
3	2	2	2	1	1	.11080	4	4	0	3	3	1	.08722
6	0	6	5	1	5	.09849	5	3	2	4	2	3	.10389
6	1	6	5	0	5	.10310	5	4	1	5	1	4	.09948
6	1	5	5	2	4	.10059	4	4	0	4	1	3	.09912
4	2	3	3	1	2	.10945	5	2	3	4	1	4	.11159
3	3	0	3	0	3	.10559							

O_3													
Transition						$\gamma(N_2)$	Transition						$\gamma(N_2)$
21	16	6	20	15	5	0.06460	30	15	15	29	14	16	0.06539
28	15	13	27	14	14	.06549	24	16	8	23	15	9	.06483
35	14	22	34	13	21	.06414	31	15	17	30	14	16	.06533
22	16	6	21	15	7	.06472	25	16	10	24	15	9	.06484
29	15	15	28	14	14	.06544	32	15	17	31	14	18	.06527
23	16	8	22	15	7	.06479	19	17	3	18	16	2	.06236

Table 20. N_2-Broadened Halfwidths for Selected H_2O and O_3 Transitions as Supplied to Smithsonian Astrophysics Institute (units are cm^{-1}/atm)

Transition						γ (cm^{-1}/atm)
J"	Ka"	Kc"	J'	Ka'	Kc'	
12	11	1	12	12	0	0.06639
28	8	20	29	9	21	0.06809
26	8	18	27	9	19	0.06815
32	15	17	31	16	16	0.06460
17	9	9	18	10	8	0.06875
19	9	11	20	10	10	0.06855
24	14	10	23	15	9	0.06566
10	10	0	11	11	1	0.06648
29	8	22	30	9	21	0.06806
27	8	20	28	9	19	0.06811
20	9	11	21	10	12	0.06846
18	9	9	19	10	10	0.06865
30	8	22	31	9	23	0.06805
23	14	10	22	15	7	0.06567
11	10	2	12	11	1	0.06770
28	8	20	29	9	21	0.06809
21	9	13	22	10	12	0.06837
19	9	11	20	10	10	0.06855
10	10	0	11	11	1	0.06648
31	8	24	32	9	23	0.06804
12	10	2	13	11	3	0.06823
22	14	8	21	15	7	0.06567
29	8	22	30	9	21	0.06806
22	9	13	23	10	14	0.06828
20	9	11	21	10	12	0.06846
32	8	24	33	9	25	0.06803
11	10	2	12	11	1	0.06770

Table 21. QFT-ID Results Given to Curtis Rinsland

Table 22. Halfwidths for O_2-Broadening of H_2O Calculated by Cutoff Free Theory with QFT-ID Interruption Functions, Units are cm^{-1}/atm

Transition									γ
1	1	1		2	2	1			0.0611
3	0	3		3	1	2			0.0595
2	2	1		3	1	2			0.0574
3	1	2		3	1	4			0.0574
4	1	3		4	2	2			0.0579
2	1	1		2	2	0			0.0581
5	1	4		5	2	3			0.0574
9	2	7		9	3	6			0.0484
4	2	3		4	3	2			0.0474
5	2	4		5	3	3			0.0456
3	0	3		4	1	4			0.0568
7	3	4		7	4	3			0.0514
5	1	5		5	2	4			0.0458
1	1	0		2	2	1			0.0594
6	2	5		6	3	4			0.0430
5	3	3		6	2	4			0.0521
1	1	1		2	2	0			0.0582
4	2	3		5	1	4			0.0535
8	1	7		8	2	6			0.0443
4	1	4		5	0	5			0.0494
4	3	1		4	4	0			0.0426
4	0	4		5	1	5			0.0509
7	2	6		7	3	5			0.0400
6	3	4		6	4	3			0.0417
2	1	1		3	2	3			0.0578

Brian Connor, a graduate student of Dr. Alex Delgarno, at Harvard University Center for Astrophysics contacted us in regard to halfwidths and temperature dependence of the halfwidth for ozone. Although Brian's actual thesis work is on LIDAR he needed information on the lines involved with his LIDAR setup. He did FTS measurements on several transitions of ozone, to help confirm his measurements he requested QFT-ID calculations for the halfwidth and temperature dependence. The results supplied to Brian are given in Table 23.

Dr. Jens Bösenberg, of the Max-Planck-Institute for Meteorology, requested pressure shift information in reference to setting up a differential absorption LIDAR in the 725 mm wavelength range for atmospheric water vapor studies. Jens has shown that the neglect of the pressure shift can cause considerable error in DIAL measurements at some km heights. The table of pressure shifts from earlier calculations (see Appendix B3) was sent to him and QFT-ID calculations were done for the specific lines of interest (see Table 24).

Table 23. Halfwidths and Temperature Coefficients (n) of Ozone

Transition	γ_{N_2} (cm^{-1}/atm)	γ_{O_2} (cm^{-1}/atm)	γ_{air} (cm^{-1}/atm)	n_{N_2}	n_{O_2}
$^{4}_{1\ 3}$ $^{4}_{0\ 4}$	0.07967	0.05683	0.07487	0.787	0.617
$^{6}_{1\ 5}$ $^{6}_{0\ 6}$	0.07918	0.05649	0.07441	0.773	0.620
$^{28}_{5\ 23}$ $^{29}_{4\ 26}$	0.06961	0.05158	0.06583	-	-
$^{14}_{3\ 11}$ $^{15}_{2\ 14}$	0.07144	0.05421	0.06782	-	-

```
        JMAX=   30KMAX=   20
        D1=      .18500E-17 Q1=      .15420E-25 Q2=     -.28000E-25 T=      .29600E+03 MREDUCED=      .18320E-22
        B2=      .20000E+01 BMIN=      .32300E-07 GEVEN=      .60000E+01 GOOD=      .30000E+01 ALPHA=      .25000E+01
        AID= 1.00 V=      .75379E+05 ADQ=      .57921E-07 FACT=      .31090E+14DIPCOR=      .10000E+01
EPS=  135.94000         RM=      .30710E-07
                        CALCULATIONS ARE FOR (000)-(000) TRANSITIONS
 3  1  3  4  1  4  000000    142.27845 224.83874  .97947E-01  .78760E-01  .19142E-01  .45518E-04 -.14329E-03
 .17821E-02 -.43400E-02 -.25579E-02  .50889E+01     .00071
 3  0  3  4  0  4  000000    136.76138 222.05292  .10060E+00  .80098E-01  .20467E-01  .34024E-04 -.84276E-04
 .32138E-02 -.67534E-02 -.35395E-02  .50942E+01     .00068
 4  0  4  3  0  3  000000    222.05292 136.76138  .10060E+00  .80098E-01  .20467E-01  .34024E-04 -.84276E-04
 .32138E-02  .35395E-02  .67534E-02  .50942E+01     .00068
 5  1  4  6  1  5  000000    399.45897 542.90904  .95878E-01  .76354E-01  .19492E-01  .32519E-04 -.52076E-04
 .31172E-02 -.95107E-02 -.63935E-02  .49629E+01     .00080
 4  3  2  4  3  1  000000    382.51983 383.84546  .88177E-01  .71658E-01  .16145E-01  .37443E-03 -.32079E-04
 .21296E-02  .42661E-02  .63957E-02  .47994E+01     .00070
 3  3  0  3  1  3  000000    285.41977 142.27845  .93386E-01  .76648E-01  .16514E-01  .22407E-03  .75443E-04
 .77134E-02 -.34968E-02  .42166E-02  .49950E+01     .00068
 3  3  1  3  3  0  000000    285.22053 285.41977  .85683E-01  .67876E-01  .17260E-01  .54692E-03 -.36379E-03
 .13145E-02  .12041E-01  .13356E-01  .46376E+01     .00058
 2  2  1  2  2  0  000000    134.90164 136.16389  .95226E-01  .77822E-01  .17331E-01  .73581E-04 -.18128E-04
-.89669E-04 -.98097E-03 -.10706E-02  .50117E+01     .00067
 1  1  0  1  1  1  000000     42.37159  37.13708  .10091E+00  .82465E-01  .18400E-01  .47784E-04 -.37800E-05
 .56944E-02  .12835E-03  .58227E-02  .51728E+01     .00066
 4  2  3  4  2  2  000000    300.36346 315.78071  .96494E-01  .78340E-01  .18121E-01  .33750E-04  .15149E-05
-.94739E-03 -.13194E-02 -.22668E-02  .50249E+01     .00074
 2  1  2  2  1  1  000000     79.49628  95.17558  .10070E+00  .81481E-01  .19171E-01  .46838E-04  .28857E-05
 .17212E-02 -.38833E-02 -.21620E-02  .51361E+01     .00065
 4  1  4  4  1  3  000000    224.83874 275.49730  .99332E-01  .79949E-01  .19337E-01  .46376E-04 -.13594E-04
-.13398E-02 -.31693E-02 -.45091E-02  .50859E+01     .00070
 1  1  1  2  1  2  000000     37.13708  79.49628  .10080E+00  .81088E-01  .19666E-01  .51666E-04 -.43204E-05
 .11313E-02 -.50964E-02 -.39651E-02  .51241E+01     .00070
 1  0  1  2  0  2  000000     23.79419  70.09048  .10360E+00  .83833E-01  .19740E-01  .30792E-04 -.18015E-04
 .38081E-02 -.10712E-01 -.69036E-02  .52102E+01     .00076
 3  0  3  4  1  4  000000    136.76138 224.83874  .10004E+00  .79746E-01  .20252E-01  .38195E-04 -.88845E-04
 .46496E-02 -.67975E-02 -.21479E-02  .50842E+01     .00073
 5  2  3  6  2  4  000000    446.51331 602.77810  .10083E+00  .76761E-01  .23972E-01  .99739E-04  .19043E-06
-.49927E-02 -.66637E-03 -.56590E-02  .49696E+01     .00072
```

Table 24. QFT-ID Calculations of Halfwidths and Pressure Shifts of N_2-Broadening of H_2O

7.0 REFERENCES

1. L. S. Rothman, R. R. Gamache, A. Barbe, A. Goldman, J. R. Gillis, L. R. Brown, R. A. Toth, J.-M. Flaud and C. Camy-Peyret, Appl. Opt. 22, 2247 (1983).

2. L. S. Rothman, A. Goldman, J. R. Gillis, R. R. Gamache, H. M. Pickett, R. L. Poynter, N. Husson and A. Chedin, Appl. Opt. 22, 1616 (1983).

3. Quarterly Status Report No. 4, Contract No. F19628-78-C-0197 (1979).

4. R. W. Davies, Phys. Rev. A12, 927 (1975).

5. R. R. Gamache and R. W. Davies, "Theoretical Calculations of N_2-Broadened Halfwidths of H_2O Using Quantum Fourier Transform Theory," Appl. Opt. 22, 4013 (1983).

6. S. A. Clough, F. X. Kneizys, L. S. Rothman and W. O. Gallery, Proc. Soc. Photo. Opt. Instrum. Eng. 277, 152 (1981).

7. P. W. Anderson, Phys. Rev. 76, 647 (1949); 80, 511 (1950). C. J. Tsao and B. Curnutte, Jr., J. Quant. Spectrosc. Radiat. Transfer 2, 41 (1962).

8. J. M. Hoell, C. N. Harward, C. H. Bair and B. S. Williams, Ozone Air Broadening Coefficients in the 9 μm Region, Optical Engineering, May/June (1982).

9. S. Lundqvist, J. Margolis and J. Reid, Appl. Opt. 21, 3109-3112 (1982).

10. J. Margolis, J. Quant. Spectrosc. Radiat. Transfer 29. 539-542 (1983).

11. C. Meunier, P. Marche and A. Barbe, J. Mol. Spectrosc. 95, 271-275 (1982).

12. J.-Y. Mandin, J.-M. Flaud and C. Camy-Peyret, CNRS Bâtiment 221, Campus d'Orsay, 91405 Orsay-Cedex, private communications (1983).

13. G. D. T. Tejwani and E. S. Yeung, J. Chem. Phys. 63, 1513 (1975).

14. J. S. Murphy and J. E. Boggs, J. Chem. Phys. 47, 691 (1967).

15. M. Cattani, Phys. Lett. A38, 147 (1972).

16. E. T. Salesky and D. Korff, Phys. Lett. A72, 431 (1979).

17. D. Robert and J. Bonamy, J. Phys. (Paris) 40, 923 (1979).

18. R. W. Tipping, Thesis, Department of Physics, The Pennsylvania State University (1969); R. H. Tipping and R. M. Herman, J. Quant. Spectrosc. Radiat. Transfer 10, 881 (1970); R. H. Tipping and R. M. Herman, J. Quant. Spectrosc. Radiat. Transfer 10, 897 (1970).

19. J. Bonamy, L. Bonamy and D. Robert, J. Chem. Phys. 67, 4441 (1977).

20. J. I. Gersten, Phys. Rev. A4, 98-108 (1970).

21. M. Berard and P. Lallemand, J. Quant. Spectrosc. Radiat. Transfer 19, 387 (1978).

22. R. W. Davies and B. A. Oli, J. Quant. Spectrosc. Radiat. Transfer 20, 95-120 (1978).

23. R. S. Eng, A. R. Calawa, T. C. Harman, P. L. Kelley and A. Javan, Appl. Phys. Lett. 21, 303 (1972); R. S. Eng, P. L. Kelley, A. Mooradian, A. R. Calawa and T. C. Harman, Chem. Phys. Lett. 19, 524 (1973); R. S. Eng, P. L. Kelley, A. R. Calawa, T. C. Harman and K. W. Nill, Molec. Phys. 28, 653 (1974).

24. H. Oelhaf, A. Leupolt and H. Fischer, Appl. Opt. 22, 647-649 (1983).

25. A. Barbe, P. Marché, C. Meunier and P. Jouve, J. Physique 44 (1983).

26. J. M. Colmont and N. Monnanteuil, J. Mol. Spectrosc. 104, 122-128 (1984).

27. B. J. Connor and H. E. Radford, Center for Astrophysics, Harvard College Observatory, Cambridge, MA 02138, private communications (1984).

28. J. Bonamy, D. Robert and C. Boulet, J. Quant. Spectrosc. Radiat. Transfer 31, 23-34 (1984).

29. N. Monnanteuil and J. M. Colmont, J. Quant. Spectrosc. Radiat. Transfer 29, 131-136 (1983).

A P P E N D I X A

Presentations made under contract

A1. The 38th Symposium on Molecular Spectroscopy, Paper ME13, June 13, 1983.

A2. The 1983 Workshop on Ozone, AFGL, November 17, 1983.

A3. The 39th Symposium on Molecular Spectroscopy, Paper MF8, June 11, 1984.

A4. Quadrennial Ozone Symposium, Halkidiki, Greece, September 3-7, 1984.

A1.

THEORETICAL DETERMINATION OF N_2-BROADENED HALFWIDTHS OF OZONE

R. R. GAMACHE, R. W. DAVIES, AND L. S. ROTHMAN

For $^{16}O_3$, accurate N_2-broadened halfwidths are difficult to obtain for a large number of transitions. Recent measurements[1] have allowed assigning average air-broadened halfwidths of ozone for A-type bands, α=0.083 cm^{-1}/atm, and for B-type bands, α=0.077 cm^{-1} at 296 K. These measurements, however, were not extensive enough to give J-dependence of the halhwidths. Theoretical N_2-broadened halfwidths have been determined for a number of ν_2 (A-type) and ν_1 (B-type) transitions of ozone. The halfwidths have been evaluated using the Anderson-Tsao-Curnutte theory of collisional broadening and by the more rigorous Quantum Fourier Transform theory due to Davies.[2] In the calculations, contributions to the halfwidth from dipole-quadrupole interaction and quadrupole-quadrupole interaction are considered. Both methods are compared with experiment. From the study, air-broadened halfwidths will be calculated for an extensive list of transitions for ozone, and these will appear on a future AFGL Main Gas Compilation.

---

1. J. M. Hoell, C.H. Harward, C.H. Bair, and B. S. Williams, Opt. Eng. 21, 3109(1982).
2. R. W. Davies, Phys Rev.A12, 927(1975).

This work was supported by the Air Force Office of Scientific Research, through task 2310G1.

Address of Gamache: The Center for Atmospheric Research, University of Lowell Research Foundation 450 Aiken St., Lowell, MA 01854.
Address of Davies: GTE/Sylvanis, 40 Sylvan Rd., Waltham, MA 02154.
Address of Rothman: Optics Division, Air Force Geophysics Laboratory, Hanscom AFB, MA 01731.

A2. SECOND ORDER PERTURBATION THEORY APPROACHES TO COLLISIONAL BROADENING OF OZONE

Robert R. Gamache
University of Lowell
Center for Atmospheric Research
450 Aiken Street
Lowell, MA 01854

Richard W. Davies
GTE Laboratories
110 Sylvan Road
Waltham, MA 02254

Laurence S. Rothman
AFGL/OPI
Hanscom AFB, MA 01731

A summary of the various second order perturbation theory approaches to collisional broadening of ozone is presented. The theories include the Anderson-Tsao-Curnutte method,[1] the quantum Fourier transform method[2] and the linked-cluster approach for a cutoff free theory.[3] In addition these methods are generalized to use approximate trajectories which better represent actual trajectories. Calculations are done on ozone perturbed by nitrogen and it is demonstrated that the non-linear trajectory approaches give much better results than the classical path methods.

REFERENCES

1. P. W. Anderson, Phys. Rev. 76, 647 (1949); 80, 511 (1950); C. J. Tsao and B. Curnutte, Jr., J. Quant. Spectrosc. Radiat. Transfer 2, 41 (1962).

2. R. W. Davies, Phys. Rev. A12, 927 (1975).

3. R. P. Leavitt and D. Korff, J. Chem. Phys. 74, 2180 (1981).

A3.

THEORETICAL N_2-, O_2-, AND AIR-BROADENED HALFWIDTHS OF $^{16}O_3$ CALCULATED BY QUANTUM FOURIER TRANSFORM THEORY WITH REALISTIC COLLISION DYNAMICS.

R.R.GAMACHE, R.W.DAVIES, AND L.S.ROTHMAN

We have evaluated collision broadened halfwidths of ozone with nitrogen and oxygen as the perturbing gases. Calculations using conventional Anderson theory[1] or quantum Fourier transform theory[2] are shown to be some 25 to 35% too low when compared to the experimental measurements[3,4]. We show that it is important to consider more realistic collision dynamics in the calculations. By replacing the classical path trajectories by non-linear trajectories with constant velocities chosen to give the equations of motion exact to first order in time we develop the interruption function in terms of the actual distance of closest approach determined by the intermolecular potential . This improvement to the theory results in N_2- and O_2- broadened halfwidths which are in good agreement with the experimental measurements.

Air-broadened halfwidths have been evaluated from the nitrogen and oxygen results via the formula

$$\gamma_{air} = 0.79\ \gamma_{N_2} + 0.21\ \gamma_{O_2} .$$

The results agree with the air-broadened measurements[3] to better than 5%.

1. P.W.Anderson, Phys.Rev.76, 647 (1949); 80, 511 (1950).
2. R.W.Davies, Phys.Rev.A12, 927 (1975).
3. C.Meunier, P.Marche, and A.Barbe, J.Mol.Spectrosc.95, 271 (1982).
4. J.Margolis, J.Quant.Spectrosc.Radiat.Transfer29, 539 (1983).

This work was supported by the Air Force Office of Scientific Research through AFGL task 2310G1.

Address of Gamache: The Center for Atmospheric Research, University of Lowell Research Foundation, 450 Aiken Street, Lowell, MA 01854.
Address of Davies: GTE/Sylvania, 40 Sylvan Road, Waltham, MA 02154.
Address of Rothman: Optical Physics Division, Air Force Geophysics Laboratory, Hanscom AFB, Bedford, MA 01731.

Time required 10 minutes
Session in which paper is recommended for presentation is 5, High Resolution IR and Theory.

A4.

THEORETICAL N_2-, O_2-, AND AIR-BROADENED HALFWIDTHS OF $^{16}O_3$ CALCULATED BY QUANTUM FOURIER TRANSFORM THEORY WITH REALISTIC COLLISION DYNAMICS.

R.R.GAMACHE, UNIVERSITY OF LOWELL
R.W.DAVIES, GTE/SYLVANIA LABORATORY
L.S.ROTHMAN, AIR FORCE GEOPHYSICS LABORATORY

DR. ROBERT GAMACHE
THE CENTER FOR ATMOSPHERIC RESEARCH
UNIVERSITY OF LOWELL RESEARCH FOUNDATION
450 AIKEN STREET,LOWELL,MA 01854 USA

We have evaluated collision broadened halfwidths of ozone with nitrogen and oxygen as the perturbing gases. Calculations using conventional Anderson theory[1] or quantum Fourier transform theory[2] are shown to be some 25 to 35% too low when compared to the experimental measurements[3,4]. Several improvements to the theory have been tested including explicit velocity integration, cutoff free theory (linked cluster theorem), and non-linear trajectories. We show that it is most important to consider more realistic collision dynamics in the calculations. The final calculations employ the the QFT method with realistic collision dynamics and the resulting halfwidths are in good agreement with the measurements (within 10%).

Air-broadened halfwidths have been evaluated from the nitrogen and oxygen results via the formula

$$\gamma_{air} = 0.79\ \gamma_{N_2} + 0.21\ \gamma_{O_2} .$$

The results agree with the air-broadened measurements[3] to better than 5%.

1. P.W.Anderson, Phys.Rev.76, 647 (1949); 80, 511 (1950).
2. R.W.Davies, Phys.Rev.A12, 927 (1975).
3. C.Meunier, P.Marche, and A.Barbe, J.Mol.Spectrosc.95, 271 (1982).
4. J.Margolis, J.Quant.Spectrosc.Radiat.Transfer29, 539 (1983).

A P P E N D I X B

Publications made under contract

B1. L. S. Rothman, A. Goldman, J. R. Gillis, R. R. Gamache, H. M. Picket, R. L. Poynter, N. Husson and A. Chedin, "AFGL Trace Gas Compilation: 1982 Version," Appl. Opt. 22, 1616-1627 (1983).

B2. L. S. Rothman, R. R. Gamache, A. Barbe, A. Goldman, J. R. Gillis, L. R. Brown, R. A. Toth, J.-M. Flaud and C. Camy-Peyret, "AFGL Atmospheric Absorption Line Parameters Compilation: 1982 Edition," Appl. Opt. 22, 2247-2256 (1983).

B3. R. R. Gamache and R. W. Davies, "Theoretical Calculations of N_2-Broadened Halfwidths of H_2O Using Quantum Fourier Transform Theory," Appl. Opt. 22, 4013-4019 (1983).

B4. R. R. Gamache, R. W. Davies and L. S. Rothman, "Theoretical N_2-, O_2-, and Air-Broadened Halfwidths of Ozone Calculated by Quantum Fourier Transform Theory with Realistic Collision Dynamics," Proceedings of the Quadrennial Ozone Symposium, Sept. 1984, Ed. by C. S. Zerefor and A. Ghayi, D. Reidel Publishing Co., Dordrecht (1985).

B5. R. R. Gamache and R. W. Davies, "Theoretical N_2-, O_2- and Air-Broadened Halfwidths of $^{16}O_3$ Calculated by Quantum Fourier Transform Theory with Realistic Collision Dynamics," J. Mol. Spectrosc. 109, 283-299 (1985).

B6. R. R. Gamache and L. S. Rothman, "Theoretical N_2-Broadened Halfwidths of $^{16}O_3$," Appl. Opt. 24, 1651-1656 (1985).

Reprinted from Applied Optics, Vol. 22, page 1616, June 1, 1983

B1.

AFGL trace gas compilation: 1982 version

L. S. Rothman, A. Goldman, J. R. Gillis, R. R. Gamache, H. M. Pickett,
R. L. Poynter, N. Husson, and A. Chedin

The new edition of the AFGL trace gas compilation is described. The latest version provides the necessary parameters for the computation of absorption or emission spectra of major bands of twenty-one gases in the region from 0 to 10,000 cm^{-1}. Emphasis on this edition has been on the addition of numerous millimeter and submillimeter transitions, the inclusion of bands of significance in upper atmospheric processes, and strong IR bands of trace constituents likely to be used for remote detection. The sources for the additions and modifications of the absorption parameters are summarized.

I. Introduction

Two years have elapsed since the second edition of the AFGL Trace Gas Compilation.[1] This compilation is a data bank of molecular absorption parameters appropriate to a broad spectrum of applications including calculation of high-resolution transmission and emission in planetary atmospheres, comparison with laboratory absorption cell measurements, and remote sensing and retrieval of profiles in the atmosphere. The Trace Gas Compilation is an extension to minor terrestrial infrared active atmospheric absorbers of the main AFGL Atmospheric Absorption Line Parameters Compilation[2] that contains analogous data for the seven most significant atmospheric absorbers. As with the previous edition,[1] several new molecular species have been added as well as additional bands and updates of the existing species. The major efforts incorporated into this new version include pure rotational transitions,[3] trace absorbers significant in the far infrared, and sequence bands of significance in upper atmospheric photochemistry. The new edition now encompasses twenty-one molecules summarized in Table I. The parameters and format of the compilation remain as before, i.e., each transition being cataloged in terms of the resonant frequency in vacuum cm^{-1}, the line intensity in cm^{-1}/molecule cm^{-2} at 296 K, the air-broadened halfwidth (HWHM) in cm^{-1}/atm, the lower-state energy in cm^{-1}, the quantum identifications (vibrational, rotational, electronic level, hyperfine, and splitting designation if necessary to uniquely specify the transition), and the entry date, isotope, and molecule codes. Representative examples of the card image format of transitions are shown in Table II.

The data presently available on the compilation (edition of Sept. 1982) are summarized in Table III. The discussion in Sec. II outlines the additions and modifications that have been made for this latest edition. Primary sources are given for the new or modified parameters on the compilation, and it is requested that these be referenced when the data are used.

II. Discussion of New or Updated Data

The ground $^2\Pi$ state of nitric oxide (NO) pure rotation data from Ref. 3 have replaced the previous microwave transitions on the atlas. The molecular constants for NO were determined by fitting the spectrum of NO to the fine structure Hamiltonian of Amiot *et al.*[4] along with the hyperfine Hamiltonian of Meerts.[5] The observed radio frequency lines used in the fit are from Ref. 6, and the observed millimeter lines used in the fit are from Jet Propulsion Laboratory measurements[3] by Pickett and Cohen. The accuracy of the line positions is generally better than 0.0005 cm^{-1}, and the line intensities are accurate to ~1%. The self-broadened halfwidths of Abels and Shaw[7] have been added to the data. Because nitrogen has nuclear spin = 1, the data contain quantum numbers describing the hyperfine interaction. To specify these transitions, a branch letter (P,Q,R) was chosen to indicate the change in nuclear spin quantum numbers along with the nuclear spin F'' of the lower state. These appear before the

L. S. Rothman is with U.S. Air Force Geophysics Laboratory, Optical Physics Division, Hanscom Air Force Base, Massachusetts 01731; A. Goldman and J. R. Gillis are with University of Denver, Physics Department, Denver, Colorado 80208; R. R. Gamache is with University of Lowell, Center for Atmospheric Research, Lowell, Massachusetts 01854; H. M. Pickett and R. L. Poynter are with California Institute of Technology, Jet Propulsion Laboratory, Pasadena, California 91109; N. Husson and A. Chedin are with Ecole Polytechnique, Laboratoire de Météorologie Dynamique, 91128 Palaiseau, France.
Received 26 January 1983.

Table I. Natural Isotopic Abundances of Compilation Constituents

Molecule	Isotope	Relative Natural Abundance	Molecule	Isotope	Relative Natural Abundance
NO (8)	46	0.99390	OCS (19)	622	0.93719
	56	0.00369		624	0.04163
	48	0.00203		632	0.01052
				822	0.00192
SO_2 (9)	626	0.94543			
	646	0.04200	H_2CO(20)	126	0.98622
				136	0.01107
NO_2(10)	646	0.99150		128	0.00202
NH_3(11)	4111	0.99585	HOCl(21)	165	0.75337
	5111	0.00370		167	0.24407
HNO_3(12)	146	0.98897	N_2 (22)	44	0.99261
OH (13)	61	0.99744	HCN (23)	124	0.98509
	81	0.00204		134	0.01106
	62	0.00015		125	0.00366
HF (14)	19	0.99985	CH_3Cl(24)	215	0.74658
				217	0.24187
HCl (15)	15	0.75519			
	17	0.24466	H_2O_2(25)	1661	0.99489
HBr (16)	19	0.50532	C_2H_2(26)	1221	0.97763
	11	0.49452			
			C_2H_6(27)	1221	0.97704
HI (17)	17	0.99985			
			PH_3 (28)	1111	0.99955
ClO (18)	56	0.75438			
	76	0.24411			

rotational branch and J'' quantum number in each line when hyperfine effects are present in a level [see Table II(c)].

On this edition of the atlas, bands of both nitric oxide and the hydroxyl radical (see below) have been added that are expected to be seen in emission in the upper atmosphere in nonlocal thermodynamic equilibrium conditions. The intensities have been calculated for equilibrium distribution at the 296 K standard; as a result, some intensities appear with very small exponents prior to scaling by subsequent upper atmospheric emission codes. A word of caution is thus in order for users of the compilations with computers incorporating small bit capacity/word—the intensity field should perhaps be read in a F6.3,1X,I3 format rather than the usual E10.3 and a decision made on the size of the exponent (I3).

The $X^2\Pi \leftarrow X^2\Pi \Delta v = 1$ sequence bands from (1–0) through (5–4) and the $\Delta v = 2$ series from (2–0) through (6–4) of the principal isotope of nitric oxide have been calculated by Gillis and Goldman.[8] Hamiltonian constants are from Refs. 4, 9, and 10. In addition, the fundamental bands of $^{15}N^{16}O$ and $^{14}N^{18}O$ have been added to the compilation. Hamiltonian constants for the isotopic bands are from Refs. 11 and 4, respectively. The eigenvectors were used to compute the intensities, and all bands involving $v' \leq 2$ include Λ-doubling. The intensity of the fundamental of the principal isotope is based on the high-resolution measurements of Mandin *et al.*[12] Intensities for other $^{14}N^{16}O$ bands were formed using Billingsley's Einstein A coefficients[13] scaled so that his (1–0) band Einstein A coefficient yields the intensity derived from Ref. 12. This scaling should be valid since Green *et al.*[14] show that ratios of Billingsley's band Einstein A coefficients[13] ending in the same upper state agree with experimental observations for the bands of interest, with the exception of the (2–0) band, whose intensity has been taken from Ref. 15. Intensities for the isotopic bands were derived by multiplying the principal isotope fundamental by the abundance ratios of Table I. The halfwidths used previously on the compilation were assumed for all bands.[7]

Table II. Examples of Line Format on Compilation

A) General Format

F[a]	I[b]	N[c]	E"[d]	Transition Quantum Designation				D[e]	A[f]	M[g]
				Vibrational Assignment		Electronic Rotational Hyperfine Splitting				
				V'	V"					
F10.4-F10.6	E10.3	F5.3	F10.3	A8	A8	A9	A10	I2	I4	I2

B) Coalescing Rotational Multiplets (Example for HNO_3)

Four parent lines (only K_a' and K_a'' differ)

F	I	N	E"	Vib Assignment	J'	K_a'	K_c'	J"	K_a''	K_c''	D	A	M
17.753332	6.494E-23	.130	292.087	ROT	29	13	16	28	14	15	382	146	12
17.753332	3.852E-22	.130	292.087	ROT	29	14	16	28	14	15	382	146	12
17.753332	6.494E-23	.130	292.087	ROT	29	14	16	28	13	15	382	146	12
17.753332	3.852E-22	.130	292.087	ROT	29	13	16	28	13	15	382	146	12
Resulting line from coalescing													
17.753332	9.003E-21	.130	292.087	ROT	29		16	28		15	382	146	12

C) Hyperfine Transition Designation (Example for ClO)

F	I	N	E"	Vib Assignment	ET[h]	$B^iP''B^jJ''S^k$	D	A	M
34.046537	9.720E-25	.085	770.941	0	0	1/2-1/2 Q20R 26.5	382	56	18

a. line frequency, cm^{-1}
b. line intensity, cm^{-1}/molec cm^{-2}
c. half-width at half maximum, cm^{-1}/atm
d. lower state energy, cm^{-1}
e. AFGL date code
f. AFGL isotope code
g. AFGL molecule code
h. electronic transition
i. hyperfine branch letter
j. rotational branch letter
k. symmetry label (Λ-doubling)

For this edition, the combination band of **sulfur dioxide** (SO_2) was updated, and the hot band of the main isotope and combination band of the second most abundant isotope in the 4-μm region were added. The line positions and intensities for these bands were calculated by Pine and Dang-Nhu.[16] Their line positions have a precision of ~0.0005 cm^{-1}, and the accuracy of the intensities is of the order of 1%.

Recent diode laser measurements[17] of intensities of the ν_2 band of **nitrogen dioxide** (NO_2) led to an improved value of the total band intensity. The line intensities of this band were normalized in the latest atlas to the calculation of Devi *et al.*[17]

Pure rotation and rotation–inversion bands in the far infrared for **ammonia** (NH_3) were added to the compilation.

The pure rotation transitions in the ground state of $^{14}NH_3$ and $^{15}NH_3$ and the rotation–inversion transitions in the ν_2 level of $^{14}NH_3$ were completely reinvestigated. The absolute intensity formulation was reviewed in the case of rotation and rotation–inversion lines of molecules with C_{3v} symmetry. A reliable set of spectroscopic parameters was computed for more than 2000 lines between 0.2 and 0.5 cm^{-1} in the microwave region[3] and beyond 0.5 cm^{-1} from a subset of the GEISA catalog[18] that met the intensity cutoff criterion (see Appendix A). The details concerning the far-infrared study are given in Ref. 19.

Recently, Urban *et al.*[20] remeasured the far-infrared spectrum of $^{14}NH_3$ with 0.010-cm^{-1} resolution in the 35–278-cm^{-1} range using a Fourier transform spectrometer. They were able to assign the ground-state

inversion–rotation transitions of $^{14}NH_3$ up to $J'' = 13$ and the lines of the inversion–rotation transitions in the ν_2 excited state up to $J'' = 11$. We used their data up to $J'' = 13$ and $J'' = 11$ in the ground and ν_2 states, respectively, to improve the line positions given in Ref. 19.

In the region from 8 to 32 μm a systematic study up to $J'' = 20$ of the line parameters of the ν_2 band of $^{14}NH_3$ and $^{15}NH_3$ and the $2\nu_2$–ν_2 band of $^{14}NH_3$ was undertaken.[21] (The ν_2 parameters of the main isotope, however, were not altered from the 1980 version).[1] The recent results of Urban *et al.*,[22] combined with those of

Table III. Absorption Bands Present on Compilation

Molecule/ isotope	Band v'	Band v''	Origin (cm^{-1})	Range (cm^{-1})	No. of lines	$\sum S_i$ [a]
NO						
46	0	0		0–99	599	3.441
46	5	4	1763.8766	1463–2020	416	7.7E-33
46	4	3	1791.8403	1488–2051	416	3.8E-29
46	3	2	1819.8392	1514–2081	416	2.0E-25
48	1	0	1827.2844	1601–2039	679	1.054
56	1	0	1842.9177	1609–2061	699	1.917
46	2	1	1847.8808	1540–2112	831	0.108
46	1	0	1875.9711	1566–2142	833	500.284
46	6	4	3499.8115	3177–3733	416	3.3E-34
46	5	3	3555.7169	3231–3791	416	1.3E-30
46	4	2	3611.6795	3285–3849	416	5.4E-27
46	3	1	3667.7198	3339–3908	416	1.4E-23
46	2	0	3723.8526	3392–3967	832	8.079
SO_2						
626	000	000		0–175	4132	238.984
626	010	000	517.75	433–617	3326	389.914
626	100	000	1151.7135	1047–1262	5812	351.914
626	001	000	1362.0295	1316–1394	2075	3080.023
646	101	000	2475.8300	2463–2497	287	0.603
626	111	010	2492.4438	2463–2516	654	2.110
626	101	000	2499.8701	2463–2527	1883	39.542
NO_2						
646	010	000	749.6541	599–900	4594	52.989
646	001	000	1616.852	1550–1657	3276	6112.775
646	101	000	2906.0691	2833–2938	1586	257.910
NH_3						
4111	0000	0000		0–415	490	1773.197
4111	0100	0100		4–477	593	29.063
5111	0000	0000		0–408	377	6.563
4111	0200	0100	789.537	309–1244	655	23.462
5111	0100	0000	945.282[b]	637–1244	584	7.967
4111	0100	0000	949.878[b]	608–1266	721	2151.304
4111	0001	0000	1630.165	1263–2056	1523	410.065
4111	0200	0000	1739.425	1239–2154	613	4.168
HNO_3						
146	Pure rot.			0–43	4182	58.191
146	$2\nu_9$		896.4187	891–899	1079	189.975
146	ν_4		1324.9	1326–1336	24	2744.290
146	ν_2		1709.5676	1670–1750	7492	2014.242

Continued

Ref. 23 for the hot band, were used to improve the line positions. Further studies on these bands are in progress at the Laboratoire de Météorologie Dynamique and at the Jet Propulsion Laboratory[24] and will be incorporated in the compilations in the future.

The perpendicular ν_4 and the parallel $2\nu_2$ bands of ammonia from 5 to 8 μm were also added to the compilation. Theoretical details of these and the above bands can be found in Refs. 21 and 25.

For the compilation of the line strengths of ν_4 we adopted the value 4.10×10^{-18} cm^{-1}/molecule cm^{-2} at 296 K.[26] That value is ~10% lower than the experimental determination of McKean and Schatz[27]; one can remark that these authors indicated that their experimental errors were too high by 20%. Moreover, recent determinations[28] of a single line strength in the ν_4 band of NH_3 using laser techniques show that the value given in Ref. 27 should be too high because of the $2\nu_2$ band,

Table III. Continued

Molecule/ isotope	Band v'	Band v"	Origin (cm^{-1})	Range (cm^{-1})	No. of lines	$\sum S_i$ [a]
OH						
61	0	0		0-84	113	313.105
81	0	0		0-7	65	9.3E-26
62	0	0		0-2	90	1.1E-27
61	9	8	2237.0640	1287-2812	352	6.5E-68
61	8	7	2414.6890	1429-3048	352	3.8E-63
61	7	6	2585.4810	1560-3268	352	3.9E-58
61	6	5	2751.7015	1687-3482	352	6.7E-53
61	5	4	2915.2998	1810-3690	352	5.6E-47
61	4	3	3077.7771	1931-3895	352	2.5E-40
61	3	2	3240.3604	2052-4099	352	2.5E-33
61	2	1	3404.0410	2172-4303	352	4.1E-26
61	1	0	3569.6432	2293-4509	352	96.995
61	9	7	4651.7530	3503-5080	352	3.7E-63
61	8	6	5000.1700	3821-5483	352	1.0E-57
61	7	5	5337.1825	4123-5874	352	5.3E-52
61	6	4	5667.0013	4416-6253	352	5.6E-46
61	5	3	5993.0769	4703-6624	352	1.2E-39
61	4	2	6318.1375	4986-6991	352	4.7E-33
61	3	1	6644.4014	5268-7358	352	3.4E-26
61	2	0	6973.6842	5552-7726	352	36.183
61	9	6	7237.2340	5895-7582	352	2.7E-58
61	8	5	7751.8715	6384-8136	352	9.7E-53
61	7	4	8252.4823	6852-8674	352	7.0E-47
61	6	3	8744.7784	7308-9204	352	1.1E-40
61	5	2	9233.4373	7757-9730	352	3.2E-34
61	4	1	9722.1785	8202-9985	326	1.8E-27
61	3	0	10214.046	8648-9998	152	6.6E-22
HF						
19	0	0		41-589	15	5703.728
19	1	0	3961.4429	3381-4339	25	1547.412
19	2	0	7750.7949	7143-7993	22	49.615
HCl						
17	0	0		20-383	19	262.030
15	0	0		20-383	19	806.803
17	1	0	2883.8850	2486-3136	33	147.189
15	1	0	2885.9765	2459-3139	34	452.786
17	2	0	5663.9276	5303-5824	27	3.480
15	2	0	5667.9832	5271-5830	29	10.707
17	3	0	8340.9407	8124-8449	18	2.3E-22
15	3	0	8346.7771	8058-8455	21	7.1E-22

Continued

which overlaps the ν_4 and is included in the measurement of the total band strength. For this reason we did not choose the other experimentally determined value of band intensity 150 ± 5 cm^{-1}/atm cm at 299 K given in Ref. 29.

The $2\nu_2$ vibration–rotation parallel band is qualitatively similar to the ν_2 band (see Ref. 21 for theoretical details). The $S \rightarrow A$ and $A \rightarrow S$ subbands were studied as independent bands. Up to $J'' = 12$ the transition wave numbers of Urban *et al*[22] were used. Higher ro-

Table III. Continued

Molecule/ isotope	Band v'	Band v"	Origin (cm^{-1})	Range (cm^{-1})	No. of lines	$\sum S_i$ [a]
HBr						
11	0	0		16-339	21	234.581
19	0	0		16-339	21	239.782
11	1	1		64-130	5	6.7E-24
19	1	1		64-130	5	6.8E-24
11	1	0	2558.5308	2195-2773	36	72.324
19	1	0	2558.9105	2195-2773	36	73.916
11	2	0	5026.6005	4712-5160	28	0.755
19	2	0	5027.3408	4713-5161	28	0.771
11	3	0	7404.1928	7204-7495	20	1.9E-22
19	3	0	7405.2610	7205-7496	20	2.0E-22
11	4	0	9690.9914	9506-9758	18	9.5E-23
19	4	0	9692.3579	9507-9759	18	9.7E-23
HI						
1	0	0		12-286	23	106.693
1	1	1		49-137	8	1.8E-23
17	1	0	2229.5817	2117-2398	26	1.758
1	2	0	4379.2261	4117-4489	32	0.633
17	3	0	6448.0348	6176-6520	30	0.343
17	4	0	8434.7076	8190-8488	26	5.9E-22
ClO						
76	0	0		0-100	2607	18.673
56	0	0		0-100	2575	58.302
76	1	0	835.4802	763-883	402	11.861
56	1	0	842.5595	769-891	436	36.979
OCS						
622	00^00	00^00		0-40	99	8.034
624	00^00	00^00		0-40	99	0.365
632	00^00	00^00		0-38	93	9.4E-22
822	00^00	00^00		0-32	84	1.6E-22
622	10^00	00^00	858.9669	817-891	181	109.782
622	00^01	00^00	2062.2	2016-2089	181	7881.287
H_2CO						
126	000000	000000		0-100	610	310.095
136	000000	000000		0-73	563	5.633
128	000000	000000		0-48	367	0.694
126	000002	000000	2500	2743-2812	5	4.548
126	001100	000000	2655	2734-2735	1	0.589
126	001001	000000	2719.156	2700-2879	105	138.588
126	100000	000000	2782.457	2723-2843	424	828.793
126	000010	000000	2843.326	2703-2982	595	974.235
126	010100	000000	2905	2734-2999	28	38.133
126	010001	000000	3000.066	2896-2957	3	8.550

Continued

Table III. Continued

Molecule/ isotope	Band v'	Band v"	Origin (cm^{-1})	Range (cm^{-1})	No.of lines	$\sum S_i$ [a]
HOCl						
167	010	000	1238.1208	1179-1303	1240	291.656
165	010	000	1238.6242	1174-1311	1463	896.245
165	100	000	3609.4801	3400-3800	2675	304.351
167	100	000	3609.4851	3400-3800	2345	97.686
N_2						
44	1	0	2329.9168	2001-2620	117	6.4E-27
HCN						
124	00^00	00^00		2-132	47	1026.457
134	00^00	00^00		2-98	34	12.226
125	00^00	00^00		2-101	35	4.036
124	02^00	01^10	697.957	587-823	119	24.979
124	02^20	01^10	713.076	595-851	232	103.278
124	01^10	00^00	713.459	579-844	134	823.016
124	02^00	00^00	1426.535	1298-1537	81	139.947
124	00^01	00^00	3311.4772	3158-3422	90	951.594
CH_3Cl						
217	ν_1		2967.745	2965-2969	229	4.919
215	ν_1		2967.777	2965-2969	255	15.432
217	ν_4		3039.1761	2986-3162	1260	20.164
215	ν_4		3039.2864	2978-3173	1844	58.776
217	$3\nu_6$		3041.8005	2916-3128	1221	19.276
215	$3\nu_6$		3042.8736	2907-3157	1878	66.582
H_2O_2						
1661	000001	000000	1269.136	1186-1350	2389	1283.539
C_2H_2						
1221	0000011	0000000	730.3341	646-811	104	2979.844
1221	0101111	0000000	3281.9020	3151-3387	101	507.407
1221	0010000	0000000	3294.8406	3162-3398	101	429.348
C_2H_6						
1221	ν_9		821.737	720-933	4328	145.556
PH_3						
1111	0100	0000	992.1301	708-1211	972	330.604
1111	0001	0000	1118.3131	828-1411	1914	411.320

[a] Sum of the line intensities on the compilation in units of cm^{-1}/molecule-cm^{-2} ($\times 10^{20}$ except where exponent given) at 296K.

[b] In the case of sub-bands, for example NH_3, the band origins given in column 4 are the averages of the two.

tational transitions were calculated using the constants of Gille and Lee.[30] The ground-state energy levels are the same as those calculated for ν_4 (see Ref. 25).

Absolute line intensities have never been measured in the $2\nu_2$ band. An analysis of the atmosphere of Jupiter gives the value of 1.03 cm^{-1}/atm cm at 296 K for the $2\nu_2$ band, and this value has been adopted. This band intensity is not applied to the R-branch individual line intensities. Indeed, the relatively large intensity (for an overtone band) of the $2\nu_2$ R-branch is to be contrasted to the weak Q- and P-branches. This anomalous intensity pattern is a result of the Coriolis interaction between the $2\nu_2^S$ and the ν_4 rotational levels, since these two vibrations are only 29 cm^{-1} apart. As for the ν_4 band, we must take into account the influence of those interactions in the intensity expressions. Thus the line intensities we give must be considered at best as preliminary results, and more theoretical and analytical works remain to be done.

A halfwidth value of 0.075 cm^{-1}/atm at 296 K has been adopted for all updated NH_3 bands on this edition.

The rotational spectrum of **nitric acid** ($H^{14}N^{16}O_3$) was replaced on the atlas. The data are from the revised JPL catalog[3] and consist of lines generated by constants obtained by fitting to lines with $J \leq 40$ from the observed nitric acid data of Cazzoli and DeLucia.[31] The fit to the data was in terms of Kirchhoff's[32] formulation of the asymmetric rotor Hamiltonian of Kivelson and Wilson.[33] The accuracy of the rotational transitions is generally better than 0.0001 cm^{-1}. The dipole moment was taken from the measurements of Cox and Riveros,[34] and the partition function was determined by a sum over states to $J = 40$. The resulting line intensities are accurate to 3–5%. Because of the small separation between many groups of lines for this molecule, the spectra are very dense (7259 lines in the 0–41-cm^{-1} range). Many of the lines differ in frequency by an amount not observable in field and some laboratory experiments. To facilitate the use of the atlas we coalesced some groups of lines into single lines. The criterion for coalescing is: a pair or group of lines separated in frequency by $<1 \times 10^{-5}$ cm^{-1} has been coalesced if the lines have the same rotational quantum numbers, $J' = J''$ and $K_c' = K_c''$, with $K_a' \neq K_a''$, or $K_a' = K_a''$, with $K_c' \neq K_c''$. This occurs in the data for groups of 2, 3, and 4 lines. The resulting line is composed of the average of the frequencies and lower-state energies of the parent lines (these are usually the same as in the individual lines), and the line intensity is the sum of the individual line intensities of the parent lines. The quantum numbers that differed in the parent line (either K_a or K_c) are replaced by a blank, thus allowing lines resulting from coalescing to be identified in the atlas. An example of coalescing is given in Table II(b). The data were reduced to 4186 lines by coalescing.

A frequency-dependent intensity cutoff (see Appendix A) was applied to the data. The criteria used were 1.02×10^{-22} cm^{-1}/molecule cm^{-2} at 41.15 cm^{-1}. The cutoff procedure reduced the data to 4182 lines, to which a constant halfwidth of 0.13 cm^{-1}/atm as reported by Brockman *et al.*[35] was added.

Line parameters for the ν_2 band at 5.8 μm were recalculated using the Hamiltonian constants of Maki and Wells.[36] The set of rovibrational constants for the upper state have been fit to a standard deviation of 0.0012 cm^{-1}. The relative line intensities adopted are consistent with the results of Ref. 36; however, laboratory measurements[37] suggest that the absolute line intensities of this band in the present compilation may be too low by ~65%.

The 1982 atlas contains microwave data for the ground $^2\Pi_{3/2}$ and $^2\Pi_{1/2}$ states of the **hydroxyl radical** (OH). Data are for the main isotope OH and for the isotopic species OD and ^{18}OH. A complete description of the calculational method and microwave data is reported in Ref. 38. The procedure refitted the spectra of OH and OD to all the available data. For ^{18}OH most of the molecular parameters were estimated by isotopic scaling of the known ^{16}OH and OD parameters; the more critical molecular parameters of ^{18}OH were then fitted to observed transitions. The data account for 125 lines between 0 and 84 cm^{-1} for ^{16}OH, 235 lines between 0 and 4 cm^{-1} for ^{16}OD, and 113 lines between 0 and 10 cm^{-1} for ^{18}OH. As discussed in Ref. 1, a constant halfwidth of 0.083 cm^{-1}/atm was added to the data. All lines that have a strength $>10^{-30}$ cm^{-1}/molecule cm^{-2} or are laboratory measurements were retained. The reported strengths are accurate to a few percent. The accuracy of the line positions is J dependent and is better than 0.005 cm^{-1}.

Goldman[39] calculated the $X^2\Pi \leftarrow X^2\Pi \Delta v = 1$, 2, and 3 series of $^{16}O^1H$ through $v' = 9$. Hamiltonian constants are from Ref. 40. Intensities are calculated using the individual transition Einstein A coefficients of Mies.[41] For the (1–0), (2–1), (3–2), and (4–3) bands these individual Einstein A coefficients were scaled to give the band Einstein A coefficients reported by Agrawalla *et al.*[42] Mies' Einstein A coefficients[41] were used directly for all other bands. Further normalization will be required for the atmospheric OH bands based on the recent work of Werner *et al.*[43]

No modifications were made to the hydrogen halides for this edition.

Data from the JPL catalog[3] for the **chlorine monoxide** species $^{35}Cl^{16}O$ and $^{37}Cl^{16}O$ are now on the atlas. The data are the pure rotation band of the ground vibrational state for the $^2\Pi$ state of each chlorine monoxide species. The molecular constants were determined by fitting the observed spectrum to a fine-structure Hamiltonian and a hyperfine Hamiltonian including off-diagonal matrix elements. The observed spectrum below 6.7 cm^{-1} (200 GHz) was from the measurements of Kakar *et al.*[44]; the spectrum above 6.7 cm^{-1} was from measurements of Cohen and Pickett at the Jet Propulsion Laboratory.[3] The uncertainties for the transition frequencies of ^{35}ClO and ^{37}ClO are J-dependent and increase from 0.00001 cm^{-1} at $J = 20.5$ to 0.005 and 0.02 cm^{-1} for the isotopes, respectively, at the highest J listed. The partition function for both Ω

= 1/2 and 3/2 states was determined by a sum over states to $F = 86$. The line intensities are accurate to 1–2%.

Because both isotopic species of chlorine have nonzero nuclear spin, the data must contain the nuclear spin quantum numbers for the states, i.e., F',F''. These appear in the data as a branch letter for the transition (P,Q,R) given by $F' - F''$ and the nuclear spin quantum number of the lower state F''. They occur between the vibration state quantum numbers and the branch and lower state J for the rotational transition as shown in Table II(c). In each species, lines having the same frequency to within 1×10^{-5} cm^{-1}, the same rotational and nuclear quantum numbers but different symmetry, were coalesced into one line. For these lines the symmetry designation + or − was dropped, the frequency and lower-state energy averaged, and the line intensities added to produce the coalesced line. The frequency-dependent cutoff (Appendix A) was applied to the data; the criteria from the main isotope were 1.00×10^{-26} cm^{-1}/molecule cm^{-2} at 100 cm^{-1}.

The (1–0) fundamental chlorine monoxide is unchanged from the 1980 AFGL trace gas compilation,[1] except that the line positions were recalculated using the Hamiltonian constants determined from the high-resolution study of Maki *et al.*[45]

Carbonyl sulfide (OCS) pure rotation bands for the isotopic species: $^{16}O^{12}C^{32}S$, $^{16}O^{13}C^{32}S$, $^{16}O^{12}C^{34}S$, and $^{18}O^{12}C^{32}S$, were added to the atlas. The frequencies and lower-state energies were calculated using the standard linear triatomic molecule formulas (for example, see Ref. 46) including the hyperfine interaction. The molecular parameters were determined by a least-squares fit to the data sets of Dubrulle *et al.*[47] and Lovas.[48] The positional accuracy is J dependent and generally better than 0.005 cm^{-1}. The line intensities were calculated using the dipole moment reported by Reinartz and Dymanus[49] for $^{16}O^{12}C^{32}S$. For the less abundant species (624, 632, and 822 in the AFGL isotopic code) the dipole moment was assumed to be the same as the parent species. The resulting intensities are accurate to ~5%. The pressure-broadened halfwidth was set at a default value 0.07 cm^{-1}/atm as discussed in Ref. 44.

The new **formaldehyde** (H_2CO) data are for the pure rotation band. Three isotopic species are present in these data; $H_2{}^{12}C^{16}O$, the main isotope, and the minor species $H_2{}^{13}C^{16}O$ and $H_2{}^{12}C^{18}O$ (136 and 128). The experimental data are summarized in Ref. 3. Formaldehyde is an asymmetric rotor, thus the rotational energy and transitions are obtained by solving the basic rigid asymmetric rotor Hamiltonian plus terms representing centrifugal distortion. Here the Hamiltonian formulation of Kirchhoff[32] was used to evaluate the rotational and centrifugal distortion constants for H_2CO. For the isotopes 126 and 136, roughly 600 lines for each are calculated in the 0–100-cm^{-1} region; for 128 there are ~450 lines calculated from 0 to 50 cm^{-1}. The line positions are accurate to 0.005 cm^{-1}, with the accuracy increasing to 0.00005 cm^{-1} for very low J transitions. The line intensities are accurate to ≈2–5%; the dipole moment value used in the calculation was taken from the measurement of Kondo and Oka.[50]

The remaining molecular species identified as 21–28 in Table I are new to the trace gas compilation.

Two vibration–rotation bands of **hypochlorous acid** (HOCl) were considered for this atlas. The molecule is of interest in stratospheric monitoring because of its role as a chlorine sink in the atmosphere. The bending mode at 1238 cm^{-1} was investigated by Sams and Olson.[51] One should consult the latter reference for the estimated precision of the line positions. Unresolvable multiplets have been coalesced as described previously in the section for nitric acid. The intensities for this band were based on measurements performed at the National Bureau of Standards.[52]

The HOCl ν_1 band in the 2.8-μm region consists of both A and B type transitions. Both types of transition have approximately the same intensity. Strong B type transitions occur in the 3400–3800-cm^{-1} range, while A type transitions are strong only in the 3525–3650-cm^{-1} range. Line positions and intensities at 296 K were generated for the A and B type transitions of HOCl for both the 35 and 37 isotopes of Cl using the Hamiltonian constants of Wells *et al.*[53] The intensities for the ν_1 band of HOCl are unknown, and the following assumptions were made: (1) for isotopically pure species, the band intensities of $HO^{35}Cl$ and $HO^{37}Cl$ are approximately equal; (2) for a simple isotopic species, the sum of all the A type transition intensities equals the sum of all the B type transition intensities (as concluded in Ref. 53). The band intensity for both isotopic species at natural abundance (75.54% $HO^{35}Cl$ and 24.41% $HO^{37}Cl$) was arbitrarily set to ≈100 cm^{-1}/atm cm at 296 K. The final set of line parameters contains all transitions with $J' \leq 40$ and $K_a' \leq 16$ from both isotopic species in natural abundance with intensity >0.5% that of the strongest line. Because HOCl is a very nearly prolate symmetric rotor ($\kappa \approx -0.9987$), Watson's Hamiltonian[54] is not optimum for this molecule. In addition, K_a' must be limited to ~16 to prevent the calculation of unphysical values of energy levels.

An arbitrary halfwidth of 0.06 cm^{-1}/atm was assumed for both bands.

Nitrogen (N_2) is included on this edition of the compilation owing to its contribution to atmospheric absorption through electric quadrupole transitions.[55] The vibration–rotation band at 2330 cm^{-1} consists of O, Q, and S transitions. An estimated air-broadening coefficient of 0.06 cm^{-1}/atm at 296 K was assumed.[56] (The O_2 quadrupole lines have been included in the Main compilation.[2])

Hydrogen cyanide (HCN) has been detected in both the troposphere[57] and stratosphere.[58] This molecule is known to contribute in certain spectral regions to temperature profile retrieval.[59]

The pure rotation bands of $H^{13}C^{14}N$ and $H^{12}C^{15}N$ from the JPL catalog,[3] edition 2, have been added to the atlas. Because of the nonzero nuclear spin of ^{13}C, ^{14}N, and ^{15}N, the hyperfine interaction between the nuclear electronic quadrupole and spin rotation is included in the calculations. The molecular constants were de-

termined by exact matrix diagonalization of the Hamiltonian fitting to the observed lines reported by Pearson *et al.*[60] Line position accuracy is J dependent ranging from 1×10^{-6} cm^{-1} for the R 0 line of both isotopic species at ~3 cm^{-1}, to 0.015 cm^{-1} for the R 33 line of $H^{13}C^{14}N$ at 97 cm^{-1} and 0.003 cm^{-1} for the R 34 line of $H^{12}C^{15}N$ at 100 cm^{-1}. For the calculation of the line intensities the dipole moment was assumed to be the same as for the main isotope, 2.984 D.[61] The accuracy of the intensities is ≈5%. The first fourteen lines of data for $H^{13}C^{14}N$ arise from hyperfine splitting of three lines ($R0$, $R1$, and $R2$). Because the separation of the lines is so small (1×10^{-5} cm^{-1}), the fourteen lines have been coalesced back to the three parent lines. Three lines for the main isotope from the JPL catalog were included in the atlas. These lines contain the hyperfine splitting, and additional quantum numbers appear before the rotational quantum numbers. The branch letter corresponding to the change in nuclear spin quantum numbers (P,Q,R) and the nuclear spin F of the lower state was added to the data. These lines were retained because their separation is observable in many laboratory and some field experiments. The remaining lines of the principal isotope were calculated by A. Goldman.

The line parameters of the ν_2, $2\nu_2$, $2\nu_2$–ν_2, and ν_3 bands of HCN were also added to the compilation. Line positions for $2\nu_2$ were calculated using the Hamiltonian constants of Maki.[62] Intensities for $2\nu_2$ were calculated using rigid rotor line strengths and are normalized to the band intensity of Smith.[63] Line positions for ν_2 and $2\nu_2 - \nu_2$ were calculated using the Hamiltonian constants of Maki[62] and the band origin from Wang and Overend.[64] The total band intensity of $2\nu_2$–ν_2 was derived from scaling the ν_2 band intensity of Hyde and Hornig[65] by the 2-D harmonic oscillator matrix element and the Boltzmann factor. Line positions for ν_3 were calculated using the Hamiltonian constants of Maki.[62] The band intensity used is the average of available published values[63,66] for this band and is corrected for the ~7% contribution from the $\nu_3 + \nu_2 - \nu_2$ band. Line positions for all bands are accurate to ±0.005 cm^{-1}. A halfwidth of 0.06 cm^{-1}/atm was adopted for all bands; however, preliminary measurements by Smith[67] indicate a J dependence of the halfwidth and that an average value of 0.12 cm^{-1}/atm would be more appropriate.

The parameters for the ν_1, ν_4, and $3\nu_6$ bands of **methyl chloride** (CH_3Cl) around 3.3 μm were provided by Dang-Nhu.[68] This molecule is considered to be a natural source for chlorine in the upper atmosphere. The ν_1 band was studied at high resolution by Dang-Nhu *et al.*[69] and is a candidate for detection since the Q branches coincide with a relative gap in the methane spectrum. The ν_4 and $3\nu_6$ bands were also studied and analyzed using a high-resolution Fourier transform spectrometer.[70] References 69 and 70 should be consulted for an understanding of the reliability of the parameters of these complex perturbed bands. A constant value of 0.08 cm^{-1}/atm was assumed for the halfwidths.

Interest in **hydrogen peroxide** (H_2O_2) is related to its prominent role in atmospheric photochemistry. It is expected to be a sink species for odd hydrogen radicals. Although it has been proposed to be in higher concentration than OH, it has yet to be detected in the terrestrial atmosphere or extraterrestrially. The ν_6 band is the strongest fundamental, and the parameters on the compilation were provided by Hillman.[71] The line positions for this band were calculated with a general asymmetric rotor program with a fit to some 600 observations.[72] The ground state was constrained to the submillimeter analysis,[73] and the standard deviation of the fit is of the order of 0.005 cm^{-1}. Unresolvable multiplets were coalesced on the atlas. The intensities were calculated and are in general agreement with experiment.[72] A value of 0.10 cm^{-1}/atm was assumed for the Lorentz halfwidth.[71]

The linear molecule **acetylene** (C_2H_2) was identified in atmospheric absorption spectra.[74] Line parameters for the ν_5 band were calculated to an estimated accuracy of 0.001 cm^{-1} using the Hamiltonian constants of Hietanen and Kauppinen.[75] The band intensity is based on the value of Varanasi and Bangaru.[76]

In the 3-μm region the two strongest bands of acetylene were provided by Rinsland.[77] Details of the laboratory study that measured the line positions and intensities are given in Ref. 78. A constant halfwidth of 0.08 cm^{-1}/atm was applied to this molecule.

Interest in **ethane** (C_2H_6) was spurred by its detection in the atmospheres of the Jovian planets. There is also wide interest in this hydrocarbon for remote sensing in terrestrial tropospheric problems. In this edition of the atlas the ν_9 fundamental has been introduced. The transitions came from Daunt *et al.*,[79] with the relative intensities corrected to agree with recent experiments.[80] A halfwidth of 0.10 cm^{-1}/atm was assumed.

Finally, two bands of **phosphine** (PH_3), ν_2 and ν_4, were added to the atlas. This species is presently of interest in studies of planetary atmospheres. The parameters are described in Ref. 81, and a constant halfwidth of 0.075 cm^{-1}/atm was assumed.

We thank M. A. H. Smith, C. P. Rinsland, and J. C. Larsen, who, in conjunction with their efforts on behalf of NASA upper atmospheric programs, graciously provided much valuable data and suggestions. We also wish to thank M. Dang-Nhu of Orsay, J. J. Hillman of NASA, and A. G. Maki of NBS for providing data prior to publication.

Appendix A: Frequency-Dependent Intensity Cutoff Criterion

Intensity criteria were developed[82] for the main IR active constituents of the terrestrial atmosphere by assuming normal concentration of a species and an extreme atmospheric path. The path was taken to be the atmospheric path tangent to the earth's surface and extending from space to space. Lines having <10% absorption at the line center were omitted from the atlas. Although an absolute line intensity cutoff was

established, exceptions were immediately necessary (see Ref. 82). For trace gas constituents of the atmosphere, similar considerations are not possible because both the notion of concentration and tangent path seemed inappropriate.

As microwave data were added to the atlases it became obvious that the intensity cutoff criterion had to account for the effect of the radiation field[83] in the line intensity at low frequency. The frequency-dependent cutoff developed[1] to account for this is

$$I(\nu) = \frac{I_c'\nu}{\nu_c} \tanh\left(\frac{c_2\nu}{2T_0}\right), \tag{A1}$$

where I_c' is the standard intensity cutoff (main gases only) at the defined frequency ν_c (e.g., $I_c' = 3.0 \times 10^{-27}$ cm^{-1}/molecule cm^{-2} and $\nu_c = 2000$ cm^{-1} for H_2O), ν is the frequency of the line in vacuum wave numbers, c_2 is the second radiation constant (hc/k), and T_0 is the atlas temperature 296 K. The cutoff given by Eq. (A1) is well-defined for the main constituents of the atmosphere, where I_c' and ν_c are known. To use Eq. (A1) for the trace gases a static cutoff intensity I_c' and frequency ν_c must be defined. Care must be taken in defining I_c' for Eq. (A1) so that $I(\nu)$ goes smoothly into I_c' at the cutoff frequency.

The cutoff parameters are determined by using ν and I of the strongest intensity line of the principal isotope from the lines at high frequency in the data. The intensity cutoff is then chosen to be 2 orders of magnitude weaker than this line, and the frequency of this line is ν. Thus

$$I(\nu = \nu_c) = I_{\text{strongest line}} \times 10^{-2}, \tag{A2}$$

and one solves for the static cutoff via

$$I_c' = \frac{I(\nu = \nu_c)}{\tanh\left(\frac{c_2\nu_c}{2T_0}\right)}. \tag{A3}$$

Using the static intensity cutoff defined by Eq. (A3) along with ν_c gives the desired criterion for Eq. (A1) to be applied to the individual line intensities for the trace gases.

References

1. L. S. Rothman *et al.*, Appl. Opt. **20**, 1323 (1981).
2. L. S. Rothman, Appl. Opt. **20**, 791 (1981); for latest edition of the Main Compilation, see L. S. Rothman *et al.*, Appl. Opt. submitted for publication (1983).
3. R. L. Poynter and H. M. Pickett, "Submillimeter, Millimeter and Microwave Spectral Line Catalogue," JPL Publication 80-23, Revision 1 (Jet Propulsion Laboratory, California Institute of Technology, Pasadena, Calif., 1981), and Edition 1 of the same catalog.
4. C. Amiot, R. Bacis, and G. Guelachvili, Can. J. Phys. **56**, 251 (1978).
5. W. L. Meerts, Chem. Phys. **14**, 421 (1976).
6. W. L. Meerts and A. Dymanus, J. Mol. Spectrosc. **44**, 320 (1972).
7. L. L. Abels and J. H. Shaw, J. Mol. Spectrosc. **20**, 11 (1966).
8. J. R. Gillis and A. Goldman, Appl. Opt. **21**, 1161 (1982).
9. L. D. G. Young, A. T. Young, S. A. Clough, and F. X. Kneizys, J. Quant. Spectrosc. Radiat. Transfer **20**, 317 (1978).
10. C. Amiot and J. Verges, J. Mol. Spectrosc. **81**, 424 (1980).
11. C. Amiot and G. Guelachvili, J. Mol. Spectrosc. **76**, 86 (1979).
12. J.-Y. Mandin, C. Amiot, and G. Guelachvili, Ann. Phys. **5**, 91 (1980).
13. F. P. Billingsley II, J. Mol. Spectrosc. **61**, 53 (1976).
14. B. D. Green, G. E. Caledonia, and R. E. Murphy, J. Quant. Spectrosc. Radiat. Transfer **26**, 215 (1981).
15. G. Chandraiah and C. W. Cho, J. Mol. Spectrosc. **47**, 134 (1973).
16. A. S. Pine and M. Dang-Nhu, J. Mol. Spectrosc. **84**, 132 (1980).
17. V. M. Devi *et al.*, J. Mol. Spectrosc. **88**, 251 (1981).
18. N. Husson, A. Chedin, N. A. Scott, I. Cohen-Hallaleh, and A. Berroir, "La Banque de Données GEISA Mise à Jour 3," Laboratoire de Météorologie Dynamique Note 116 (1982).
19. N. Husson, A. Goldman, and G. Orton, J. Quant. Spectrosc. Radiat. Transfer **27**, 505 (1982).
20. S. Urban *et al.*, J. Mol. Spectrosc. **88**, 274 (1981).
21. N. Husson, A. Chedin, and N. A. Scott, "Paramètres Spectroscopiques de la Molécule d'Ammoniac dans la Région 32–7.5 μm (Bandes ν_2 et $2\nu_2-\nu_2$)," Laboratoire de Météorologie Dynamique Note 90 (1979).
22. S. Urban *et al.*, J. Mol. Spectrosc. **79**, 455 (1980).
23. J. J. Hillman, D. E. Jennings, and J. L. Faris, Appl. Opt. **18**, 1808 (1979); G. Baldacchini, S. Marchetti, and V. Montelatici, J. Mol. Spectrosc. **86**, 115 (1981); J. P. Sattler, L. S. Miller, and T. L. Worchesky, J. Mol. Spectrosc. **88**, 347 (1981).
24. R. L. Poynter and J. S. Margolis, Mol. Phys. **11**, 1 (1983).
25. N. Husson and A. Chedin, "Line Parameters of Infrared Absorption Bands of Ammonia in Connection with the Voyager IRIS Mission," Laboratorie de Météorologie Dynamique Note 115 (1982).
26. R. Hanel *et al.*, Science **204**, 972 (1979); **206**, 952 (1979).
27. D. C. McKean and P. N. Schatz, J. Chem. Phys. **24**, 316 (1956).
28. L. A. Farrow and R. E. Richton, J. Chem. Phys. **70**, 2166 (1979).
29. W. L. France and D. Williams, *J. Opt. Soc. Am.* **56**, 70 (1966).
30. J. C. Gille and T. H. Lee, J. Appl. Sci. **26**, 932 (1969).
31. G. Cazzoli and F. C. DeLucia, J. Mol. Spectrosc. **76**, 131 (1979).
32. W. H. Kirchhoff, J. Mol. Spectrosc. **41**, 333 (1972).
33. D. Kivelson and E. B. Wilson, Jr., J. Chem. Phys. **20**, 1575 (1952).
34. A. P. Cox and J. M. Riveros, J. Chem. Phys. **42**, 3106 (1965).
35. P. Brockman, C. H. Bair, and F. Allario, Appl. Opt. **17**, 91 (1978).
36. A. G. Maki and J. S. Wells, J. Mol. Spectrosc. **82**, 427 (1980).
37. A. Goldman, T. G. Kyle, and F. S. Bonomo, Appl. Opt. **10**, 65 (1971).
38. R. A. Beaudet and R. L. Poynter, J. Phys. Chem. Ref. Data **7**, 311 (1978).
39. A. Goldman, Appl. Opt. **21**, 2100 (1982).
40. J. A. Coxon, Can. J. Phys. **58**, 933 (1980); J. A. Coxon and S. C. Foster, Can. J. Phys. **60**, 41 (1982).
41. F. H. Mies, J. Mol. Spectrosc. **53**, 150 (1974).
42. B. S. Agrawalla, A. S. Manocha, and D. W. Setser, J. Phys. Chem. **85**, 2873 (1981).
43. H. J. Werner, P. Rosmus, and E. A. Reinsch, "MCSCF, MCSCF-SCEP, and SCEP-CEPA Calculations of Infrared Transition Rates for the Electronic Ground States of OH, OH^- and OH^+," J. Chem. Phys. (1982), submitted for publication.
44. R. K. Kakar, E. A. Cohen, and M. Geller, J. Mol. Spectrosc. **70**, 243 (1978).
45. A. G. Maki, F. J. Lovas, and W. B. Olson, J. Mol. Spectrosc. **92**, 410 (1982).
46. C. H. Townes and A. L. Schawlow, *Microwave Spectroscopy* (McGraw-Hill, New York, 1955).
47. A. Dubrulle, J. Demaison, J. Burie, and D. Boucher, Z. Naturforsch. Teil A **35**, 471 (1980).
48. F. J. Lovas, J. Phys. Chem. Ref. Data **7**, 1445 (1978).

49. J. M. L. J. Reinartz and A. Dymanus, Chem. Phys. Lett. **24**, 346 (1974).
50. K. Kondo and T. Oka, J. Phys. Soc. Jpn. **15**, 307 (1960).
51. R. L. Sams and W. B. Olson, J. Mol. Spectrosc. **84**, 113 (1980).
52. R. L. Sams and A. G. Maki, NBS; private communication.
53. J. S. Wells, R. L. Sams, and W. J. Lafferty, J. Mol. Spectrosc. **77**, 349 (1979).
54. J. K. G. Watson, Mol. Phys. **15**, 479 (1968).
55. A. Goldman, J. Reid, and L. S. Rothman, Geophys. Res. Lett. **8**, 77 (1981).
56. C. Camy-Peyret, J.-M. Flaud, L. Delbouille, G. Roland, J. W. Brault, and L. Testerman, J. Phys. Lett. **42**, 279 (1981).
57. C. P. Rinsland, M. A. H. Smith, P. L. Rinsland, A. Goldman, J. W. Brault, and G. M. Stokes, J. Geophys. Res. **87**, 11119 (1982).
58. M. T. Coffey, W. G. Mankin, and R. J. Cicerone, Science **214**, 333 (1981).
59. M. T. Coffey and A. Goldman, Appl. Opt. **20**, 3480 (1981).
60. E. F. Pearson, R. A. Creswell, M. Winnewisser, and G. Winnewisser, Z. Naturforsch. Teil A **31**, 1394 (1976).
61. G. Tomasevich, Thesis, Harvard U. (1970).
62. A. G. Maki, J. Mol. Spectrosc. **58**, 308 (1975).
63. I. W. M. Smith, J. Chem. Soc. Faraday Trans. 2 **77**, 2357 (1981).
64. V. K. Wang and J. Overend, Spectrochim. Acta Part A **29**, 687 (1973).
65. G. E. Hyde and D. F. Hornig, J. Chem. Phys. **20**, 647 (1952).
66. J. H. Jaffe, "Refraction of Gases in the Infrared," in *Advances in Spectroscopy*, H. W. Thompson, Ed. (Interscience, New York, 1961), pp. 263–291; J. Finzi, J. H. S. Wang, and F. N. Mastrup, J. Appl. Phys. **48**, 2691 (1977); K. Kim and W. T. King, J. Chem. Phys. **71**, 1967 (1979).
67. M. A. H. Smith, NASA Langley; private communication.
68. M. Dang-Nhu, CNRS, Orsay; private communication.
69. M. Dang-Nhu, M. Morillon-Chapev, G. Graner, and G. Guelachvili, J. Quant. Spectrosc. Radiat. Transfer **26**, 515 (1981).
70. M. Dang-Nhu, M. Morillon-Chapey, G. Graner, and G. Guelachvili, Can. J. Phys. **60**, 1328 (1982).
71. J. J. Hillman, NASA Goddard; private communication.
72. J. J. Hillman, D. E. Jennings, W. B. Olson, and A. Goldman; private communication.
73. J. J. Hillman, J. Mol. Spectrosc. **95**, 236 (1982).
74. A. Goldman *et al.*, J. Geophys. Res. **86**, 12143 (1981).
75. J. Hietanen and J. Kauppinen, Mol. Phys. **42**, 411 (1981).
76. P. Varanasi and B. R. P. Bangaru, J. Quant. Spectrosc. Radiat. Transfer **14**, 839 (1974).
77. C. P. Rinsland, NASA Langley; private communication.
78. C. P. Rinsland, A. Baldacci, and K. N. Rao, Astrophys. J. **49**, 487 (1982).
79. S. J. Daunt *et al.*, J. Mol. Spectrosc. **86**, 327 (1981).
80. G. S. Orton, JPL, and D. E. Jennings, NASA Goddard; private communication.
81. A. Goldman, G. R. Cook, and F. S. Bonomo, J. Quant. Spectrosc. Radiat. Transfer **24**, 211 (1980); G. Tarrago, M. Dang-Nhu, and A. Goldman, J. Mol. Spectrosc. **88**, 311 (1981).
82. R. A. McClatchey *et al.*, "AFCRL Atmospheric Absorption Line Parameters Compilation," AFCRL-TR-0096 (1973).
83. S. A. Clough, F. X. Kneizys, L. S. Rothman, and W. O. Gallery, Proc. Soc. Photo. Opt. Instrum. Eng. **277**, 152 (1981).

Reprinted from Applied Optics, Vol. 22, page 2247, August 1, 1983

B2.

AFGL atmospheric absorption line parameters compilation: 1982 edition

L. S. Rothman, R. R. Gamache, A. Barbe, A. Goldman, J. R. Gillis, L. R. Brown, R. A. Toth, J.-M. Flaud, and C. Camy-Peyret

The latest edition of the AFGL atmospheric absorption line parameters compilation for the seven most active infrared terrestrial absorbers is described. Major modifications to the atlas for this edition include updating of water-vapor parameters from 0 to 4300 cm^{-1}, improvements to line positions for carbon dioxide, substantial modifications to the ozone bands in the middle to far infrared, and improvements to the 7- and 2.3-μm bands of methane. The atlas now contains ~181,000 rotation and vibration–rotation transitions between 0 and 17,900 cm^{-1}. The sources of the absorption parameters are summarized.

I. Introduction

A new edition of the AFGL atmospheric absorption line parameters compilation was submitted for public distribution in Oct. 1982. This edition supersedes the last version of Sept. 1980.[1] The atmospheric absorption line parameters compilation, or *main* tape, provides the basic absorption parameters of the seven most active infrared molecular absorbers of significance in terrestrial atmospheric transmission and radiance studies. There is also a similar compilation of data for trace and pollutant molecular species.[2] These data bases are distributed in the form of magnetic tapes by the National Climatic Center of NOAA, Digital Product Section, Federal Building, Asheville, N.C. 28801. The main compilation presently covers the spectral range from 0 to 17,900 cm^{-1}, with an attempt to include at least all transitions contributing more than 10% absorption over a terrestrial atmospheric path defined from space to space tangent to the surface of the earth. A representative example of the card image format of the transitions is shown in Fig. 1. The previous data bank has been utilized in a wide range of applications such as spectroscopic detection of trace or weakly absorbing features in the atmosphere,[3] atmospheric modeling efforts,[4] laser transmission studies,[5] and general studies of remote sensing of atmospheric characteristics[6] and molecular spectroscopic theory.[7]

The salient achievements of this new edition have been the updating of parameters for the isotopic variants of water vapor in the region from 0 to 4300 cm^{-1}, the improvement of line positions of carbon dioxide, substantial modifications to the ozone bands in the middle to far infrared, and improvements to the 7-μm bands and addition to the 2.3-μm combination bands of methane. All modifications and additions to the compilation are described molecule by molecule in Sec. II.

II. New or Modified Data

The ground-state pure rotation band of the normal isotope of water (H_2O) has been recalculated and has replaced the earlier data on the atlas. Watson-type constants[8] for the band were determined by a fit to fifteen microwave lines[9] and more than 200 infrared lines.[10] The constants yield eigenvalues, which were used to calculate line positions, and wave functions, which were used to evaluate line intensities. The resulting line intensities are accurate to ~15%. The line positions were compared with line positions generated using energy levels of Flaud *et al.*[10] The confidence in the line positions of this band can be estimated from the following three criteria used to enter the line positions into the compilation: (1) all microwave observations by DeLucia *et al.*[9] were used in preference to the calculations and were written in F10.6 format; (2) calculated lines were written in F10.5 format; and (3) lines

L. S. Rothman is with U.S. Air Force Geophysics Laboratory, Optical Physics Division, Hanscom Air Force Base, Massachusetts 01731; R. R. Gamache is with University of Lowell, Center for Atmospheric Research, Lowell, Massachusetts 01854; A. Barbe is with Université de Reims, Laboratoire de Physique Moléculaire 51062-Reims, France; A. Goldman and J. R. Gillis are with University of Denver, Physics Department, Denver, Colorado 80208; L. R. Brown and R. A. Toth are with California Institute of Technology, Jet Propulsion Laboratory, Pasadena, California 91109; and J.-M. Flaud and C. Camy-Peyret are with Laboratoire de Physique Moléculaire et d'Optique Atmosphérique, Campus d'Orsay, 91405-Orsay, France.

Received 24 March 1983.

F[a]	I[b]	H[c]	E"[d]	Transition Quantum Designation (Rotational, Vibrational, Electronic, Splitting)	D[e]	A[f]	M[g]
F10.3-F10.6	E10.3	F5.4	F10.3	Format: species dependent	I3	I4	I3

Fig. 1. Example of line format on compilation: *a*, Resonant line transition in vacuum cm^{-1}; *b*, Line intensity in cm^{-1}/molecule cm^{-2} at 296 K; *c*, Air-broadened halfwidth (HWHM) in cm^{-1}/atm at 296 K; *d*, Lower-state energy in cm^{-1}; *e*, AFGL date code; *f*, Isotopic variant code; *g*, Molecular species code.

Table I. Summary of New or Updated Water Bands for 1982 Compilation

BAND ORIGIN	ISO†	BAND V'	BAND V"	SUM OF LINE INTENSITIES§	RANGE (CM-1)	# LINES	JMAX	SMIN§	SMAX§
	161	0 0 0	0 0 0	5.268E-17	0-1648	1728	23	1.01 E-32	2.67 E-18
	171	0 0 0	0 0 0	1.943E-20	6- 906	622	17	1.00 E-26	9.83 E-22
	181	0 0 0	0 0 0	1.066E-19	6- 977	766	18	1.02 E-26	5.39 E-21
	171	0 1 0	0 1 0	7.921E-24	21- 449	117*	11	1.00 E-26	4.23 E-25
	181	0 1 0	0 1 0	4.632E-23	21- 559	202*	12	1.02 E-26	2.35 E-24
	161	0 2 0	0 2 0	1.016E-23	26- 503	129*	11	1.01 E-26	5.34 E-25
	161	1 0 0	1 0 0	5.977E-25	86- 302	27*	8	1.01 E-26	5.08 E-26
	161	0 0 1	0 0 1	3.072E-25	86- 292	19*	6	1.01 E-26	3.14 E-26
1515.163	181	0 3 0	0 2 0	5.135E-24	1271-1932	121*	9	1.03 E-26	1.66 E-25
1550.774	181	0 2 0	0 1 0	1.644E-23	1287-1960	187*	10	1.00 E-26	4.91 E-25
1553.853	171	0 2 0	0 1 0	2.464E-24	1343-1860	86*	8	1.04 E-26	8.80 E-26
1588.279	181	0 1 0	0 0 0	2.101E-20	1009-2220	852	16	1.02 E-26	5.85 E-22
1591.325	171	0 1 0	0 0 0	3.823E-21	1063-2156	668	15	1.00 E-26	1.07 E-22
1594.7498	161	0 1 0	0 0 0	1.038E-17	640-2822	1807	20	3.17 E-27	2.90 E-19
2153.288	181	0 0 1	0 1 0	2.267E-25	2066-2267	16*	5	1.01 E-26	2.08 E-26
2723.6799	162	1 0 0	0 0 0	6.338E-22	2332-3133	1333	17	1.01 E-27	9.75 E-24
2782.0117	162	0 2 0	0 0 0	8.468E-23	2486-3362	953	15	1.00 E-27	1.23 E-24
3072.046	161	0 3 0	0 1 0	7.303E-23	2813-3917	313	12	1.00 E-26	1.83 E-24
3139.053	181	0 2 0	0 0 0	1.325E-22	2806-4046	388	13	1.01 E-26	4.53 E-24
3144.978	171	0 2 0	0 0 0	2.409E-23	2887-3994	247	11	1.00 E-26	5.49 E-25
3632.961	181	1 1 0	0 1 0	7.920E-26	3624-3790	3*	4	1.51 E-26	3.53 E-26
3640.245	161	1 1 0	0 1 0	1.946E-22	3172-4145	365	13	1.00 E-26	1.25 E-23
3649.685	181	1 0 0	0 0 0	9.468E-22	3108-4194	553	14	1.00 E-26	7.77 E-23
3653.143	171	1 0 0	0 0 0	1.699E-22	3223-4127	387	13	1.02 E-26	9.37 E-24
3707.4667	162	0 0 1	0 0 0	1.416E-21	3236-4122	1651	17	1.01 E-27	1.75 E-23
3719.891	161	0 2 1	0 2 0	1.158E-24	3570-3869	49*	7	1.01 E-26	5.11 E-26
3722.189	181	0 1 1	0 1 0	5.356E-24	3525-3912	101*	9	1.01 E-26	1.93 E-25
3728.937	171	0 1 1	0 1 0	6.618E-25	3591-3858	34*	6	1.00 E-26	3.63 E-26
3736.522	181	0 1 1	0 1 0	2.923E-21	3203-4282	527	15	1.01 E-26	9.81 E-23
3741.567	181	0 0 1	0 0 0	1.393E-20	3160-4341	711	16	1.00 E-26	4.37 E-22
3748.318	171	0 0 1	0 0 0	2.516E-21	3227-4243	529	15	1.00 E-26	7.89 E-23
4099.9559	162	1 1 0	0 0 0	6.426E-23	3843-4497	860	15	1.00 E-27	9.36 E-25
4145.4734	162	0 3 0	0 0 0	3.504E-23	3679-4640	602	14	1.01 E-27	8.76 E-25

*NEW BAND FOR PRESENT COMPILATION.

† Isotope code: 161 is $H_2{}^{16}O$, 181 is $H_2{}^{18}O$, 162 is HDO, etc.

§ Units of $cm^{-1}/(molecule\text{-}cm^{-2})$ at 296K.

Table II. Bands of Carbon Dioxide on 1982 Compilation in Which Both Upper and Lower States Have Been Refit

Band Origin	Band* v'	Band* v"	Iso†
471.512	20003	11101	626
479.839	13302	12201	626
544.287	11102	10001	626
568.846	13302	04401	626
594.290	20002	11101	626
597.052	10002	01101	628
597.340	11102	02201	626
608.829	10012	01111	626
615.897	20003	11102	626
617.350	10002	01101	636
618.029	10002	01101	626
636.752	01111	00011	636
647.063	11102	10002	626
648.479	01101	00001	636
648.787	02201	01101	636
649.078	03301	02201	636
654.869	01111	00011	626
655.259	02211	01111	626
662.374	01101	00001	628
662.776	02201	01101	628
664.730	01101	00001	627
667.031	11101	10001	636
667.380	01101	00001	626
667.752	02201	01101	626
668.115	03301	02201	626
668.472	04401	03301	626
681.531	13301	12201	626
683.869	12201	11101	626
688.672	11101	10001	626
703.470	10001	01101	628
703.539	21101	20001	626
710.770	10011	01111	626
711.300	10001	01101	627
720.280	20001	11101	626
720.805	10001	01101	626
721.584	10001	01101	636
738.674	20002	11102	626
739.829	11101	02201	636
739.950	21101	12201	626
741.726	11101	02201	626
757.479	12201	03301	626
770.538	13301	04401	626
771.266	11101	10002	636
791.448	11101	10002	626
828.254	12201	11102	626
829.529	21101	20002	626
864.665	20001	11102	626
883.145	01111	11101	636
898.548	02211	12201	626
913.425	00011	10001	636
917.647	10011	20001	626
927.186	01111	11101	626
941.696	10012	20002	626
952.307	21101	20003	626
960.959	00011	10001	626
963.984	00011	10001	627
966.269	00011	10001	628
1017.659	00011	10002	636
1043.637	10011	20002	626
1063.735	00011	10002	626
1064.474	10012	20003	626
1071.542	01111	11102	626
1072.687	00011	10002	628
1259.426	10002	00001	628
1365.844	10001	00001	628
1376.030	10001	00001	627
1880.988	20003	01101	626
1905.433	13302	02201	626
1932.472	11102	00001	626
2003.767	20002	01101	626
2037.093	11101	00001	636
2076.856	11101	00001	626
2093.345	12201	01101	626
2107.125	13301	02201	626
2112.490	21101	10001	626
2129.756	20001	01101	626
2157.675	10012	10001	636
2165.544	21101	02201	626
2170.850	11112	11101	626
2180.701	20012	20001	626
2182.479	20013	20002	626
2205.297	10012	10001	628
2224.657	10012	10001	626
2248.362	01121	01111	636
2250.606	11111	11101	636
2260.051	02211	02201	636
2260.061	00021	00011	636
2261.909	10012	10002	636
2262.849	10011	10001	636
2265.972	00011	00001	638
2271.760	01111	01101	636
2283.488	00011	00001	636
2288.390	13311	13301	626
2290.681	13312	13302	626
2299.214	04411	04401	626
2299.240	02221	02211	626
2301.053	12211	12201	626
2301.800	01111	01101	828
2301.909	10021	10011	626
2302.372	10022	10012	626
2302.523	20011	20001	626
2305.256	20013	20003	626
2306.691	20012	20002	626
2307.383	02211	02201	628
2309.290	10011	10001	628
2311.668	03311	03301	626
2311.701	01121	01111	626
2311.715	10012	10002	628
2313.772	11111	11101	626
2314.049	00011	00001	828

CONTINUED

that differed by more than ± 0.005 cm^{-1} from positions generated using combination differences of vibration–rotation levels[10] were replaced by these latter estimates and written in F10.4 format.

In a comparison of the 1980 data[1] for the ν_2 band of water in the 1500–2500-cm^{-1} region with the long path field measurements of Haught and Dowling[11] and Hanley *et al.*[12] it was found that many of the lines of the 1980 ν_2 data were much too strong. Inspection showed that the lines that were overestimated exceeded the values in the 1978 atlas[13] and corresponded to weak lines in the band. This fact was pointed out by Benedict[14] who suggested that, in the 1980 ν_2 data, transitions with $\Delta K_a \geq 3$ were being inadequately represented

Table II. Continued

Band Origin	Band* v'	Band* v"	Iso†
2315.235	11112	11102	626
2319.738	01111	01101	628
2324.141	02211	02201	626
2324.183	00021	00011	626
2326.598	10011	10001	626
2327.433	10012	10002	626
2332.113	00011	00001	628
2336.633	01111	01101	626
2340.014	00011	00001	627
2349.143	00011	00001	626
2367.083	10011	10002	636
2415.708	10011	10002	628
2428.513	20011	20002	626
2429.375	10011	10002	626
2429.469	20012	20003	626
2458.158	11111	11102	626
2614.242	20002	00001	628
2618.637	21102	01101	628
2641.231	20002	00001	627
2757.183	20001	00001	628
3450.902	13312	03301	636
3460.466	21113	11102	636
3465.440	20013	10001	626
3473.712	12212	02201	636
3482.235	20013	10002	636
3482.833	21112	11101	636
3490.398	10012	00001	638
3497.495	30001	01101	636
3498.755	11112	01101	636
3500.675	21101	00001	626
3517.324	20012	10001	636
3525.205	10012	00001	828
3527.616	30014	20003	626
3527.737	10012	00001	636
3527.999	13312	03301	626
3550.719	30012	20001	626
3556.774	30013	20002	626
3566.070	10022	00011	626
3568.216	20013	10002	626
3571.141	10012	00001	628
3580.326	11112	01101	626
3587.546	10011	00001	638
3589.652	20012	10001	626
3612.842	10012	00001	626
3621.291	20011	10001	636
3621.558	20012	10002	636
3623.384	21112	11102	636
3625.165	21111	11101	636
3632.911	10011	00001	636
3638.065	10011	00001	828
3639.222	11111	01101	636
3641.568	12211	02201	636
3641.676	13311	03301	636
3667.548	10021	00011	826
3675.134	10011	00001	628
3676.709	30012	20002	626
3679.552	30013	20003	626
3692.428	20012	10002	626
3705.948	30011	20001	626
3711.474	20011	10001	626
3714.783	10011	00001	626
3723.249	11111	01101	626
3725.525	20011	10002	636
3726.647	12211	02201	626
3727.399	13311	03301	626
3799.487	30012	20003	626
3814.251	20011	10002	626
4005.946	00021	01101	626
4687.799	30014	10001	626
4748.062	20013	00001	636
4786.704	31113	11101	626
4790.575	30014	10002	626
4839.735	30013	10001	626
4853.625	20013	00001	626
4887.387	20012	00001	636
4931.089	31113	11102	626
4942.511	30013	10002	626
4946.823	31112	11101	626
4959.670	30012	10001	626
4977.837	20012	00001	626
4991.353	20011	00001	636
5013.781	21111	01101	636
5062.446	30012	10002	626
5099.659	20011	00001	626
5114.899	30011	10001	626
5168.600	01121	00001	636
5217.675	30011	10002	626
5247.834	10022	01101	626
5291.133	02221	01101	626
5315.714	01121	00001	626
5349.312	10021	01101	626
5584.394	00031	10001	626
5687.170	00031	10002	626
6075.984	30014	00001	626
6196.180	31113	01101	626
6227.920	30013	00001	626
6347.855	30012	00001	626
6356.299	31112	01101	626
6503.084	30011	00001	626
6745.114	01131	01101	636
6780.212	00031	00001	636
6860.435	03331	03301	626
6897.754	02231	02201	626
6905.769	10031	10001	626
6907.144	10032	10002	626
6935.136	01131	01101	626
6972.579	00031	00001	826
8192.552	10032	00001	626
8293.953	10031	00001	626

* The vibrational quantum identification is $v_1 v_2 \ell v_3 r$ (see Ref. 25)

† Isotope code: 626 is $^{12}C^{16}O_2$, 628 is $^{12}C^{16}O^{18}O$, etc.

in the least-squares fitting procedure. Subsequent work has shown this to be correct, and for the new atlas we have replaced the line intensities for transitions of this band with $\Delta K_a \geq 3$ with the corresponding 1978 values until further analysis can be performed on this problem.

The bands in the 6.3- and 2.7-μm regions and the pure rotation bands shown in Table I (except for HDO and the data discussed above) have been updated by incorporating data from Flaud *et al.*[15] All bands in Table I with an asterisk after the number of lines correspond to data previously absent from the atlas. In general the accuracy of the line positions is better than ± 0.005 cm^{-1}, and the line intensities are accurate to ~20% (with the weaker lines being somewhat less accurate). The combination and overtone bands are much more uncertain, however, and all the data show a deterioration of accuracy for high J lines.

Improvements were made for the ν_1, $2\nu_2$, ν_3, $\nu_1 + \nu_2$, and $3\nu_2$ bands of monodeuterated water. The data are from the work of Toth *et al.*[16] The line positions are accurate to ± 0.0004 cm^{-1} for all unblended lines and slightly blended lines of medium to strong intensity. The line intensities were calculated by the F-factor formalism and included the following corrections: centrifugal distortion, $\Delta\kappa$ effect, Coriolis-type resonance interactions between the states (100) and (020), and Fermi-type resonance interactions between the states (110) and (030). For lines for which the $\Delta\kappa$ effect is minimal and the resonant effects are minor contributions to the resultant line strengths, calculated lines are 5% or better, which usually represents the medium to strong lines. The accuracy of the weak lines are uncertain up to 20%. These data totally replace the previously existing corresponding data on the atlas.

The air-broadened halfwidths generated for the bands in Table I were from the calculations of Gamache and Davies.[17] For the $H_2{}^{17}O$ and $H_2{}^{18}O$ data, no separate calculations were performed for $J \geq 16$; the values for these lines were extrapolated from the $H_2{}^{16}O$ calculations.

Recent high-resolution measurements of several isotopic species of **carbon dioxide** (CO_2) have provided access to many ro-vibration levels not observed before. The high-temperature measurements of Esplin and Rothman[18] have determined high rotational levels, while the experiments of Bailly *et al.*[19] have reached high vibrational levels in the 4.3-μm region. These observations have been combined with new laser sequence bands observed by Siemsen *et al.*[20] and weak isotopic species bands observed in the long path measurements of Hoke and Shaw[21] and Baldacci *et al.*[22] Together with the high-resolution observations that went into the previous atlas, these new observations have produced a self-consistent set of energy levels which have led to improved line positions of interest in atmospheric problems. The least-squares procedure[23] has affected a majority of the 518 bands on the compilation. Table II presents the bands that have had both the upper- and lower-state molecular constants refit since the last atlas. The accuracy should be assessed in terms of the highest rotational levels reached for a particular energy level.[23] Extrapolation beyond these levels or to levels involved in weak transitions that have no experimental verification presents the problem of diverging series. Nevertheless, the new fit has provided accuracies of better than 0.001 cm^{-1} for most transitions emanating from vibrational term values <2500 cm^{-1} for the two principal isotopic species of carbon dioxide.

With the exception of several weak bands in the 3.6–3.8-μm region,[21,24] the intensities have not been updated for this edition and remain as calculated for the 1980 edition.[25] It is expected that this situation will be remedied in the near future as new intensity measurements become available.[26]

Several bands of the principal isotope of **ozone** (O_3) from the earlier atlases have been updated for this edition as well as the addition of three new bands: $2\nu_2 - \nu_2$, $\nu_2 + \nu_3$, and $\nu_1 + \nu_2$. The recalculated bands discussed below are the three fundamentals and the hot bands that existed in the 10-μm region. A summary of the updated and new bands is given in Table III.

Line positions and intensities for ν_2 and $2\nu_2 - \nu_2$ were generated as described in Ref. 27. The band intensity for the fundamental is 6.284×10^{-19} cm^{-1}/molecule cm^{-2} and for the hot band, 4.16×10^{-20} cm^{-1}/molecule cm^{-2}, based on the total band intensity of McCaa and Shaw.[28] The compilation includes all lines in this region within 4 orders of magnitude in intensity of the strongest line with J up to 68 and K_a up to 24 for ν_2, and 3 orders of magnitude of intensities with J up to 68 and K_a up to 20 for $2\nu_2 - \nu_2$. Line positions are accurate to better than 0.004 cm^{-1}, and the intensities are accurate to within 15%. Comparisons of synthetic spectra to observed atmospheric spectra[29] have demonstrated good agreement. The updating of this region extends the ozone band parameters to include the weak lines that have been interfering with the detection of the numerous trace species being searched for in this region.[30]

Line positions for the $^{16}O_3$ ν_1 and ν_3 Coriolis interacting bands have been calculated using the Watson Hamiltonian[8] with Coriolis coupling terms and Hamiltonian constants supplied from Barbe *et al.*[31] This has resulted in an improvement in the line positions of ν_3 and especially ν_1. The intensities were calculated with a dipole moment derivative ratio between the two bands as determined by Flaud *et al.*[32] and normalized to a total band intensity of 1.462×10^{-17} cm^{-1}/molecule cm^{-2}, achieved by multiplying the intensities of Ref. 32 by 1.113 as recommended by Secroun *et al.*[33] All lines with intensity $> 1 \times 10^{-5}$ of the strongest line and J up to 70 and K_a up to 25 are included in the compilation. The line positions in the updated data in this region are accurate to better than 0.004 cm^{-1}, and the majority of the line intensities have accuracies better than 10%. A further check for reliability was performed by comparing generated spectra to observed atmospheric spectra,[29] and good agreement was obtained.

Line positions for the hot bands in the 10-μm region have not been changed from the 1980 atlas values. For the line intensities, however, the overall intensity cor-

Table III. Summary of New or Updated Ozone Bands for 1982 Compilation

BAND ORIGIN	ISO	BAND V'	BAND V"	SUM OF LINES§ INTENSITIES	RANGE (CM-1)	# LINES	JMAX	SMIN§	SMAX§
698.343	666	0 2 0	0 1 0	4.164E-20	573- 865	4591•	67	9.36 E-26	9.35 E-23
700.9316	666	0 1 0	0 0 0	6.283E-19	560- 895	6340	69	1.40 E-25	1.40 E-21
1007.650	666	1 0 1	1 0 0	6.152E-20	948-1036	1185	50	5.59 E-24	1.90 E-22
1015.808	666	0 0 2	0 0 1	1.743E-19	958-1048	1534	55	5.65 E-24	5.43 E-22
1025.596	666	0 1 1	0 1 0	4.503E-19	969-1068	1544	45	5.59 E-24	1.38 E-21
1042.084	666	0 0 1	0 0 0	1.394E-17	950-1238	5813	71	4.20 E-25	4.19 E-20
1095.329	666	1 1 0	0 1 0	1.104E-20	979-1174	901	44	5.56 E-24	8.41 E-23
1103.141	666	1 0 0	0 0 0	6.711E-19	950-1250	5203	71	4.19 E-25	1.77 E-20
1726.5277	666	0 1 1	0 0 0	5.373E-20	1657-1910	1709•	55	1.15 E-24	1.67 E-22
1796.2606	666	1 1 0	0 0 0	2.266E-20	1681-1927	2137•	54	1.15 E-24	1.07 E-22

•NEW BAND FOR PRESENT COMPILATION.

§ Units of $cm^{-1}/(molecule\text{-}cm^{-2})$ at 296K.

rection suggested by Secroun *et al.*[33] has been made to all the lines.

In the 5.8-μm region the combination bands $\nu_2 + \nu_3$ and $\nu_1 + \nu_2$ have been added to the compilation. The line positions have been computed using the rotational and coupling constants of Barbe *et al.*,[34] and their accuracy should be better than 0.004 cm^{-1} for $J \leq 45$ or $K_a \leq 11$. The accuracy is then decreasing when extrapolating to higher J or K_a. The relative intensities have been verified with an atmospheric spectrum from Ref. 29, and their average relative precision should be of the order of 20%. The absolute intensities have been calibrated according to the results of McCaa and Shaw.[28] The average overall accuracy on the line intensities can be estimated to be ~30% (varying from10 to 100%).

Recent work by Hoell *et al.*[35] and by Lundqvist *et al.*[36] has made it possible to improve the values of the air-broadened halfwidths for ozone on the atlas. For the 1978 atlas[13] a constant value of 0.11 cm^{-1}/atm was adopted for all ozone lines, and in the last atlas[1] the value of 0.1 cm^{-1}/atm was adopted for all updated data. These values were from one and five measurements, respectively. Although not sufficient to conclusively determine J-dependence, Refs. 35 and 36 do allow the assigning of average halfwidths for A- and B-type bands separately. The value adopted for A-type bands is 0.083 cm^{-1}/atm, and the corresponding B-type band value is 0.077 cm^{-1}/atm. The halfwidths for all the bands in Table III adopt these new values (hence on the whole compilation there exists these three different sets of inputs to the halfwidths depending on the entry date of particular transitions). It has, however, been pointed out[37] that a value of 0.066 cm^{-1} for the A-type bands may be more appropriate, and the whole issue of ozone halfwidths is currently under investigation.[38]

It should be noted that updated parameters for the pure rotation transitions of ozone below 100 cm^{-1} are available from the submillimeter catalog of Poynter and Pickett,[39] and these transitions, when extended to the range presently covered on the AFGL atlas, will update the parameters of a future edition. In addition, recent analysis of the $\nu_1 + \nu_2 + \nu_3$ band at 2785 cm^{-1} has resulted in significantly improved line positions and intensities which became available after the release of the present atlas.[40]

The pure rotation band of the principal isotope of **nitrous oxide** (N_2O) from Ref. 39 has replaced the existing band on the atlas. NNO is a linear triatomic molecule, the frequencies and lower-state energies for the data being calculated by the standard formulas.[41] The molecular parameters were determined by a least-squares fit to the data summarized by Lovas.[42] These transitions cover the range from 0 to 50 cm^{-1}, and the accuracy is generally better than 5×10^{-6} cm^{-1}. The dipole moment used to evaluate intensities is from Scharpen *et al.*,[43] with an estimated accuracy of the line intensities of ~2%. The air-broadened halfwidths appended to the data were based on the values given by Toth.[44]

The pure rotation band of monodeuterated **methane** (CH_3D) obtained from Ref. 39 has been added to the atlas. The $J = 0 \rightarrow 1$ line has been measured by Pickett *et al.*[45] The predicted lines are based on the constants given by Chakerian and Guelachvili.[46] The accuracy of the line positions is generally better than 0.0001 cm^{-1}. The dipole moment was measured by Ozier *et al.*[47] and by Wofsey *et al.*[48] The calculated line intensities are estimated to be accurate to 2%. Air-broadened halfwidths were evaluated using the O_2- and N_2-broadened halfwidths of Tejwani and Fox[49] corrected to 296K.

The methane parameters have been revised in the regions covering 1071–1735 and 4136–4667 cm^{-1}. Table IV summarizes the updates giving the band origin in cm^{-1}, the upper and lower vibrational code (v' and v''), the isotope code (iso: 211, 311, 212 for $^{12}CH_4$, $^{13}CH_4$, and CH_3D, respectively), the range in cm^{-1} in which the transitions fall on the atlas (σ_{low} and σ_{high}), the summation of line intensities in cm^{-1}/molecule cm^{-2}, the number of transitions considered in the atlas, the minimum and maximum intensities included in the

Table IV. Summary of New or Updated Methane Bands for 1982 Compilation

BAND ORIGIN	BAND** V'	V"	ISO†	RANGE (CM-1)	SUM OF LINE§ INTENSITIES	# LINES	SMIN	SMAX	JMAX'
	ROT		212	7- 101	4.241E-26	80*	5.57 E-30	1.51 E-27	13
1302.7719	00000111	00000000	311	1183-1384	5.692E-20	353	2.92 E-24	1.08 E-21	17
1310.7606	00000111	00000000	211	1071-1544	5.041E-18	1420	2.90 E-24	9.55 E-20	22
1533.3367	01100001	00000000	211	1378-1735	5.503E-20	810	2.91 E-24	1.05 E-21	18
1533.526	01100001	00000000	311	1417-1645	3.990E-22	69	2.96 E-24	1.48 E-23	12
4223.497	10000111	00000000	211	4136-4279	2.399E-19	172	1.90 E-22	5.24 E-21	13
4340.	00011112	00000000	211	4147-4490	4.078E-19	958*	1.56 E-23	5.53 E-21	14
4540.	01111002	00000000	211	4409-4667	6.247E-20	388*	2.05 E-23	1.21 E-21	12
NO QU# ID			211	4136-4667	8.457E-20	537*	4.00 E-23	1.87 E-21	

*NEW BAND FOR PRESENT COMPILATION.

** For the bands other than the monodeuterated species, the vibrational quantum identification is $v_1 v_2 l_2 v_3 l_3 v_4 l_4$ (see Ref. 68).

† Isotope code: 211 is $^{12}CH_4$, 311 is $^{13}CH_4$, 212 is CH_3D.

§ The summation of intensities on the compilation only provides a lower limit to the band intensity since weak transitions are excluded.

We wish to acknowledge the contributions of the following colleagues toward this program: D. Bailly, J. W. Brault, G. Graner, G. Guelachvili, H. M. Pickett, R. L. Poynter, C. P. Rinsland, and M. A. H. Smith. This effort has been supported by the Air Force Office of Scientific Research through AFGL task 2310G1.

band (S_{min} and S_{max}), and the maximum J' in the list (upper-state rotational value). As can be seen in Table IV, no changes have been made in the 3- and 1.6-μm regions for this edition.

The 1980 parameters for the 1071–1735-cm^{-1} region were based on the simultaneous calculation of the ν_2 and ν_4 fundamentals given by Orton and Robiette[50] using the work of Gray and Robiette.[51] The 1982 parameters are a revision of the original calculation to include recent experimental work.[52–59] The ν_2 and ν_4 line positions are now generally computed using the calculated ground state[60–62] and experimentally determined upper states obtained from assignment of spectral data.[52–54] The spectra utilized[54] were recorded at 0.005- and 0.01-cm^{-1} resolution with a Fourier transform spectrometer (FTS) at Kitt Peak National Observatory. The absolute calibration of line positions (on which the upper states are based) was made using CO_2 lines[63] arising from residual carbon dioxide at 0.05 Torr in the FTS enclosure. The accuracies of the line positions vary from 0.001 cm^{-1} for the strong unblended lines to 0.003 cm^{-1} for the forbidden $^{13}CH_4$ lines and other weak features. The line intensities are the calculated values from the 1980 list[1] lowered by 2% to conform with a ν_4 band strength of 128 cm^{-2} atm^{-1} at 296K.[54–58] A Herman-Wallis factor of $(1 - 0.0034\ m)^2$ was applied, correcting an error in the 1980 calculation.[50,59] An additional adjustment has been made to all ν_2 intensities,[53,54]

$$S_{\nu_2} = S_{\nu_2}(\nu_2,\nu_4)_{calc} \times 0.767 \times (1 - 0.022\ m)^2,$$

where $m = -J'', 0, J'' + 1$ for the P-, Q-, and R-branch lines, respectively. The $^{13}CH_4$ line intensities were scaled to be 1.1% of the corresponding ν_4 line intensities, representing the natural isotopic abundance of ^{13}C. The accuracy for the line intensities varies from 4% for the allowed lines to 10% for the forbidden ν_2 and ν_4 lines. All lines with calculated intensities of 2.9×10^{-24} cm^{-1}/molecule cm^{-2} or greater were included in the list.

The parameters for the 4136–4667-cm^{-1} region were obtained from direct measurement of experimental spectra. This portion of the compilation has been described elsewhere[64] so that only a brief description is recounted here. The 1980 list contained 181 lines of the $\nu_1 + \nu_4$ band from 4136 to 4268 cm^{-1}. The present compilation has 2055 features partially assigned to $\nu_1 + \nu_4$, $\nu_3 + \nu_4$, and $\nu_2 + \nu_3$. The minimum intensity of lines included in this second region is 1.5×10^{-23} cm^{-1}/molecule cm^{-2}. The air-broadened halfwidths for this region and the ν_4 region are the same as those in the 1980 compilation.[1]

The parameters of methane are still incomplete even for the 2–11-μm region. The 7-μm region parameters do not include features arising from three hot bands, $\nu_3 - \nu_4$ (1710 cm^{-1}), $2\nu_4 - \nu_4$, and $\nu_2 + \nu_4 - \nu_2$ (1310 cm^{-1}). These bands are expected to contribute an additional 500–1000 lines to the compilation with individual line intensities of not more than 10^{-22} cm^{-1}/molecule cm^{-2}. In the 2.5-μm region, two bands, $3\nu_4$ (3868 cm^{-1}) and $2\nu_4 + \nu_2$ (4125 cm^{-1}), give rise to lines with intensities of 10^{-22} cm^{-1}/molecule cm^{-2}, but these absorptions are not yet included in the parameter list. However, work is in progress to correct these deficiencies.[54] Above 5000 cm^{-1} the CH_4 parameters are of limited use in making synthetic spectra for comparison purposes. Only 142 lines of $2\nu_3$ at 6005 cm^{-1} are listed. After the 1982 compilation was issued an error was detected in the parameters for this latter band: the individual line intensities are too low by a factor of ~2.5.[65,66] However, work on the higher bands[66,67] of CH_4 indicates that the simple formalism by which the $2\nu_3$ intensities were originally calculated[68] may not provide adequate relative line strengths. In addition, many strong absorptions arise between 5000 and 6000 cm^{-1} from bands other than $2\nu_3$. Unfortunately, no systematic measurement and analysis of high-resolution data for the 2–1.6-μm region of methane are currently underway to provide the comprehensive parameters needed for remote sensing applications.

All bands of **oxygen** (O_2) were modified to some extent in this atlas. The summary in Table V, therefore, covers all oxygen transitions presently in the compilation. In the third column the two-letter symbol identifies which of the three electronic transitions is occurring, i.e., XX signifies a band within the electronic ground state ($X^3\Sigma_g^-$), AX signifies a transition between the singlet delta electronic level ($a^1\Delta_g$) and the ground electronic level, and BX denotes a transition between the singlet sigma level ($b^1\Sigma_g^+$) and the ground state. Within these transitions are superimposed the vibrational transitions as indicated in the columns under v' and v''.

In the first group of transitions in Table V (transitions within the electronic ground state), besides a recalculation that very slightly altered the intensities of the magnetic dipole transitions, the electric quadrupole transitions were also included.[69] The band at 1556 cm^{-1} represents solely the latter type of transition.

New constants for the singlet delta level of oxygen[70] have improved the line positions of all the bands in the second group in Table V. In addition, the (0–1) vibrational band at 6326 cm^{-1} was added in anticipation of its significance in upper atmospheric radiance problems. The cutoff criterion was lowered to accommodate this band, and the band intensity was adopted from Jones and Harrison.[71] The other band intensities in this region were based on the work of Badger *et al.*[72]

The atmospheric A bands (13120 cm^{-1}), B bands (14525 cm^{-1}), and γ bands (15900 cm^{-1}) were refined in terms of the intensity calculation. These bands have been based on total band intensity measurements of Miller *et al.*,[73] Giver *et al.*,[74] and Miller *et al.*,[75] respectively. Good agreement was found between calculations based on the these measurements and the high-resolution long path-length observations performed by Nakagawa *et al.*[76] The (0–1) band and the (1–1) band intensities were estimated from Krupenie[77] and Galkin.[78]

For the millimeter electronic fine structure parameters (60 GHz) and the submillimeter pure rotation transitions, the halfwidths adopted were those given in Ref. 77. All other transitions assumed the halfwidths of Ref. 74.

Table V. Summary of All Oxygen Bands on Main Compilation

BAND ORIGIN	ISO†	ELEC	BAND* V'	V"	SUM OF LINE§ INTENSITIES	RANGE (CM-1)	# LINES	SMIN§	SMAX§
	66	XX	0	0	7.231E-24	1- 276	161	2.07 E-35	5.18 E-25
	67	XX	0	0	4.537E-27	1- 132	465	3.71 E-30	4.05 E-29
	68	XX	0	0	3.033E-26	1- 214	218	1.20 E-35	1.15 E-27
	66	XX	1	1	3.764E-27	1- 207	100	2.09 E-35	2.68 E-28
1556.379	66	XX	1	0	6.152E-27	1407- 1706	146	3.68 E-30	1.49 E-28
6326.033	66	AX	0	1	1.129E-28	6284- 6410	47	1.24 E-30	4.99 E-30
7882.425	66	AX	0	0	1.816E-24	7664- 8065	157	1.47 E-29	6.23 E-26
7883.738	68	AX	0	0	6.745E-27	7809- 7984	147	1.48 E-29	1.24 E-28
9365.877	66	AX	1	0	8.626E-27	9264- 9469	88	1.79 E-29	3.06 E-28
11564.516	66	BX	0	1	7.798E-27	11483-11617	47	2.76 E-29	3.11 E-28
12969.269	66	BX	1	1	9.418E-26	12847-13011	59	4.65 E-29	3.71 E-27
13120.909	66	BX	0	0	1.946E-22	12899-13166	91	3.47 E-29	7.71 E-24
13122.972	68	BX	0	0	7.921E-25	12981-13165	136	3.51 E-29	1.52 E-26
14488.826	68	BX	1	0	4.960E-26	14373-14520	108	3.03 E-29	9.58 E-28
14506.26	67	BX	1	0	1.831E-26	14453-14537	45	6.62 E-29	1.16 E-27
14525.661	66	BX	1	0	1.218E-23	14317-14558	79	6.37 E-29	4.82 E-25
15828.247	68	BX	2	0	8.884E-29	15846-15849	3	2.94 E-29	2.99 E-29
15902.418	66	BX	2	0	3.782E-25	15719-15928	67	3.48 E-29	1.50 E-26

† Isotope code: 66 is $^{16}O_2$, 68 is $^{16}O^{18}O$.

* Column under ELEC: XX is transition within electronic ground state ($X\,^3\Sigma_g^-$); AX is transition between electronic ground state and singlet delta electronic state ($a\,^1\Delta$); BX is transition between electronic ground state and singlet sigma electronic state ($b\,^1\Sigma_g^+$).

§ Units of $cm^{-1}/(molecule\text{-}cm^{-2})$ at 296K.

The accuracy of the line positions depends to a great degree on the rotational level attained in the measurements of a vibronic state. For an estimate of the accuracies of a transition in Table V we cite the original references.[70,79] Similarly, for the intensities, with the exception of the millimeter electronic fine structure spectrum and the submillimeter pure rotation spectrum which are based on fundamental properties such as the Bohr magneton and hence are accurate to a few percent, the original band intensity observations should be consulted.[71-75,77,78,80]

The atlas now contains ~181,000 transitions of the major isotopic variants of the molecules water vapor, carbon dioxide, ozone, nitrous oxide, carbon monoxide, methane, and oxygen, while covering the 0–17,900-cm^{-1} spectral range. A continuing program is in progress to improve the accuracy and completeness of the atlases for diverse applications relating to molecular absorption and radiance problems. Complete tables of the bands presently in the compilation can be obtained from L. S. Rothman.

References

1. L. S. Rothman, Appl. Opt. 20, 791 (1981); a graphical presentation of the 1980 atlases can be found in J. H. Park, L. S. Rothman, M. A. H. Smith, D. J. Richardson, and J. C. Larsen, NASA Ref. Publ. 1084 (1981).
2. L. S. Rothman *et al.*, Appl. Opt. 22, 1616 (1983).
3. M. T. Coffey, W. G. Mankin, and R. J. Cicerone, Science London 214, 333 (1981); J. M. Hoell, C. N. Harward, and W. Lo, Opt. Eng. 21, 320 (1982); C. P. Rinsland, M. A. H. Smith, J. M. Russell, J. H. Park, and C. B. Farmer, Appl. Opt. 20, 4167 (1981); C. P. Rinsland *et al.*, J. Geophys. Res. 87, 3119 (1982); D. T. Cassidy and J. Reid, Appl. Opt. 21, 2527 (1982).
4. D. C. Robertson, L. S. Bernstein, R. Haimes, J. Wunderlich, and L. Vega, Appl. Opt. 20, 3218 (1981); V. Oinas, J. Quant. Spectrosc. Radiat. Transfer 26, 381 (1981); H. J. Liebe, Radio Sci. 16, 1183 (1981); S. A. Clough, F. X. Kneizys, L. S. Rothman, and W. O. Gallery, Proc. Soc. Photo-Opt. Instrum. Eng. 277, 152 (1981); W. M. Wehrbein and C. B. Leovy, J. Atmos. Sci. 39, 1532 (1982).
5. D. H. Leslie and G. L. Trusty, Appl. Opt. 20, 1941 (1981); T. A. Wiggins, Appl. Opt. 20, 3431 (1981).
6. J. R. Drummond and C. T. Mutlow, Nature London 294, 431 (1981); C. P. Rinsland *et al.* Appl. Opt. 21, 4351 (1982).
7. R. L. Armstrong, Appl. Opt. 21, 2141 (1982); K. K. Lehmann, G. J. Scherer, and W. Klemperer, J. Chem. Phys. 77, 2853 (1982).
8. J. K. G. Watson, Mol. Phys. 15, 479 (1968).
9. F. C. DeLucia, P. Helminger, R. L. Cook, and W. Gordy, Phys. Rev. A 5, 478 (1972).
10. J.-M. Flaud, C. Camy-Peyret, and J. P. Maillard, Mol. Phys. 32, 499 (1972).
11. K. M. Haught and J. A. Dowling, Opt. Lett. 1, 121 (1977).
12. S. T. Hanley, J. A. Dowling, R. F. Horton, J. A. Curcio, C. O. Gott, M. Woytko, and J. Storvick, "1978 WSMR Atmospheric Transmission," NRL-MR-4199 (1980) (Defense Technical Information Center ADB-049676L).
13. L. S. Rothman, Appl. Opt. 17, 3517 (1978).
14. W. S. Benedict, U. Maryland; private communication.

15. J.-M. Flaud, C. Camy-Peyret, and R. A. Toth, *Selected Constants: Water Vapor Line Parameters from Microwave to Medium Infrared* (Pergamon, Oxford, 1981).
16. R. A. Toth, V. D. Gupta, and J. W. Brault, Appl. Opt. **21**, 3337 (1982); R. A. Toth and J. W. Brault, Appl. Opt. **22**, 908 (1983); N. Papineau, C. Camy-Peyret, J.-M. Flaud, and G. Guelachvili, J. Mol. Spectrosc. **92**, 451 (1982).
17. R. R. Gamache and R. W. Davies, to be submitted to Appl. Opt.
18. M. P. Esplin and L. S. Rothman, J. Mol. Spectrosc. **100**, in press (1983).
19. D. Bailly, R. Farrenq, G. Guelachvili, and C.Rosetti, J. Mol. Spectrosc. **90**, 74 (1981).
20. K. J. Siemsen, National Research Council of Canada; private communication; F. R. Petersen, J. S. Wells, A. G. Maki, and K. J. Siemsen, Appl. Opt. **20**, 3635 (1981).
21. M. L. Hoke and J. H. Shaw, Appl. Opt. **21**, 935 (1982).
22. A. Baldacci, C. P. Rinsland, M. A. H. Smith, and K. N. Rao, J. Mol. Spectrosc. **94**, 351 (1982).
23. L. S. Rothman, M. P. Esplin, D. Bailly, R. Farrenq, G. Guelachvili, C. Rosetti, and K. J. Siemsen, to be submitted to J. Mol. Spectrosc.
24. M. L. Hoke and J. H. Shaw, Appl. Opt. **22**, 328 (1983).
25. L. S. Rothman and L. D. G. Young, J. Quant. Spectrosc. Radiat. Transfer **25**, 505 (1981).
26. C. P. Rinsland, College of William and Mary; private communication.
27. A. Goldman, J. R. Gillis, D. G. Murcray, A. Barbe, and C. Secroun, J. Mol. Spectrosc. **96**, 279 (1982).
28. D. J. McCaa and J. H. Shaw, J. Mol. Spectrosc. **25**, 374 (1968).
29. A. Goldman, R. D. Blatherwick, F. J. Murcray, J. W. VanAllen, F. H. Murcray, and D. G. Murcray, Appl. Opt. **21**, 1163 (1982).
30. H. Oelhaf, A. Leupolt, and H. Fischer, Appl. Opt. **22**, 647 (1983).
31. A. Barbe, C. Secroun, P. Jouve, A. Goldman, and D. G. Murcray, J. Mol. Spectrosc. **86**, 286 (1981); A. Barbe, U. Reims, A. Goldman, U. Denver, and J. S. Margolis, JPL; private communication.
32. J.-M. Flaud, C. Camy-Peyret, and L. S. Rothman, Appl. Opt. **19**, 655 (1980).
33. C. Secroun, A. Barbe, P. Jouve, P. Arcas, and E. Arié, J. Mol. Spectrosc. **85**, 8 (1981).
34. A. Barbe, C. Secroun, P. Jouve, C. Camy-Peyret, and J.-M. Flaud, J. Mol. Spectrosc. **75**, 103 (1979).
35. J. M. Hoell, C. N. Harward, C. H. Bair, and B. S. Williams, Opt. Eng. **21**, 548 (1982).
36. S. Lundqvist, J. Margolis, and J. Reid, Appl. Opt. **21**, 3109 (1982).
37. C. Meunier, P. Marché, and A. Barbe, J. Mol. Spectrosc. **95**, 271 (1982).
38. R. R. Gamache, R. W. Davies, and L. S. Rothman, in *Proceedings, Thirty-Eighth Symposium on Molecular Spectroscopy, Ohio State U.* (1983), paper ME13.
39. R. L. Poynter and H. M. Pickett, "Submillimeter, Millimeter and Microwave Spectral Line Catalogue," JPL Publication 80-23, Revision 1 (Jet Propulsion Laboratory, California Institute of Technology, Pasadena, 1981).
40. A. Barbe and C. Secroun, U. Reims, A. Goldman and J. R. Gillis, U. Denver; private communication.
41. C. H. Townes and A. L. Schawlow, *Microwave Spectroscopy* (McGraw-Hill, New York, 1955).
42. F. J. Lovas, J. Phys. Chem. Ref. Data **7**, 1445 (1978).
43. L.H. Scharpen, J. S. Muenter, and V. W. Laurie, J. Chem. Phys. **53**, 2513 (1970).
44. R. A. Toth, J. Mol. Spectrosc. **40**, 605 (1971).
45. H. M. Pickett, E. A. Cohen, and T. G. Phillips, Astrophys. J. Lett. **236**, 43 (1980).
46. C. Chakerian and G. Guelachvili, J. Mol. Spectrosc. **84**, 447 (1980).
47. I. Ozier, W. Ho, and G. Birnbaum, J. Chem. Phys. **51**, 4873 (1969).
48. S. C. Wofsey, J. S. Muente , and W. Klemperer, J. Chem. Phys. **53**, 4005 (1970).
49. G. D. T. Tejwani and K. Fox, J. Chem. Phys. **61**, 759 (1974).
50. G. S. Orton and A. G. Robiette, J. Quant. Spectrosc. Radiat. Transfer **24**, 81 (1980).
51. D. L. Gray and A. G. Robiette, Mol. Phys. **32**, 1609 (1976).
52. A. G. Robiette, J. Mol. Spectrosc. **86**, 143 (1981).
53. B. Lutz, C. Pierre, G. Pierre, and J. P. Champion, Astrophys. J. Supp. Ser. **48**, 507 (1982).
54. L. R. Brown, (unpublished work).
55. L. R. Brown, J. S. Margolis, R. H. Norton, and B. A. Stedry, Appl. Spectrosc. **37**, 287 (1983).
56. G. Restelli and F. Cappellani, Chem. Phys. Lett. **92**, 439 (1982).
57. D. E. Jennings and A. G. Robiette, J. Mol. Spectrosc. **94**, 369 (1982).
58. J. H. G. Bode and W. M. A. Smith, J. Phys. Chem. **84**, 198 (1980).
59. G. S. Orton and A. G. Robiette, J. Quant. Spectrosc. Radiat. Transfer **29**, 283 (1983).
60. G. Tarrago, M. Dang-Nhu, G. Poussigue, G. Guelachvili, and C. Amiot, J. Mol. Spectrosc. **57**, 246 (1975).
61. C. W. Holt, M. C. L. Gerry, and I. Ozier, Can. J. Phys. **53**, 1791 (1975).
62. L. W. Pinkley, K. N. Rao, M. Dang-Nhu, G. Tarrago, and G. Poussigue, J. Mol. Spectrosc. **63**, 402 (1976).
63. G. Guelachvili, J. Mol. Spectrosc. **75**, 251 (1979).
64. L. R. Brown and L. S. Rothman, Appl. Opt. **21**, 2425 (1982).
65. J. S. Margolis, J. Quant. Spectrosc. Radiat. Transfer **13**, 1097 (1973).
66. K. Fox, G. W. Halsey, S. J. Daunt, W. E. Blass, and D. E. Jennings, J. Chem. Phys. **72**, 4657 (1980).
67. J. W. Brault, K. Fox, D. E. Jennings, and J. S. Margolis, Astrophys. J. **247**, 1101 (1981).
68. K. Fox, "Analysis of Vibration-Rotation Spectra of Methane," AFCRL-TR-0738 (1974) (Defense Technical Information Center AD-776061).
69. L. S. Rothman and A. Goldman, Appl. Opt. **20**, 2182 (1981).
70. C. Amiot and J. Verges, Can. J. Phys. **59**, 1391 (1981); L. S. Rothman, Appl. Opt. **21**, 2428 (1982); J. W. Brault, R. C. M. Learner, and M. A. Brown, in *Proceedings, Thirty-Seventh Symposium on Molecular Spectroscopy, Ohio State U.* (1982), paper TA2.
71. A. V. Jones and A. W. Harrison, J. Atmos. Terr. Phys. **13**, 45 (1958).
72. R. M. Badger, A. C. Wright, and R. F. Whitlock, J. Chem. Phys. **43**, 4345 (1965).
73. J. H. Miller, R. W. Boese, and L. P. Giver, J. Quant. Spectrosc. Radiat. Transfer **9**, 1507 (1969).
74. L. P. Giver, R. W. Boese, and J. H. Miller, J. Quant. Spectrosc. Radiat. Transfer **14**, 793 (1974).
75. J. H. Miller, L. P. Giver, and R. W. Boese, J. Quant. Spectrosc. Radiat. Transfer **16**, 595 (1976).
76. T. Nakagawa, T. Yamanouchi, and M. Tanaka, J. Quant. Spectrosc. Radiat. Transfer **27**, 615 (1982).
77. P. H. Krupenie, J. Phys. Chem. Ref. Data **1**, 423 (1972).
78. V. D. Galkin, Opt. Spectrosc. **47**, 266 (1979).
79. W. Steinbach and W. Gordy, Phys. Rev. A **11**, 729 (1975); T. Amano and E. Hirota, J. Mol. Spectrosc. **53**, 346 (1974); D. L. Albritton, W. J. Harrop, A. L. Schmeltekopf, and R. N. Zare, J. Mol. Spectrosc. **46**, 103 (1973).
80. W. S. Benedict and L. D. Kaplan, J. Quant. Spectrosc. Radiat. Transfer **4**, 453 (1964); J. Reid, R. L. Sinclair, A. M. Robinson, and A. W. R. McKellar, Phys. Rev. A **24**, 1944 (1981).

Reprinted from Applied Optics, Vol. 22, page 4013, December 15, 1983

B3.

Theoretical calculations of N_2-broadened halfwidths of H_2O using quantum Fourier transform theory

Robert R. Gamache and Richard W. Davies

N_2-broadened halfwidths for the pure rotation band of H_2O have been calculated for some 1600 transitions using quantum Fourier transform (QFT) theory. The QFT method corresponds to a quantum mechanical second-order perturbation development of collisional broadening within the binary collision approximation. Self-broadened halfwidths as well as pressure shifts were also calculated in this study but are not presented here. The N_2-broadened halfwidths were used to form the data base of H_2O halfwidths present on the AFGL main gas Atlas and replace the earlier Anderson calculations by Benedict and Kaplan.

I. Introduction

Although water vapor is a minor constituent of the terrestrial atmosphere its vibrational–rotational structure is such that it is of major importance for considering the absorption of infrared radiation in the atmosphere.[1] It is known to play a prominent role in determining atmospheric transmission to solar or laser radiation and the heat balance of the lower atmosphere.[2]

High resolution atmospheric transmission models[3] consider the absorption of radiation by a molecule[4] in terms of the spectral parameters: the spectral transition frequency ν, the line intensity S, the collision broadened halfwidth γ, and the lower state energy E''. From a knowledge of the above parameters, theoretical spectra can be computed for diagnosing experimental observations, designing new systems and experiments, understanding atmospheric properties, etc. It is the purpose of the AFGL Line Atlases to catalog these spectral parameters for the main IR absorbers of the atmosphere[5] and for trace gas constituents[6] of the atmosphere. Many high resolution measurements[7] have been performed yielding accurate parameters for the line positions, lower state energies, and line intensities of water vapor. Absent from the literature are similar extensive measurements of collision-broadened halfwidths for H_2O. Thus one must rely on theory to evaluate halfwidths in order to extend the data base.

For water vapor some accurate measurements of halfwidths are available[8–22] to compare with theoretical calculations. These measurements usually concentrate on medium-to-strong intensity lines that are isolated (no overlap with adjacent lines) in the spectrum.

The purpose of this paper is to report calculations of N_2-broadened halfwidths for water vapor that form the data base used to evaluate the air-broadened widths for H_2O present on the AFGL main gas compilation. These calculations were performed using the quantum Fourier transform (QFT) theory[23] of collisional broadening and replace the earlier Anderson-Tsao-Curnutte[24] (ATC) values of Benedict and Kaplan.[25]

The QFT method was derived[23] using graphical many-body techniques and corresponds to a complete quantum mechanical treatment of the problem. However, within the binary collision approximation, the main differences between the QFT formalism and ATC theory are (a) QFT theory rigorously conserves momentum and energy in the collision process (in the ATC approach both angular deflection and change in kinetic energy of the colliding molecules are ignored) and (b) the QFT treatment includes a Boltzmann average over the initial translational state (ATC simply uses the mean relative thermal velocity). The QFT method is expected to be more appropriate especially for weak transitions. This can be seen from Ref. 26 where a limited comparison of QFT, ATC, and experimental results was presented for N_2 broadening of H_2O. An explicit comparison of QFT, ATC, and experimental results has also been carried out by Mandin *et al.*[27] for self-broadening of H_2O. Both methods of calculation indicated an improvement over the previous results tabulated by Benedict and Kaplan.[25] The general

When this work was initiated both authors were with University of Lowell, Center for Atmospheric Research, Lowell, Massachusetts 01854; R. W. Davies is now with GTE Laboratories, Inc., 40 Sylvan Road, Waltham, Massachusetts 02254.
Received 17 August 1983.
0003-6935/83/244013-07$01.00/0.

tendency is for the QFT treatment to yield somewhat narrower halfwidths, particularly for weaker transitions involving large collisional energy denominators. This is primarily due to the more rapid fall-off of the QFT resonance functions [the analog of the ATC $F(k)$, $f(k)$ functions] for large rotational energy differences. Part of this more rapid fall-off is in turn due to the fact that an explicit Boltzmann average over velocities is included in the QFT theory. It is known that a similar average of the ATC theory also leads to narrower linewidths, however, this is frequently not done because of the increased computational time.

Due to computation limitations, halfwidths for ~100 transitions were tabulated in Ref. 26. New techniques have allowed us to extend the calculations to generate the present data base of N_2-broadened halfwidths of water (1600 transitions), as well as self-broadened halfwidths and line shifts for the same transitions. The N_2-broadened halfwidths of H_2O are presented in Table I. Tables of self-broadened halfwidths and pressure shifts of H_2O are available on request to one of the authors (RRG).

In Sec. II we briefly describe the theory as applied to N_2 broadening of water vapor lines. Section III describes the molecular constants and data necessary to perform the calculations, and the numerical results are presented.

II. Theoretical

The quantum Fourier transform theory of second-order pressure shifts and widths was derived in detail in Ref. 23. A comparison of QFT theory with ATC theory and a casting of the QFT equations into a form similar to the ATC equations were presented in Ref. 26. Readers interested in the general theory are referred to the above articles. Here we briefly summarize the theory as applied to N_2 broadening of water vapor.

The charge distribution of H_2O can be approximated as a sum of a dipole and a quadrupole term. The leading term for N_2 is the quadrupole term. These give rise to the following interactions: dipole (H_2O) interacting with quadrupole (N_2) and quadrupole (H_2O) interacting with quadrupole (N_2). Because of the relative magnitudes of the dipole and quadrupole moments of water, the second term (q–q interaction) contributes at most 10% to the halfwidth[28] (usually the contribution is ~3–5%). In our calculations we consider only the dipole (H_2O)–quadrupole (N_2) interaction in the formalism. A similar procedure was employed in the earlier calculations of Benedict and Kaplan.[25]

The halfwidth for the radiative transition $i \rightarrow f$ is given by (cm^{-1}/atm)

$$\gamma_{if} = \left(\frac{nv}{2\pi c}\right) \sum_{J_2} \rho(J_2)\sigma_{if,J_2}, \tag{1}$$

where n is the perturber density (N_2) at 1-atm pressure and temperature T ($n = n_0\,273/T$), c = velocity of light, v is the mean relative thermal velocity given by $v = [8\,k_B T/\pi m]^{1/2}$, m is the reduced mass, and $\rho(J_2)$ is the Boltzmann factor for perturber state J_2.

For the dipole–quadrupole interaction, QFT theory yields

$$\sigma_{if,J_2} = \pi \left[b_0^2 + \int_{b_0}^{\infty} 2b\,db\, s_{if,J_2}(b)\right], \tag{2}$$

or

$$\sigma_{if,J_2} = \pi b_0^2 [1 + S_{if,J_2}(b_0)], \tag{3}$$

where, in a notation similar to Benedict and Kaplan,[25]

$$s_{if,J_2}(b) = \left(\frac{2\alpha^4}{225\pi}\right)\left(\frac{d_1 Q_2}{\hbar v}\right)^2 b^{-6} \times \left[\sum_{i'J_2'} D(i,i')Q(J_2,J_2')g(k_i) + \sum_{f'J_2'} D(f,f')Q(J_2,J_2')g(k_f)\right], \tag{4}$$

$$S_{if,J_2}(b_0) = \left(\frac{2\alpha^4}{225\pi}\right)\left(\frac{d_1 Q_2}{\hbar v}\right)^2 b_0^{-6} \times \left[\sum_{i'J_2'} D(i,i')Q(J_2,J_2')G(k_i) + \sum_{f'J_2'} D(f,f')Q(J_2,J_2')G(k_f)\right]. \tag{5}$$

In the above equations d_1 is the dipole moment of the radiator (H_2O), Q_2 is the quadrupole moment of the perturber (N_2), and b is the impact parameter. The various $D(i,i')$ are reduced dipole matrix elements of the radiator which satisfy the sum rule

$$\sum_{i'} D(i,i') = 1. \tag{6}$$

The $Q(J_2,J_2')$ are reduced quadrupole matrix elements of the perturber, and the sum on J_2' is determined by quadrupole transition selection rules. The functions $g(k)$ and $G(k)$ are the resonance functions of QFT theory; for the d–q case these are given by

$$g(k) = \exp\left(-\frac{4}{\pi}\frac{k^2}{\alpha^2}\right), \tag{7}$$

$$G(k) = 2k^4 \int_k^{\infty} \frac{k'dk'}{(k')^6} g(k') \qquad (k > 0). \tag{8}$$

In the above expressions k is the resonance factor

$$k_i = \frac{2\pi c b}{v}(E_i - E_{i'} + E_{J_2} - E_{J_2'}), \tag{9}$$

where the energies are in cm^{-1} and correspond to the rotation–vibration energy difference between the initial (i,J_2) and final (i',J_2') collisional states.

As discussed in Ref. 26, the QFT theory may also be employed to compute pressure shifts of spectral transitions. In all our calculations the pressure shifts were evaluated, however, we shall not present these results in this paper.

The scaling parameter α was introduced in QFT theory in order to obtain a cutoff procedure similar to ATC's and is not given *a priori*. The method used for fixing α was to choose the best available value for the quadrupole moment of the perturber and then to adjust α to match a well-measured calibration line. In ATC theory the corresponding procedure is to adjust the

Table I. N_2-Broadened Halfwidths for H_2O in units of cm^{-1}/atm, Initial State Vs Transition Type $\Delta J(\Delta K_a, \Delta K_c)$

Initial State			Transition				Initial State			Transition			
J	K_a	K_c	Q(1,-1)	R(1,1)	R(3,-1)	R(-1,3)	J	K_a	K_c	Q(1,-1)	R(1,1)	R(3,-1)	R(-1,3)
0	0	0		.1055			1	1	1		.1043		.1096
1	0	1	.1162	.1121			2	1	2	.1041	.1060		.1088
2	0	2	.1101	.1104	.1007		3	1	3	.1019	.1069		.1042
3	0	3	.1080	.1069	.1005		4	1	4	.0962	.1070		.0930
4	0	4	.1067	.0975	.0953		5	1	5	.0865	.1028		.0779
5	0	5	.1000	.0812	.0853		6	1	6	.0747	.0932		.0618
6	0	6	.0868	.0628	.0738		7	1	7	.0616	.0815		.0468
7	0	7	.0694	.0466	.0621		8	1	8	.0492	.0675		.0347
8	0	8	.0514	.0341	.0518		9	1	9	.0388	.0517		.0257
9	0	9	.0363	.0251	.0436		10	1	10	.0314	.0370		.0194
10	0	10	.0256	.0189	.0373		11	1	11	.0253	.0258		.0153
11	0	11	.0188	.0150	.0318		12	1	12	.0202	.0186		.0127
12	0	12	.0147	.0125	.0268		13	1	13	.0166	.0144		.0112
13	0	13	.0122	.0111	.0241		14	1	14	.0139	.0121		.0103
14	0	14	.0109	.0103	.0220		15	1	15	.0121	.0108		.0099
15	0	15	.0102	.0099	.0188		16	1	16	.0110	.0101		.0097
16	0	16	.0098	.0097	.0166		17	1	17	.0103	.0098		.0096
17	0	17	.0096	.0096	.0148		18	1	18	.0099	.0096		.0095
18	0	18	.0096	.0095	.0132		19	1	19	.0114	.0096		.0095
19	0	19	.0095	.0095	.0120		20	1	20	.0095			
20	0	20	.0095				2	2	1		.0922		.1039
1	1	0		.1087			3	2	2	.0911	.0944		.1040
2	1	1	.1049	.1065			4	2	3	.0900	.0973		.1008
3	1	2	.1015	.1050	.0908		5	2	4	.0865	.0986		.0918
4	1	3	.1025	.1020	.0936		6	2	5	.0806	.0974		.0783
5	1	4	.1037	.0960	.0929		7	2	6	.0727	.0938		.0633
6	1	5	.1009	.0852	.0858		8	2	7	.0632	.0859		.0496
7	1	6	.0921	.0703	.0742		9	2	8	.0537	.0760		.0386
8	1	7	.0806	.0542	.0607		10	2	9	.0460	.0666		.0311
9	1	8	.0669	.0408	.0487		11	2	10	.0391	.0548		.0251
10	1	9	.0512	.0306	.0394		12	2	11	.0328	.0414		.0200
11	1	10	.0366	.0232	.0329		13	2	12	.0278	.0297		.0165
12	1	11	.0256	.0183	.0289		14	2	13	.0250	.0214		.0139
13	1	12	.0185	.0148	.0272		15	2	14	.0227	.0161		.0121
14	1	13	.0144	.0126	.0267		16	2	15	.0193	.0131		.0109
15	1	14	.0121	.0112	.0257		17	2	16	.0169	.0114		.0103
16	1	15	.0108	.0104	.0235		18	2	17	.0150	.0105		.0099
17	1	16	.0101	.0100	.0223		19	2	18	.0134	.0100		.0097
18	1	17	.0098	.0097	.0223		20	2	19	.0121			
19	1	18	.0096	.0096	.0201		3	3	1		.0725		.0948
20	1	19	.0096				4	3	2	.0743	.0773		.0983
2	2	0		.0932		.1065	5	3	3	.0770	.0810		.0982
3	2	1	.0938	.0961		.1047	6	3	4	.0766	.0838		.0934
4	2	2	.0972	.0986	.0872	.1026	7	3	5	.0740	.0857		.0851
5	2	3	.1000	.1002	.0912	.1007	8	3	6	.0688	.0858		.0728
6	2	4	.1010	.0973	.0920	.0946	9	3	7	.0609	.0843		.0589
7	2	5	.1012	.0897	.0879	.0854	10	3	8	.0525	.0803		.0471
8	2	6	.0972	.0804	.0808	.0757	11	3	9	.0456	.0719		.0388
9	2	7	.0886	.0683	.0695	.0642	12	3	10	.0400	.0643		.0324
10	2	8	.0777	.0549	.0548	.0500	13	3	11	.0352	.0570		.0270
11	2	9	.0669	.0431	.0410	.0361	14	3	12	.0326	.0473		.0242
12	2	10	.0540	.0333	.0313	.0254	15	3	13	.0308	.0377		.0221
13	2	11	.0403	.0272	.0251	.0184	16	3	14	.0278	.0288		.0188
14	2	12	.0285	.0235	.0211	.0143	17	3	15	.0252	.0227		.0166
15	2	13	.0202	.0197	.0187	.0120	18	3	16	.0239	.0186		.0148
16	2	14	.0152	.0171	.0181	.0108	19	3	17	.0236	.0141		.0133
17	2	15	.0125	.0150	.0194	.0101	20	3	18	.0211			
18	2	16	.0110	.0134	.0216	.0098	4	4	1		.0560		.0838
19	2	17	.0103	.0121	.0232	.0096	5	4	2	.0604	.0625		.0900
20	2	18	.0098				6	4	3	.0642	.0664		.0939
3	3	0		.0740		.0904	7	4	4	.0658	.0677		.0936
4	3	1	.0791	.0817		.0910	8	4	5	.0652	.0689		.0882
5	3	2	.0871	.0886	.0800	.0921	9	4	6	.0621	.0674		.0790
6	3	3	.0934	.0922	.0848	.0917	10	4	7	.0552	.0689		.0688
7	3	4	.0970	.0943	.0889	.0918	11	4	8	.0466	.0712		.0562
8	3	5	.0970	.0926	.0889	.0889	12	4	9	.0389	.0712		.0429
9	3	6	.0948	.0856	.0834	.0813	13	4	10	.0335	.0668		.0331
10	3	7	.0920	.0763	.0753	.0723	14	4	11	.0306	.0582		.0286
11	3	8	.0853	.0665	.0666	.0639	15	4	12	.0296	.0521		.0273
12	3	9	.0748	.0544	.0548	.0528	16	4	13	.0288	.0483		.0260
13	3	10	.0649	.0419	.0413	.0399	17	4	14	.0273	.0426		.0236
14	3	11	.0560	.0339	.0298	.0284	18	4	15	.0270	.0348		.0223
15	3	12	.0452	.0297	.0224	.0203	19	4	16	.0280	.0272		.0223
16	3	13	.0345	.0257	.0183	.0153	20	4	17	.0269			
17	3	14	.0256	.0232	.0156	.0126	5	5	1		.0443		.0679

continued

Table I. Continued

Initial State			Transition				Initial State			Transition			
J	K_a	K_c	Q(1,-1)	R(1,1)	R(3,-1)	R(-1,3)	J	K_a	K_c	Q(1,-1)	R(1,1)	R(3,-1)	R(-1,3)
18	3	15	.0195	.0227	.0139	.0111	6	5	2	.0485	.0501		.0746
19	3	16	.0156	.0203	.0130	.0103	7	5	3	.0534	.0556		.0800
20	3	17	.0111				8	5	4	.0554	.0560		.0840
4	4	0		.0566		.0751	9	5	5	.0560	.0568		.0847
5	4	1	.0624	.0643		.0765	10	5	6	.0545	.0542		.0813
6	4	2	.0698	.0711	.0657	.0778	11	5	7	.0493	.0486		.0730
7	4	3	.0765	.0768	.0714	.0791	12	5	8	.0416	.0486		.0644
8	4	4	.0820	.0805	.0763	.0802	13	5	9	.0342	.0537		.0563
9	4	5	.0859	.0832	.0806	.0819	14	5	10	.0287	.0575		.0457
10	4	6	.0875	.0836	.0816	.0819	15	5	11	.0246	.0583		.0350
11	4	7	.0852	.0800	.0781	.0781	16	5	12	.0216	.0548		.0264
12	4	8	.0816	.0715	.0701	.0701	17	5	13	.0199	.0470		.0218
13	4	9	.0789	.0631	.0626	.0626	18	5	14	.0204	.0408		.0209
14	4	10	.0724	.0554	.0554	.0557	19	5	15	.0225	.0360		.0217
15	4	11	.0622	.0451	.0452	.0457	20	5	16	.0242			
16	4	12	.0537	.0347	.0348	.0355	6	6	1		.0363		.0535
17	4	13	.0472	.0272	.0260	.0268	7	6	2	.0396	.0411		.0573
18	4	14	.0401	.0250	.0202	.0207	8	6	3	.0450	.0473		.0619
19	4	15	.0318	.0250	.0167	.0166	9	6	4	.0482	.0491		.0645
20	4	16	.0188				10	6	5	.0489	.0489		.0686
5	5	0		.0445		.0623	11	6	6	.0477	.0464		.0708
6	5	1	.0489	.0505		.0644	12	6	7	.0435	.0407		.0713
7	5	2	.0549	.0568	.0519	.0660	13	6	8	.0370	.0341		.0673
8	5	3	.0592	.0592	.0553	.0641	14	6	9	.0304	.0320		.0590
9	5	4	.0626	.0624	.0593	.0627	15	6	10	.0255	.0358		.0519
10	5	5	.0651	.0630	.0618	.0626	16	6	11	.0222	.0412		.0464
11	5	6	.0681	.0662	.0659	.0660	17	6	12	.0198	.0455		.0397
12	5	7	.0722	.0698	.0690	.0693	18	6	13	.0178	.0471		.0316
13	5	8	.0738	.0705	.0698	.0699	19	6	14	.0159	.0446		.0190
14	5	9	.0709	.0666	.0657	.0658	20	6	15	.0145			
15	5	10	.0668	.0582	.0576	.0585	7	7	1		.0309		.0441
16	5	11	.0650	.0512	.0510	.0530	8	7	2	.0338	.0354		.0470
17	5	12	.0601	.0460	.0459	.0479	9	7	3	.0391	.0413		.0498
18	5	13	.0522	.0395	.0395	.0421	10	7	4	.0430	.0442		.0505
19	5	14	.0449	.0314	.0315	.0339	11	7	5	.0444	.0443		.0498
20	5	15	.0350				12	7	6	.0429	.0413		.0506
6	6	0		.0363		.0519	13	7	7	.0387	.0359		.0533
7	6	1	.0397	.0412		.0533	14	7	8	.0328	.0294		.0573
8	6	2	.0452	.0474	.0428	.0559	15	7	9	.0267	.0240		.0583
9	6	3	.0491	.0497	.0456	.0553	16	7	10	.0221	.0219		.0549
10	6	4	.0507	.0503	.0476	.0521	17	7	11	.0195	.0232		.0473
11	6	5	.0504	.0486	.0478	.0474	18	7	12	.0179	.0268		.0410
12	6	6	.0480	.0449	.0464	.0439	19	7	13	.0166	.0315		.0348
13	6	7	.0481	.0466	.0477	.0467	20	7	14	.0153			
14	6	8	.0533	.0524	.0521	.0523	8	8	1		.0271		.0380
15	6	9	.0583	.0568	.0565	.0566	9	8	2	.0299	.0317		.0412
16	6	10	.0602	.0580	.0577	.0578	10	8	3	.0351	.0373		.0436
17	6	11	.0576	.0547	.0543	.0543	11	8	4	.0392	.0404		.0436
18	6	12	.0533	.0470	.0467	.0470	12	8	5	.0407	.0406		.0416
19	6	13	.0518	.0407	.0406	.0428	13	8	6	.0391	.0376		.0378
20	6	14	.0473				14	8	7	.0349	.0323		.0348
7	7	0		.0309		.0438	15	8	8	.0293	.0264		.0358
8	7	1	.0338	.0354		.0460	16	8	9	.0237	.0210		.0409
9	7	2	.0392	.0414	.0369	.0480	17	8	10	.0192	.0175		.0454
10	7	3	.0431	.0443	.0400	.0482	18	8	11	.0166	.0163		.0471
11	7	4	.0447	.0446	.0416	.0459	19	8	12	.0155	.0165		.0447
12	7	5	.0435	.0417	.0408	.0412	20	8	13	.0149			
13	7	6	.0395	.0365	.0375	.0352	9	9	1		.0243		.0339
14	7	7	.0342	.0309	.0333	.0302	10	9	2	.0272	.0290		.0373
15	7	8	.0317	.0303	.0316	.0305	11	9	3	.0322	.0342		.0396
16	7	9	.0353	.0350	.0350	.0351	12	9	4	.0360	.0370		.0395
17	7	10	.0411	.0406	.0405	.0406	13	9	5	.0371	.0368		.0370
18	7	11	.0461	.0452	.0451	.0452	14	9	6	.0352	.0338		.0329
19	7	12	.0482	.0470	.0468	.0469	15	9	7	.0311	.0289		.0279
20	7	13	.0463				16	9	8	.0261	.0237		.0238
8	8	0		.0271		.0379	17	9	9	.0211	.0190		.0231
9	8	1	.0299	.0317		.0410	18	9	10	.0171	.0155		.0265
10	8	2	.0352	.0373	.0330	.0432	19	9	11	.0145	.0137		.0313
11	8	3	.0392	.0404	.0362	.0430	20	9	12	.0133			
12	8	4	.0407	.0406	.0376	.0409	10	10	1		.0221		.0309
13	8	5	.0392	.0376	.0363	.0366	11	10	2	.0250	.0267		.0343
14	8	6	.0350	.0324	.0326	.0311	12	10	3	.0297	.0314		.0362
15	8	7	.0295	.0265	.0278	.0256	13	10	4	.0328	.0336		.0358
16	8	8	.0240	.0215	.0233	.0216	14	10	5	.0333	.0328		.0331
17	8	9	.0210	.0200	.0210	.0205	15	10	6	.0311	.0297		.0291
18	8	10	.0225	.0223	.0224	.0225	16	10	7	.0272	.0254		.0244

continued

AD-A162 154 MICROWAVE AND INFRARED ABSORPTION PROPERTIES OF ATMOSPHERIC SPECIES WITH.. (U) LOWELL UNIV MA CENTER FOR ATMOSPHERIC RESEARCH R R GAMACHE JUL 85 ULRF-428/CAR 2/2

UNCLASSIFIED AFGL-TR-85-0168 F19628-82-K-0043 F/G 7/4 NL

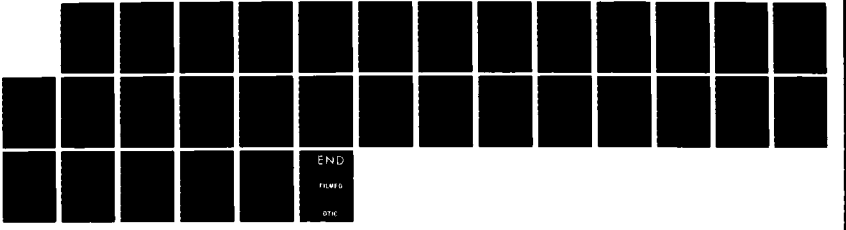

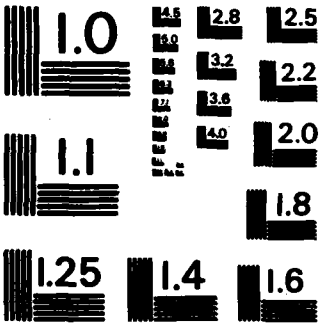

MICROCOPY RESOLUTION TEST CHART
NATIONAL BUREAU OF STANDARDS - 1963 - A

Table I. Continued

Initial State			Transition				Initial State			Transition			
J	K_a	K_c	Q(1,-1)	R(1,1)	R(3,-1)	R(-1,3)	J	K_a	K_c	Q(1,-1)	R(1,1)	R(3,-1)	R(-1,3)
19	8	11	.0265	.0264	.0263	.0265	17	10	8	.0228	.0209		.0201
20	8	12	.0315				18	10	9	.0187	.0170		.0169
9	9	0		.0243		.0339	19	10	10	.0154	.0141		.0160
10	9	1	.0272	.0290		.0373	20	10	11	.0131			
11	9	2	.0322	.0342	.0302	.0396	11	11	1		.0202		.0285
12	9	3	.0360	.0370	.0331	.0394	12	11	2	.0229	.0243		.0314
13	9	4	.0371	.0369	.0340	.0369	13	11	3	.0269	.0283		.0327
14	9	5	.0353	.0338	.0323	.0327	14	11	4	.0293	.0297		.0318
15	9	6	.0312	.0290	.0287	.0276	15	11	5	.0291	.0285		.0291
16	9	7	.0261	.0237	.0242	.0226	16	11	6	.0268	.0256		.0253
17	9	8	.0212	.0190	.0200	.0186	17	11	7	.0233	.0219		.0212
18	9	9	.0172	.0156	.0166	.0163	18	11	8	.0196	.0182		.0176
19	9	10	.0152	.0145	.0150	.0155	19	11	9	.0164	.0152		.0148
20	9	11	.0155				20	11	10	.0138			
10	10	0		.0221		.0309	12	12	1		.0184		.0260
11	10	1	.0250	.0267		.0343	13	12	2	.0207	.0217		.0281
12	10	2	.0297	.0314	.0277	.0362	14	12	3	.0239	.0249		.0288
13	10	3	.0328	.0336	.0301	.0357	15	12	4	.0254	.0256		.0275
14	10	4	.0333	.0328	.0303	.0331	16	12	5	.0248	.0243		.0249
15	10	5	.0311	.0297	.0283	.0290	17	12	6	.0226	.0217		.0216
16	10	6	.0272	.0254	.0249	.0244	18	12	7	.0198	.0187		.0183
17	10	7	.0228	.0209	.0211	.0200	19	12	8	.0169	.0158		.0155
18	10	8	.0187	.0170	.0176	.0165	20	12	9	.0144			
19	10	9	.0154	.0141	.0147	.0143	13	13	1		.0164		.0232
20	10	10	.0131				14	13	2	.0182	.0189		.0245
11	11	0		.0202		.0285	15	13	3	.0206	.0213		.0247
12	11	1	.0229	.0243		.0314	16	13	4	.0215	.0216		.0233
13	11	2	.0269	.0283	.0252	.0327	17	13	5	.0208	.0205		.0210
14	11	3	.0293	.0297	.0268	.0318	18	13	6	.0191	.0185		.0184
15	11	4	.0291	.0285	.0265	.0291	19	13	7	.0171	.0162		.0159
16	11	5	.0268	.0256	.0244	.0253	20	13	8	.0149			
17	11	6	.0233	.0219	.0214	.0212	14	14	1		.0144		.0201
18	11	7	.0196	.0182	.0184	.0176	15	14	2	.0157	.0162		.0209
19	11	8	.0164	.0152	.0156	.0147	16	14	3	.0174	.0179		.0208
20	11	9	.0138				17	14	4	.0180	.0182		.0196
12	12	0		.0184		.0260	19	14	6	.0168	.0164		.0160
13	12	1	.0207	.0217		.0281	20	14	7	.0153			
14	12	2	.0239	.0249	.0224	.0268	15	15	1		.0126		.0171
15	12	3	.0254	.0256	.0234	.0275	16	15	2	.0136	.0140		.0176
16	12	4	.0248	.0243	.0226	.0249	17	15	3	.0148	.0154		.0175
17	12	5	.0226	.0217	.0208	.0216	19	15	5	.0162	.0163		.0158
18	12	6	.0198	.0187	.0185	.0183	20	15	6	.0156			
19	12	7	.0169	.0158	.0163	.0155	16	16	1		.0111		.0145
20	12	8	.0144				17	16	2	.0121	.0127		.0151
13	13	0		.0164		.0232	19	16	4	.0150	.0133		.0156
14	13	1	.0182	.0189		.0245	20	16	5	.0119			
15	13	2	.0206	.0213	.0194	.0247	17	17	1		.0100		.0130
16	13	3	.0215	.0216	.0199	.0233	19	17	3	.0114	.0114		.0137
17	13	4	.0208	.0205	.0194	.0210	20	17	4	.0095			
18	13	5	.0191	.0185	.0184	.0184	18	18	1				.0114
19	13	6	.0171	.0162	.0170	.0159	19	18	2				.0095
20	13	7	.0149										
14	14	0		.0144		.0201							
15	14	1	.0157	.0162		.0209							
16	14	2	.0174	.0179	.0167	.0208							
17	14	3	.0180	.0182	.0175	.0196							
18	14	4		.0176	.0173								
19	14	5	.0168	.0164	.0150	.0160							
20	14	6	.0153										
15	15	0		.0126		.0171							
16	15	1	.0136	.0140		.0176							
17	15	2	.0148	.0154	.0141	.0175							
19	15	4	.0162	.0163	.0144	.0158							
20	15	5	.0156										
16	16	0		.0111		.0145							
17	16	1	.0121	.0127		.0151							
19	16	3	.0150	.0133		.0156							
20	16	4	.0119										
17	17	0		.0100		.0130							
19	17	2	.0114	.0114		.0137							
20	17	3	.0095										
18	18	0	.0095	.0132		.0114							
19	18	1	.0095	.0120		.0095							

quadrupole moment value of the perturber to fit a calibration line (for example, see Ref. 25).

All that remains is to evaluate b_0, the minimum impact parameter; this is obtained by solving the implicit equation

$$s_{if,J_2}(b_0) = 1. \tag{10}$$

The formulas in this section provide a complete description of the theory except for the introduction of the parameter b_{min} employed in the earlier calculations of Benedict and Kaplan.[25] This minimum physically believable value of the cutoff is used as follows: if $b_{min} < b_0$ [as determined by Eq. (10)] use b_0 in the calculation, otherwise use b_{min} in place of b_0. The dependence of the results on the choice of b_{min} for the H_2O–N_2 system is discussed below.

In Ref. 26 it was found that, to obtain a fit to the very narrow (high J) lines measured by Eng *et al.*,[18–20] it was necessary to reduce the constant b_{min} to a value of the order of 1.4 Å. This is much smaller than the Benedict and Kaplan choice of 3.2 Å and can really only be regarded as a phenomenological adjustment. In addition, for intermediate J lines it was found that the choice, b_{min} = 1.4 Å, tended to underestimate the halfwidths for a number of transitions. Therefore, in compiling the present results for the AFGL Atlas, it was decided to use a compromise value of b_{min} = 1.75 Å. It should also be noted, from the results presented in Ref. 26, that the strong (low J) lines are totally insensitive to reducing b_{min} below the Benedict and Kaplan value of 3.2 Å. Therefore, for the results presented in this paper, one may anticipate that the choice of b_{min} plays a minor role for transitions with various $J \lesssim 10$.

III. Results and Summary

Calculations of N_2-broadened halfwidths were performed for ground state transitions of $H_2{}^{16}O$. Wave functions were calculated using a Watson-type Hamiltonian and the constants provided by Clough.[29] The reduced dipole matrix elements for H_2O were evaluated using the expansion of μ given by Clough *et al.*[30]

The quadrupole moment of N_2, $Q = 3.04 \times 10^{-26}$ esu cm^2, was taken from Stogryn and Stogryn.[31] In all the calculations, b_{min} was set at 1.75×10^{-8} cm and the reduced mass used in Eq. (1) is 1.832×10^{-23} g.

Using the 5,2,3 → 6,1,6 microwave line studied by Becker and Autler,[8] corrected to air according to $\gamma_{N_2} = 1.1045\ \gamma_{air} \simeq 0.0961$ cm^{-1}/atm,[20] as a calibration line we fix the scaling parameter α at 2.79.

In Table I the resulting N_2-broadened halfwidths are presented in units of cm^{-1}/atm. The initial state quantum numbers, J, K_a, and K_c are given and the halfwidths are listed as a function of the type of transition, i.e., ΔJ (ΔK_a,ΔK_c), from the initial state. The table lists halfwidths for $Q(1,-1)$, $R(1,1)$, $R(3,-1)$, and $R(-1,3)$ transitions. Using the relations

$$\gamma[Q(1,-1)] = \gamma[Q(-1,1)], \tag{11}$$

and

$$\gamma[R(\Delta K_a,\Delta K_c)] = \gamma[P(-\Delta K_a,-\Delta K_c)], \tag{12}$$

halfwidths for P and $Q(-1,1)$ transitions can be obtained. The listing is further broken up into even and odd ($J + K_a + K_c$) initial states.

In summary we have calculated N_2-broadened halfwidths for ground state transitions of H_2O via quantum Fourier transform theory. The importance of accurate halfwidths for applications in infrared remote sensing or spectral analysis is well established.[32–34] The results in Table I have been used to generate a halfwidth data base for some 1600 transitions.

Using the relationship given in Ref. 20,

$$\gamma_{air} = 0.90\ \gamma_{N_2}, \tag{13}$$

we have generated air-broadened halfwidths for water. These halfwidths form the data base for H_2O for the AFGL main gas compilation.[5] In the compilation, the vibrational dependence is assumed negligible and the above air-broadened widths have been added to all water bands below 13000 cm^{-1} in the Atlas.

In general, the halfwidths presented here have a relative accuracy of ≈15% with some high J transitions and weak intensity transition being somewhat less accurate.

We would like to thank S. A. Clough and L. S. Rothman for their helpful comments and suggestions. We would also like to thank Justinne Gamache for proofing the table of halfwidths.

This work was supported by the Air Force Office of Scientific Research through AFGL task 2310G1.

References

1. H. L. Hackforth, *Infrared Radiation* (McGraw-Hill, New York, 1960).
2. V. E. Zuev, *Atmospheric Transparency in the Visible and the Infrared* (Keter, Jerusalem, 1970).
3. S. A. Clough, F. X. Kneizys, L. S. Rothman, and W. O. Gallery, Proc. Soc. Photo-Opt. Instrum. Eng. **277**, 152 (1981).
4. J. H. Van Vleck and D. L. Huber, Rev. Mod. Phys. **49**, 939 (1977).
5. L. S. Rothman, R. R. Gamache, A. Barbe, A. Goldman, J. R. Gillis, L. R. Brown, R. A. Toth, J.-M. Flaud, and C. Camy-Peyret, Appl. Opt. **22**, 2247 (1983).
6. L. S. Rothman, A. Goldman, J. R. Gillis, R. R. Gamache, H. M. Pickett, R. L. Poynter, N. Husson, and A. Chedin, Appl. Opt. **22**, 1616 (1983).
7. See Ref. 5 and references therein, especially the work of C. Camy-Peyret, J. M. Flaud, and R. Toth.
8. G. E. Becker and S. H. Autler, Phys. Rev. **70**, 300 (1946).
9. H. J. Liebe and T. A. Dillon, J. Chem. Phys. **50**, 727 (1969).
10. J. R. Rusk, J. Chem. Phys. **42**, 493 (1965).
11. R. Emery, Infrared Phys. **12**, 65 (1972).
12. L. Frenkel and D. Woods, Proc. IEEE **54**, 498 (1966).
13. J. E. Pearson, D. T. Llewellyn-Jones, and R. J. Knight, Infrared Phys. **9**, 53 (1969).
14. R. B. Sanderson and N. Ginsburg, J. Quant. Spectrosc. Radiat. Transfer **3**, 435 (1963).
15. J. R. Izatt, H. Sakai, and W. S. Benedict, J. Opt. Soc. Am. **59**, 19 (1969).
16. M. C. Guerra, M. Ketabi, A. Sanchez, M. S. Feld, and A. Javan, J. Chem. Phys. **63**, 1317 (1975).
17. F. A. Blum, K. A. Nill, P. L. Kelley, A. R. Calawa, and T. C. Harman, Science **177**, 694 (1972).
18. R. S. Eng, A. R. Calawa, T. C. Harman, P. L. Kelley, and A. Javan, Appl. Phys. Lett. **21**, 303 (1972).

19. R. S. Eng, P. L. Kelley, A. Mooradian, A. R. Calawa, and T. C. Harman, Chem. Phys. Lett. 19, 524 (1973).
20. R. S. Eng, P. L. Kelley, A. R. Calawa, T. C. Harman, and K. W. Nill, Mol. Phys. 28, 653 (1974).
21. C. K. N. Patel, Phys. Rev. Lett. 28, 649 (1972).
22. R. A. Toth, J. Quant. Spectrosc. Radiat. Transfer 13, 1127 (1973).
23. R. W. Davies, Phys. Rev. A 12, 927 (1975).
24. C. J. Tsao and B. Curnutte, J. Quant. Spectrosc. Radiat. Transfer 2, 41 (1962).
25. W. S. Benedict and L. D. Kaplan, J. Chem. Phys. 30, 388 (1959); J. Quant. Spectrosc. Radiat. Transfer 4, 453 (1964).
26. R. W. Davies and B. A. Oli, J. Quant. Spectrosc. Radiat. Transfer 20, 95 (1978).
27. J. Y. Mandin, J. M. Flaud, C. Camy-Peyret, and G. Guelachvili, J. Quant. Spectrosc. Radiat. Transfer 23, 351 (1980).
28. G. Yamamoto and T. Aoki, J. Quant. Spectrosc. Radiat. Transfer 12, 227 (1972).
29. S. A. Clough (AFGL) private communication and R. R. Gamache (ULCAR), unpublished.
30. S. A. Clough, Y. Beers, G. P. Klein, and L. S. Rothman, J. Chem. Phys. 59, 2254 (1973).
31. D. E. Stogryn and A. P. Stogryn, Mol. Phys. 11, 371 (1966).
32. M. A. H. Smith and L. L. Gordy, J. Quant. Spectrosc. Radiat. Transfer 29, 413 (1983).
33. J. M. Hoell, C. N. Harward, C. H. Bair, and B. S. Williams, Opt. Eng. 21, 548 (1982).
34. N. Monnanteuil and J. M. Colmont, J. Quant. Spectrosc. Radiat. Transfer 29, 131 (1983).

B4.

THEORETICAL N2-, O2-, AND AIR-BROADENED HALFWIDTHS OF OZONE CALCULATED BY QUANTUM FOURIER TRANSFORM THEORY WITH REALISTIC COLLISION DYNAMICS.

Robert R. Gamache, The Center for Atmospheric Research, The University of Lowell, Lowell, MA 01854 USA
Richard W. Davies, GTE/Sylvania Laboratories, Waltham, MA 02154 USA
Laurence S. Rothman, Air Force Geophysics Laboratory, Hanscom AFB, Bedford, MA USA

Abstract

We have evaluated collision broadened halfwidths of ozone with nitrogen, oxygen, and air as the perturbing gases. We show that it is important to consider more realistic collision dynamics in the calculations. By replacing the classical path trajectories by linear trajectories with constant velocities chosen to give the equations of motion exact to first order in time we develop the interruption function in terms of the actual distance of closest approach determined by the intermolecular potential and the velocity at this point. This improvement to the theory results in halfwidths which are in good agreement with experimental measurements. The temperature dependence of the halfwidth has been determined for 126 transitions for N_2-broadening and for 10 transitions for O_2-broadening. Comparison with experimental measurements is given.

1. INTRODUCTION

Because of its importance to our planet, the nature of ozone in the atmosphere must be well understood. One of the more powerful methods to study atmospheric ozone and monitor its concentration is infrared remote sensing of total column density and concentration-altitude profiles. To implement remote sensing techniques an accurate knowledge of the wavenumber, intensity, and collision broadened halfwidth of ro-vibrational transitions is necessary. Unfortunately most spectroscopic studies have concentrated on obtaining wavenumbers, strengths, and assignments. Relatively few studies have reported collisional broadened halfwidths of ozone (1-5). Together they total some hundred and fifty transitions only.

For ozone some theoretical calculations of collision broadened halfwidths have been performed (6-8). The calculations are difficult owing to the types of interactions that must be considered for ozone. In the first two studies (6-7) the molecular quadrupole constants were not well known, producing inaccurate results. The last study (8) did use improved quadrupole moment components, however only ten transitions were studied. In all of these studies the classical path Anderson-Tsao-Curnutte (ATC) method was used to determine the halfwidths, and the corresponding pressure shifts were not evaluated. We have performed conventional ATC calculations on ≈135 transitions which have been experimentally studied and find the theoretical values some 20 to 35% too low. In order to better interpret infrared remote sensing results for ozone, collision broadened halfwidths must be determined more accurately and for a broad range of transitions.

In this paper we report halfwidths and shifts for N_2- and O_2-, and air- broadening of ozone calculated by the ATC method and by the quantum Fourier transform (QFT) method with improved dynamics, ATC-ID and (QFT-ID) respectively. These theories are refined to consider more realistic collision dynamics than those obtained from classical straight path trajectories and yield much better agreement with experiment. The application of approximate trajectories in binary collision calculations was first done by Tipping and Herman (9). Their method and extensions of the method have been applied by Bonamy et. al. (10) and by Berard and Lallemand (11). In all studies, improved results were obtained using these methods.

2. THEORY

In Reference 12 a complete description of the QFT-ID theory is given, here we summarize the main features of the theory. As a starting point we take the classical path ATC method or QFT method which considers an anisotropic interaction between the radiating and perturbing molecules which is treated in the usual second order perturbation theory. As an improvement in the theory we consider approximate trajectories which better represent actual trajectories and which are described by an isotropic potential. Here as in other works (9-11) which use approximate trajectories a Lennard-Jones potential is used. The resulting equations of motion can be solved by expanding in a time series (t=0 at r=the distance of closest approach) and evaluating the integrals numerically. For ozone-perturbing gas systems this approach is too difficult and time consuming so we must rely on approximations.

The approach adopted here is to use linear trajectories with constant velocities chosen such that the equations of motion are correct to first order in time. This corresponds to replacing b (impact parameter) and v in the interruption function by the distance of closest approach r_c and the relative velocity at this point v_c as determined from the potential. This is shown in figure 1 where the classical path at b (straight solid line) is related to the first order in time trajectory at r_c (straight dashed line) by the actual trajectory (curved line) determined by a potential.

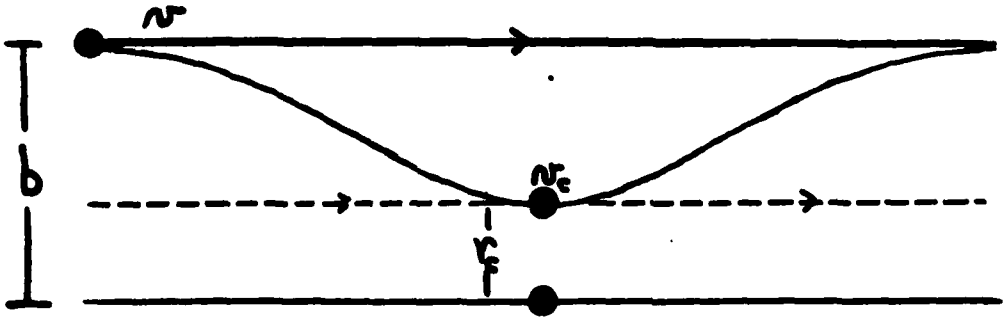

Figure 1 Comparison of classical path, first order in time and actual trajectories.

Before the interruption function can be evaluated the classical parameters b and v must be related to the distance of closest approach r_c and the relative velocity v_c. This is accomplished through the equations for conservation of energy and momentum in the collision.

3. CALCULATIONS

We have performed calculations via QFT-ID theory on the O_3-N_2 and O_3-O_2 systems. In these calculations we have considered the dipole(O_3)-quadrupole(N_2 or O_2) interaction(d-q) and the quadrupole(O_3)-quadrupole(N_2 or O_2) interaction(q-q). Explicit vibrational dependence was taken into account for the ground, ν_1 and ν_3 states of ozone using very accurate Hamiltonian constants for these states (12). The molecular constants used in the calculations are given in Ref. 12 and are in all cases reproducible and confirmed by several studies. In all calculations, the d-q and q-q interactions arising from Anderson's $S_{2\text{middle}}$ term were also included. For the QFT theory, as in ATC theory, the numerical coefficients for the middle term are just twice those given for the outer terms. The asymmetric quadrupole moment of O_3 was included using precisely the same formalism as developed by Yamamoto and Aoki (6), and our definition of quadrupole moment components is identical to theirs.

In all calculations the temperature was fixed at 296 K. The QFT scaling parameter, α, was adjusted to give the best fit to the theoretical halfwidth of three transitions computed using the ATC method, including velocity averaging. Thus the theories are on the same footing with no experimental bias in the QFT results.

4. DISCUSSION AND CONCLUSION

The assumption of linear trajectories with a constant velocity chosen to give the equations of motion correct to first order in time has produced results for N_2- and O_2-broadening well within 10% of experiment. For N_2 as the perturbing gas we can compare our results with 127 experimental measurements from Refs. 3 and 5. The average percent error for the QFT-ID calculations was 8.4% with a standard deviation of the halfwidths of 0.0086 cm^{-1}. A better comparison of the two theories can be obtained by using only the data of Meunier, Marché, and Barbe which contains error bars for each measurement and is more accurate than that of reference 5. In figure 2 we present a comparison of the QFT-ID and velocity averaged ATC-ID N_2-broadened result with the 9 $\nu_1+\nu_3$ lines studied. The average absolute percent difference (AAPD) from the QFT-ID results compared with experiment is 2.3% with a maximum difference of 4.2%. As presented above, the comparison with the complete set of 127-transitions studied does not give as good agreement, however the accuracy of most of this data is $\pm$10% whereas the accuracy of Meunier et. al. for N_2-broadening is better than $\pm$4.4%. We note most of the QFT-ID results are within or close to the error bars on the measurements of Meunier et. al., with the largest discrepancy observed being just under 0.003 cm^{-1}/atm.

In addition to the N_2-broadening, the work of Meunier et.al. contains results for O_2- and air-broadening as well. We present a comparison of our calculations with experiment in Figure 3 for O_2 as the perturbing gas, and in Figure 4 for air-broadening. For O_2-broadening Meunier et. al.'s results are accurate to 8.8%. Our QFT-ID results have an average absolute percent difference of 7.3% with the largest discrepancy being 15.6%. The QFT-ID results are quite satisfactory considering the nature of the O_2-broadening calculations. Although the air-broadening results of Meunier et. al. does not list error bars, one can estimate the accuracy to be slightly greater than 5%, the QFT-ID results agree very well with the measurements, 2.0% AAPD with a 3.9% maximum difference.

A final parameter derived from this study is the ratio of air broadening to nitrogen broadening, the usefulness of this parameter arises

from the method in which air-broadened results are usually generated, i.e. N_2-broadened results are calculated and then scaled to air-broadened values. This method saves the time necessary to calculate O_2-broadened results and is sometimes necessary since the results for O_2 calculations are more questionable. From the calculations for the 127 transitions, we find a very constant air/N_2 ratio with an average of 0.95 and a standard deviation of 0.0056. This compares well with Meunier et. al.'s value of 0.94.

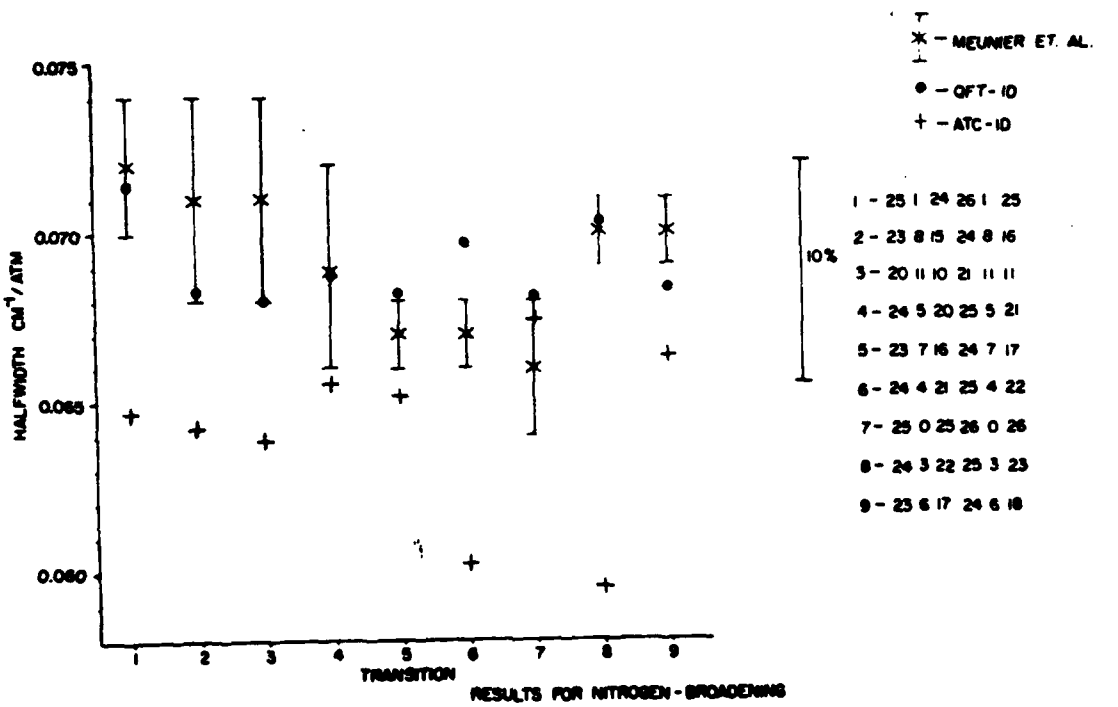

Figure 2 Comparison of QFT-ID, ATC-ID, and experimental results for N_2-broadening.

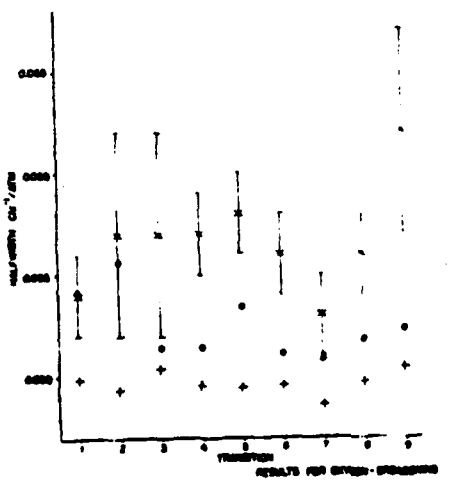

Figure 3

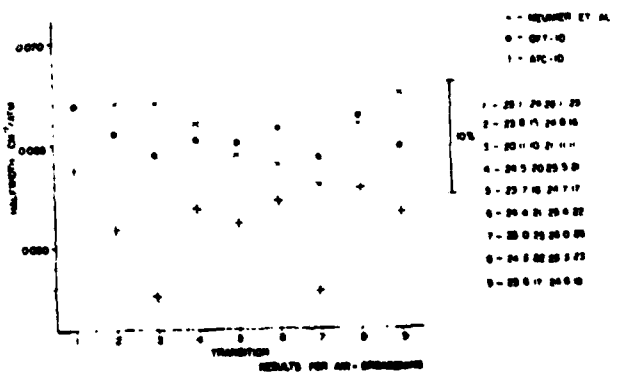

Figure 4

Comparison of QFT-ID, ATC-ID, and experimental results for O_2- and air-broadening respectively.

We have studied the temperature dependence of 125 transitions of O_2 broadened by N_2 and 10 transitions broadened by O_2. The transitions were chosen to consider a wide range of ", J_a", and to compare with experiment when possible. Nine temperatures were studied for N_2 broadening from 200-1000 K and nine for O_2 broadening from 171-500 K. The temperature dependence is given by the exponent n in the formula

$$\gamma(T) = \gamma(T_0) \left[\frac{T_0}{T}\right]^n \quad . \tag{1}$$

We have calculated n for each transition and find for N_2-broadening an average value of $\bar{n}$=0.77(0.04) (We note that one line did not give a value close to the average). For O_2 broadening we find an average of $\bar{n}$=1.08(0.04). These values compare well with the value of n reported in Ref 13 for N_2-broadening (0.71) and with the value of n reported in Ref 14 for O_2-broadening (1.3), however Ref 13 gives a value of n of 0.30 for O_2-broadening. Our values also compare well with the theoretical values from ATC calculations reported in reference 8.

REFERENCES

1. M. Lichtenstein, J.J. Gallagher, and S.A. Clough, J. Mol. Spectrosc. 40, 10(1971).
2. J.M. Hoell, C.N. Harward, C.H. Bair, and B.S. Williams, Optical Engineering, May/June (1982).
3. C. Meunier, P. Marché, and A. Barbe, J. Mol. Spectrosc. 95, 271(1982).
4. S. Lundqvist, J. Margolis, and J. Reid, Appl. Opt. 21, 3109(1982).
5. J. Margolis, J. Quant. Spectrosc. Radiat. Transfer 29, 539(1983).
6. G. Yamamoto and T. Aoki, J. Quant. Spectrosc. Radiat. Transfer 12, 227(1972).
7. G.T.D. Tejwani and E.S. Yeung, J. Chem. Phys. 63, 1513(1975).
8. J.-Y. Mandin, J.-M. Flaud and C. Camy-Peyret, "Calculs de Coefficients d'Elargissement de la Molecule D'Ozone." Final Report, CNRS,Baitment 221, Campus d'Orsay, (1983).
9. R.H. Tipping and R.M. Herman, J. Quant. Spectrosc. Radiat. Transfer 10, 897(1970), and references therein.
10. J. Bonamy, L. Bonamy, and D. Robert, J. Chem. Phys. 67, 4441(1977).
11. M. Berard and P. Lallemand, J. Quant. Spectros. Radiat. Transfer 19, 387(1978)
12. R.R. Gamache and R.W. Davies,"Theoretical N_2-, O_2-, and Air-Broadened Halfwidths of Ozone Calculated By Quantum Fourier Transform Theory with realistic Collision Dynamics." submitted to J. Mol. Spectrosc. July(1984).
13. J.M. Colmont and N. Monnanteuil, J. Mol. Spectrosc. 104, 122(1984).
14. A. Barbe, P. Marché, C. Meunier and P.Jouve, J. Physique 44(1983).

ACKNOWLEDGEMENTS

We would like to acknowledge the following colleagues for stimulating discussions and for their encouragement: S. A. Clough, and R. H. Tipping.

This work was supported by the Air Force Office of Scientific Research through AFGL task 2310G1.

B5.

JOURNAL OF MOLECULAR SPECTROSCOPY 109, 283–299 (1985)

Theoretical N_2-, O_2-, and Air-Broadened Halfwidths of $^{16}O_3$ Calculated by Quantum Fourier Transform Theory with Realistic Collision Dynamics

ROBERT R. GAMACHE

The Center for Atmospheric Research, University of Lowell Research Foundation, 450 Aiken Street, Lowell, Massachusetts 01854

AND

RICHARD W. DAVIES

GTE/Sylvania, 40 Sylvan Road, Waltham, Massachusetts 02154

We have evaluated collision-broadened halfwidths of ozone with nitrogen and oxygen as the perturbing gases. Calculations using conventional Anderson theory or quantum Fourier transform theory are shown to be some 25 to 35% too low when compared to the experimental measurements. We show that it is important to consider more realistic collision dynamics in the calculations. By replacing the classical path trajectories by linear trajectories with constant velocities chosen to give the equations of motion exact to first order in time, we develop the interruption function in terms of the actual distance of closest approach determined by the intermolecular potential and the velocity at this point. This improvement to the theory results in N_2- and O_2-broadened halfwidths which are in good agreement with the experimental measurements. Air-broadened halfwidths have been evaluated from the nitrogen and oxygen results via the formula $\gamma_{air} = 0.79\gamma_{N_2} + 0.21\gamma_{O_2}$. The results agree with the air-broadened measurements to better than 5%.

1. INTRODUCTION

Ozone is a minor constituent of the earth's atmosphere. It has been detected by its odor during thunderstorms since the earliest times. (Both "The Iliad" and "The Odyssey" of Homer give mention of this.) When giving a name to the gas in the mid 1800s, Schönbein chose the name ozone, which is from the Greek, Οζειν, to smell (*1*). Ozone plays a prominent role in relation to climate and air chemical cycles of the earth. Its concentration in the atmosphere depends on the season, time of day, altitude, and local conditions, and is usually below 2×10^{-8} vol/vol air, with some smog-infected areas recording levels some 50 times higher.

The concentration of ozone rises appreciably with altitude, reaching a maximum at approximately 25 km. It is produced mainly by high-altitude photochemical synthesis of molecular oxygen. However, some is formed at low altitudes in polluted areas. Ozone takes part in many atmospheric chemical reactions as a reactant and as a catalyst. The layer at 25 km is a very efficient absorber of solar ultraviolet radiation (less than 300 mμ) and protects life on earth from the harmful effects of

0022-2852/85 $3.00

these rays. The layer is very warm due to the heat generated by light absorption and by the exothermic decomposition of ozone; thus, it plays an important part in the temperature regulation of the lower atmosphere.

It took 20 years after Schönbein named the blueish gas ozone before its atomic formula, O_3, was established. Its structure was thought to be an equilateral triangle until, in the early 1950s, microwave spectrum investigations (*2*) determined ozone to be an asymmetric molecule with an O–O bond length of 1.278×10^{-8} cm and an angle of 116°49′ between the central and outer atoms. The O_3 molecule is an asymmetric rotor and is shown in Fig. 1 with its principle axies of inertia. The dipole moment of ozone as determined from microwave data (*3*) is 0.53×10^{-18} esu-cm, and the quadrupole moment components, as determined from molecular beam spectroscopy (*4*), are $\theta_{aa} = -1.4 \times 10^{-26}$, $\theta_{bb} = -0.7 \times 10^{-26}$, and $\theta_{cc} = 2.1 \times 10^{-26}$ esu-cm^2.

Because of its importance to our planet, the nature of ozone in the atmosphere must be well understood. One of the more powerful methods to study atmospheric ozone and monitor its concentration is infrared remote sensing of total column density and concentration–altitude profiles. To implement remote sensing techniques an accurate knowledge of the wavenumber, intensity, and collision-broadened halfwidth of rovibrational transitions is necessary (*5*). Unfortunately, most spectroscopic studies have concentrated on obtaining wavenumbers, strengths, and assignments. Relatively few studies have reported collisional-broadened halfwidths of ozone (*3, 6–9*). Together they total some 150 transitions only.

For ozone some theoretical calculations of collision-broadened halfwidths have been performed (*10–12*). The calculations are difficult owing to the types of interactions that must be considered for ozone (because of its small dipole moment, the quadrupole–quadrupole interaction must be considered as well as the dipole–quadrupole interaction for any meaningful calculation). In the first two studies (*10, 11*) the molecular quadrupole constants were not well known, producing inaccurate results. The last study (*12*) did use improved quadrupole moment components; however, only 10 transitions were studied. In all of these studies the classical path Anderson–Tsao–Curnutte (ATC) method (*13*) was used to determine the halfwidths, and the corresponding pressure shifts were not evaluated. We have performed conventional ATC calculations on ≈135 transitions which have been experimentally studied, and found the theoretical values some 20 to 35% too low.

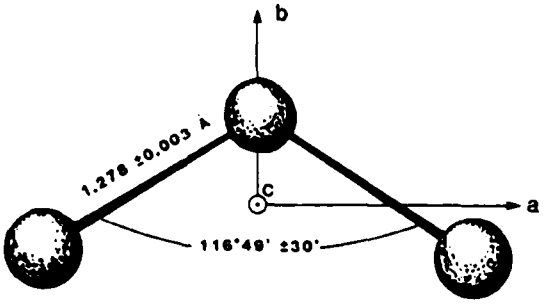

FIG. 1. Ozone molecule with its principal axes of inertia.

In order to better interpret infrared remote sensing results for ozone, collision-broadened halfwidths must be determined more accurately and for a broad range of transitions.

In this paper we report halfwidths and shifts for N_2-, O_2-, and air-broadening of ozone calculated by the ATC method and by the quantum Fourier transform (QFT) method (*14*). We further refine the theories to consider more realistic collision dynamics than those obtained from classical straight-path trajectories. Much better agreement with experiments results from this method. The application of approximate trajectories in binary collision calculations was first done by Tipping and Herman (*15–17*). Their method and extensions of the method have been applied by Bonamy *et al.* (*18*) and by Berard and Lallemand (*19*). In all studies, improved results were obtained using these methods.

In section 2 we discuss the ATC and QFT methods and the kinematic corrections considered. In section 3 results are presented for the conventional and improved dynamics (ID) calculations; this is followed by a discussion of the results in section 4.

2. THEORY

Both the pressure-induced shift and the pressure-broadening of a spectral line arise because of collisions between the radiating molecule and some perturbing gas molecules. In order to fully understand these properties, the exact dynamics of the molecular motions and the interactions at each point should be determined. This is much too difficult to do, especially if many transitions are to be studied; thus, we must rely on approximations. The first assumptions made are the so-called binary collision and impact approximations i.e., we are dealing with uncorrelated two-body collisions. Next, we assume that the kinetic energies are large enough so that we can make use of classical mechanics to describe the motions of the centers of gravity of the colliding particles. This limits the exchange of energy between kinetic and internal degrees of freedom to a very small fraction of the kinetic energy. In what follows, we assume an isotropic interaction which can be treated using classical trajectories, and an anisotropic interaction which is treated in the usual second-order perturbation theory.

The width and shift of a spectral transition $i \rightarrow f$ are given in terms of the real and imaginary part of the spectral power density of the perturbation;

$$\gamma(\mathrm{cm}^{-1}/\mathrm{atm}) = +\frac{1}{2\pi c} Re\{P_{if}(\omega)\} \tag{1}$$

and

$$\Delta\omega(\mathrm{cm}^{-1}/\mathrm{atm}) = -\frac{1}{2\pi c} Im\{P_{if}(\omega)\} \tag{2}$$

where c is the speed of light. From the equations of motion of classical mechanics $\vec{r}(t)$ and $\vec{\theta}(t)$ are obtained for each trajectory, labeled by its initial relative velocity, v, and impact parameter, b. The effect of collisions is obtained, using these trajectories, by averaging over angular orientations of the molecules, integrating over impact parameters, and finally by averaging over the relative velocity using the Maxwell–Boltzmann velocity distribution function $f(v)$. This gives

$$P_{if}(\omega) = n \int_0^\infty v f(v) dv \int_0^\infty 2\pi b db S_{if}(b, v), \tag{3}$$

where n is the number density of the perturbers and $S_{if}(b, v)$ is the interruption (or collision efficiency) function. It is the evaluation of the interruption function that is central to the solution of the problem; it depends on the initial and final state of the radiating molecule, the perturbing molecule, the type and number of interactions involved, and the collision dynamics.

With the assumption of an isotropic potential, the dynamics of the collisions are described in terms of plane trajectories that are determined by the impact parameter, b, and the initial relative velocity, v (or the total energy of motion $E = 1/2\mu v^2$, where μ is the reduced mass of the system). The equations of motion are given in polar coordinates by

$$\dot{\theta} = \frac{bv}{r^2},$$

and

$$\dot{r} = v \sqrt{1 - \frac{b^2}{r^2} - \frac{\phi(r)}{E}}. \tag{4}$$

The distance of closest approach $r_c(b, E)$ is obtained from the equation (which is a statement of conservation of energy),

$$1 - \frac{b^2}{r^2} - \frac{\phi(r)}{E} = 0. \tag{5}$$

The potential $\phi(r)$, in general, contains both an attractive and repulsive term, and Eq. (5) may have several solutions. Here only the largest r_c solution is retained, thereby discarding trajectories that correspond to stable or metastable bound states. In this work, as in other works (*15–20*) which use approximate trajectories to better represent actual trajectories, a Lennard–Jones potential is chosen:

$$\phi(r) = 4\epsilon\left[\left(\frac{\sigma}{r}\right)^{12} - \left(\frac{\sigma}{r}\right)^{6}\right]. \tag{6}$$

The above equations can be solved by expanding r and θ in a time series ($t = 0$ at $r = r_c$) and then evaluating the integrals numerically. This is very difficult and has only been carried out for some simple systems (*19*). Most treatments have been based on approximations to the dynamics.

The approximation that is made in most calculations using the ATC method is simply not to include the isotropic intermolecular potential ($\epsilon = 0$). This corresponds to the use of classical straight line trajectories in the theory, i.e.,

$$r(t) = \sqrt{b^2 + v^2 t^2}; \qquad \theta(t) = \arctan(vt/b). \tag{7}$$

This yields an interruption function, $S_{if}(b, v)$, dependent on the impact parameter and relative velocity which straightforwardly goes into Eq. (3) to evaluate the perturbation operator.

Although some (*15–17, 21*) have explicitly evaluated the velocity integral in Eq. (3), the usual procedure is to make the further assumption that the interruption

function is roughly independent of velocity. This allows the velocity integral to be done analytically, resulting in evaluation at the mean relative thermal velocity, $\bar{v} = (8kT/\pi\mu)^{1/2}$, where k is the Boltzmann constant and T is the temperature in degrees Kelvin. The solution is now contained in the impact parameter integral, which is solved via the conventional cutoff approach (*13, 15–17*). This gives a solution expressed in terms of Anderson's integrated resonance functions, F and $\tilde{F}$, and the cutoff parameter b_0. The exact form of the resonance functions and interruption functions (i.e., $S(b, v)$, for example) depends on the system and the types of interactions being considered, e.g., dipole–dipole, induction–dispersion, etc. Tabulations of the interruption functions and resonance functions for a variety of intermolecular potentials can be found in the literature (*22–24*); the last reference by Leavitt (*24*) contains formulas for symmetric and asymmetric top molecules.

Another approach to pressure shifts and collisional broadening is the quantum Fourier transform theory (QFT) developed by one of the authors (*14*). This is a quantum theory, developed using graphical perturbation theory, which proceeds by making use of the Fourier transform of the multipole interactions. Within the context of second-order perturbation theory in the anisotropic interaction (e.g., the multipole interaction), energy and momentum are rigorously conserved in the collision process. The theory is somewhat simpler to use in actual calculations than the ATC method, owing to the fact that the velocity averaging can be done analytically and the resulting resonance functions have a simpler form than the corresponding ATC resonance functions $f(k)$, $F(k)$. The QFT method has been cast (*25*) into a form similar to the ATC approach; in analogy with Eq. (3), we may write

$$P_{if} = n\bar{v}\int_0^\infty 2\pi b db S_{if}(b, \bar{v}), \tag{8}$$

where $\bar{v}$ is the means relative thermal velocity. In this connection, it should be stated that a velocity average similar to that indicated in Eq. (3) has already been carried out, and $\bar{v}$ has been used to replace temperature via $\bar{v} = (8kT/\pi\mu)^{1/2}$ in order to make the correspondence with Anderson's approach more explicit. The interruption function, $S_{if}(b, \bar{v})$, is of the same form as in ATC theory; however, the coefficients and resonance functions for the interactions are quite different. Reference (*25*) gives the relationship between the ATC and QFT coefficients and resonance functions for the dipole–dipole, dipole–quadrupole, and quadrupole–quadrupole interactions. The method of solving Eq. (8) is similar to the ATC approach, i.e., a cutoff is determined at the point where the real part of the QFT interruption function equals unity and the remaining integral is evaluated via QFT resonance functions.

Both the classical straight-path ATC method and the original QFT method contain no allowance for an isotropic potential in the dynamics. In order to better approximate the collision process, more realistic trajectories should be employed in the calculations, and here we have attempted to do this while keeping the time involved in performing a calculation small enough that many transitions can be considered. A first approach to this is to use linear trajectories with constant velocities chosen to give values of θ and r exact to first order in time (*15–17, 19*), i.e.,

$$\vec{r}(t) = \vec{r}_c + \vec{v}_c t$$

with

$$\vec{v}_c = \dot{r}(t = 0),$$

so that

$$v_c = r_c \dot{\vartheta}(0) = \frac{bv}{r_c}. \tag{9}$$

Thus

$$r(t) = \sqrt{r_c^2 + v_c^2 t^2}; \qquad \theta(t) = \arctan \frac{v_c t}{r_c}, \tag{10}$$

where r_c and v_c correspond to the distance of closest approach and the relative velocity at this point. Using equations of motion which are exact to first order in time gives an interruption function dependent on these parameters, i.e., $S(r_c, v_c)$. In order to evaluate the interruption functions, r_c and v_c must be related to the classical parameters b and v. This is accomplished through Eqs. (5) and (9). Because the solution of Eqs. (3) and (8) is in terms of r_c and v_c, we cannot use the capital F resonance function solution as before; therefore, the integrals are evaluated numerically. The above first-order-in-time approximation has been successfully applied by Tipping *et al.* (*15–17*). Bonamy *et al.* (*18*) have proceeded along similar lines, considering linear trajectories and choosing the velocity such that the equations of motion are exact to second order in time, i.e.,

$$\vec{r}(t) = \vec{r}_c + \vec{v}_c' t, \qquad \vec{r}_c \text{ perpendicular to } \vec{v}_c', \tag{11}$$

with

$$r(t) = \sqrt{r_c^2 + v_c'^2 t^2},$$

$$v_c'^2 = v_c^2 - \frac{r_c}{\mu}\left(\frac{d\phi}{dr}\right)_{r_c}, \tag{12}$$

and

$$\theta(t) = \arctan \frac{v_c' t}{r_c}.$$

Both of the above approximations to the dynamics use straight-line trajectories given in terms of the distance of closest approach, r_c; then the relative velocity v_c is adjusted to give the equations of motion correct to first and second order in time. The use of actual parabolic trajectories has been formulated and applied to inert gas systems by Gersten (*20*), for ozone, however, this approach is much too difficult and time consuming.

3. CALCULATIONS AND RESULTS

We have performed calculations via both conventional Anderson theory and QFT theory on the O_3–N_2 and O_3–O_2 systems. In these calculations we have considered the dipole(O_3)–quadrupole(N_2 or O_2) interaction(d–q) and the quadrupole(O_3)–quadrupole(N_2 or O_2) interaction(q–q). Explicit vibrational dependence was taken into account for the ground, ν_1 and ν_3 states of ozone using very accurate Hamiltonian constants for these states (*26*). The molecular constants used in the

calculations are given in Table I and are in all cases reproducible and confirmed by several studies (see references in Table I). In all calculations, the d–q and q–q interactions arising from Anderson's $S_{2\,\text{middle}}$ term were also included. For the QFT theory, as in ATC theory, the numerical coefficients for the middle term are just twice those given in Ref. (*27*) for the outer terms. The asymmetric quadrupole moment of O_3 was included using precisely the same formalism as developed by Yamamoto and Aoki (*10*), and our definition of quadrupole moment components (as given in Table I) is identical to theirs. The matrix elements of the quadrupole moment operator were computed using a program developed by one of the present authors (*28*).

In all calculations the temperature was fixed at 296 K. The QFT scaling parameter, α, was adjusted to give the best fit to the *theoretical* halfwidth of three transitions computed using the ATC method, including velocity averaging. Thus, the theories are on the same footing with no experimental bias in the QFT results.

The data base used to evaluate the calculations is from the work of Hoell *et al.* (*6*), Lundqvist *et al.* (*7*), Margolis (*8*), and Meunier *et al.* (*9*). Of these works only Ref. (*9*) gives an error analysis for each transition studied; hence, we relied on this work more heavily. The data base we have collected amounts to 118 ν_3 transitions,

TABLE I

Molecular Constants and Parameters Used in the Calculations

Molecule/Parameter	Value	Reference
Ozone		
dipole moment	0.53087×10^{-18} esu-cm	3, 4
quadrupole moments		
θ_{aa}	$-1.4(2) \times 10^{-26}$ esu-cm^2	4
θ_{bb}	$-0.7(2) \times 10^{-26}$ esu-cm^2	4
θ_{cc}	$2.1(3) \times 10^{-26}$ esu-cm^2	4
Hamiltonian constants	see Reference 26	26
Nitrogen		
quadrupole moment	-1.4 ± 0.1 esu-cm^2	34
rotational constant b_c	2.010 cm^{-1}	35
Oxygen		
quadrupole moment	-0.4 ± 0.1 esu-cm^2	34
rotational constant b_c	1.4457 cm^{-1}	35
Systems		
O_3-N_2		
reduced mass	2.9375×10^{-23} g	
Lennard-Jones parameters		
ϵ	181.5 cm^{-1}	this work
σ	3.11×10^{-8} cm	this work
O_3-O_2		
reduced mass	3.1882×10^{-23} g	
Lennard-Jones parameters		
ϵ	173.3 cm^{-1}	this work
σ	3.03×10^{-8} cm	this work
Other		
Temperature	296 K	this work
QFT Scaling Parameter α	2.99	this work

TABLE II

Contribution of Q–Q Interaction to Computed Halfwidth (cm^{-1}/atm)
(Anderson Theory, No Velocity Averaging, No ID)

ν_3 Transition								
J'	Ka'	Kc'	J"	Ka"	Kc"	γ_{DQ}	γ_{DQ+QQ}	%QQ
15	2	13	16	2	14	.05679	.06826	16.80
17	2	15	16	2	14	.05685	.06799	16.38
20	8	13	19	8	12	.04763	.06263	23.95
21	1	22	21	1	21	.05647	.06372	11.38
21	6	15	20	6	14	.04879	.06281	22.32
22	2	21	21	2	20	.05573	.06639	16.06
26	1	26	25	1	25	.05441	.06184	12.01

16 ν_1 transitions, and 9 $\nu_1 + \nu_3$ transitions. In all of our calculations both the halfwidth and the shift were evaluated. Because there appear to be no experimental shift measurements for ozone to compare with, we limit our discussion to the halfwidths.

The effect of vibrational dependence and of the inclusion of the quadrupole–quadrupole interaction were both investigated. In Table II the effect of thr q–q interaction is shown for several transitions. We compare results for the O_3–N_2 system calculated using only the dipole–quadrupole interaction with those calculated using both d–q and q–q terms. An average increase in the halfwidth of 19% was observed for the 118 ν_3 transitions when the q–q term was included. To investigate the vibrational dependence, the halfwidths of ν_3 (and ν_1) transitions were studied using explicit ground state and ν_3 (or ν_1) state matrix elements and compared with halfwidths calculated using only ground state matrix elements. The results of our calculations show the effects of the explicit vibrational state to be small, $\approx$1% on the average, with the largest difference obtained being 7%. This is somewhat expected because ozone is a heavy molecule and can be contrasted to water vapor, where vibrational dependence can affect the halfwidth by 10 to 14% (29). We conclude that the q–q interaction must be included in any meaningful calculation for the halfwidth or shift of ozone transitions, whereas explicit vibrational matrix elements are not as critical.

The results of our straight-path trajectory calculations for the O_3–N_2 system are summarized in Figs. 2 and 3, where we plot the percentage difference in the halfwidth compared with experiment vs the J level of the initial state for the ν_3 and ν_1 transitions, respectively. Both the ATC and QFT calculations are present in both figures and we note that the theory is $\approx$16% too low. If we correctly include the velocity averaging in the ATC method (see Table III) the results are $\approx$23% too low. The straight-path trajectory results for the O_3–O_2 system were some 35% too low (for both ATC and QFT methods).

We next performed ATC and QFT calculations with improved dynamics (ATC-ID and QFT-ID) correct to first order in time for 127 ν_3 and $\nu_1 + \nu_3$ transitions

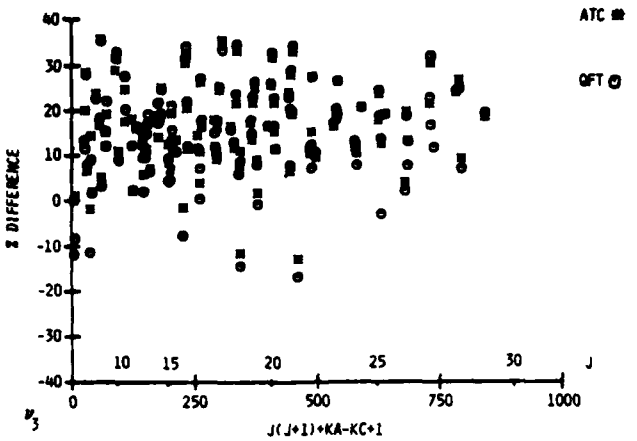

FIG. 2. Percentage difference between experimental [Refs. (*7–9*)] and theoretical (conventional ATC and QFT calculations) N_2-broadened halfwidths as a function of lower state J for 118 ν_3 transitions of ozone.

from the work of Margolis (*8*) and Meunier *et al.* (*9*). In these calculations we studied both N_2 and O_2 as perturbing gases and, using the relation

$$\gamma_{air} = 0.79\gamma_{N_2} + 0.21\gamma_{O_2}, \tag{13}$$

we generated air-broadened values for the halfwidth. In order to perform the calculations correctly to first order in time, a potential is required and here a Lennard–Jones potential was used. The Lennard–Jones parameters for the calculations were derived by taking literature values for the oxygen atom (*30*) and for the nitrogen and oxygen molecules (*31*). Using a pairwise additive scheme (*31*) for the three oxygen atoms of ozone and the perturbing molecule, N_2 or O_2, we constructed

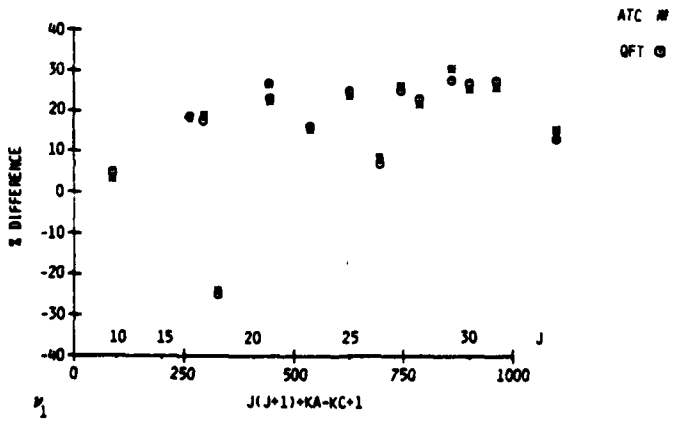

FIG. 3. Percentage difference between experimental [Refs. (*7–9*)] and theoretical (conventional ATC and QFT calculations) N_2-broadened halfwidths as a function of lower state J for 16 ν_1 transitions of ozone.

TABLE III

Effects of Velocity Averaging on N_2-Broadened Halfwidth for Six ν_3 Transitions of Ozone Computed by ATC Method and for Nine $\nu_1 + \nu_3$ Transitions of Ozone Computed by ATC-ID Method

	Transition								
	J'	Ka'	Kc'	J"	Ka"	Kc"	$\gamma_{\bar{v}}^a$ (cm^{-1}/atm)	γ^b (cm^{-1}/atm)	% Difference
ATC	3	1	2	2	1	1	0.07206	0.06717	6.79
	5	3	2	5	3	3	0.06761	0.06269	7.28
	12	2	11	11	2	10	0.06970	0.06380	8.46
	18	3	16	19	3	17	0.06634	0.06149	7.32
	26	3	24	25	3	23	0.06569	0.06082	7.42
	28	5	24	27	5	23	0.06192	0.05820	6.01
ATC-ID	25	1	24	26	1	25	0.07603	0.06743	11.3
	23	8	15	24	8	16	0.07099	0.06393	9.9
	20	11	10	21	11	11	0.07004	0.05949	15.1
	24	5	20	25	5	21	0.07199	0.06518	9.5
	23	7	16	24	7	17	0.07129	0.06427	9.8
	24	4	21	25	4	22	0.07252	0.06558	9.6
	25	0	25	26	0	26	0.07125	0.06023	15.5
	24	3	22	25	3	23	0.07390	0.06633	10.2
	23	6	17	24	6	18	0.07166	0.06468	9.7

a. mean relative thermal velocity result

b. explicit velocity integration, see eq. 3

the potential by averaging over angular orientations of the ozone molecule. This generated the values of σ and ϵ for the O_3–N_2 and O_3–O_2 systems found in Table I.

We should state that the Lennard-Jones parameters ϵ and σ were adjusted without any thought of matching experiment; in fact, all parameters were determined before halfwidth calculations were undertaken.

4. DISCUSSION AND CONCLUSION

The results from our early calculations revealed the theory to be inadequate; more accurate results would be needed to help interpret atmospheric experiments on ozone and to provide transition-dependent halfwidths for O_3 on the Air Force Geophysics Laboratory Main Gas Compilation (*32*). Improvements to the theory were investigated, including velocity averaging (see Table III), use of the linked-cluster expansion theorem to produce a cutoff-free theory (*33*), and the use of more realistic trajectories in the dynamics of the problem. As expected the first two changes decreased the halfwidths further, while the use of approximate trajectories has provided improved agreement with experiment.

The assumption of linear trajectories with a constant velocity chosen to give the equations of motion correct to first order in time has produced results for N_2- and O_2-broadening well within 10% of experiment. For N_2 as the perturbing gas we can compare our results with the 127 experimental measurements which have an accuracy of ±10%. The average absolute percentage difference (AAPD) for the QFT-ID calculations was 8.4% and that for the ATC-ID calculations without velocity averaging was 4.3%; when velocity averaging is included in the ATC-ID calculations the AAPD is around 15%. A better comparison of the two theories can be obtained by using only the data of Meunier, Marché, and Barbe, which contain error bars

TABLE IV

Comparison of QFT and ATC (with Improved Dynamics) Calculations with the Experimental N_2-Broadened Results of Meunier *et al.* (*8*) (All Units cm^{-1}/atm; Percentage Difference in Brackets)

Transition								
J'	Ka'	Kc'	J"	Ka"	Kc"	γ^a	γ^b	γ^c
25	1	24	26	1	25	0.072 ± 0.002	0.0714 (0.9)	0.06743 (-2.2)
23	8	15	24	8	16	0.071 ± 0.003	0.0683 (3.8)	0.06393 (10.0)
20	11	10	21	11	11	0.071 ± 0.003	0.0680 (4.2)	0.05949 (15.0)
24	5	20	25	5	21	0.069 ± 0.003	0.0689 (0.2)	0.06516 (2.7)
23	7	16	24	7	17	0.067 ± 0.001	0.0682 (-1.8)	0.06427 (9.5)
24	4	21	25	4	22	0.067 ± 0.001	0.0697 (-4.1)	0.06558 (5.5)
25	0	25	26	0	26	0.066 ± 0.002	0.0681 (-3.1)	0.06023 (10.1)
24	3	22	25	3	23	0.070 ± 0.001	0.0703 (0.4)	0.06633 (5.2)
23	6	17	24	6	18	0.070 ± 0.001	0.0683 (2.5)	0.06468 (10.2)

a. Reference 9
b. This work, QFT-ID
c. This work, ATC-ID

for each measurement and are accurate to 4.4%. The data for the comparison are given in Table IV (note the ATC-ID results have been velocity averaged). In Fig. 4 we present a comparison of the QFT-ID and velocity-averaged ATC-ID N_2-broadened results with the 9 $\nu_1 + \nu_3$ lines studied. The AAPD from the QFT-ID results compared with experiment is 2.3% with a maximum difference of 4.2%. From the ATC-ID result the AAPD compared with experiment is 7.8% with a maximum deviation of 15.%. We note most of the QFT-ID results are within or close to the error bars on the measurements of Meunier *et al.*, with the largest discrepancy being just under 0.003 cm^{-1}/atm.

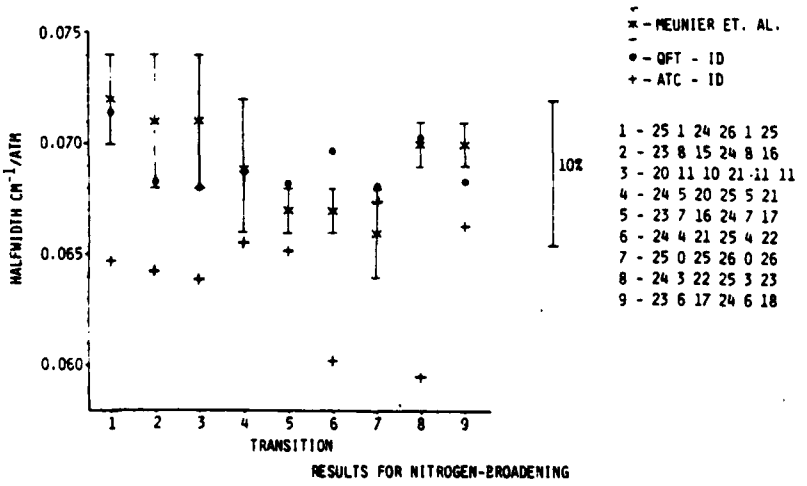

FIG. 4. Comparison of experimental N_2-broadened halfwidths [Ref. (*9*)] with ATC-ID and QFT-ID results for nine $\nu_1 + \nu_3$ transitions of ozone. Halfwidths are in units of cm^{-1}/atm. The rotational state quantum numbers are listed at the right along with an indication of a 10% error bar as a visual guide.

TABLE V

Comparison of QFT and ATC (with Improved Dynamics) Calculations with the Experimental O_2-Broadened Results of Meunier *et al.* (*8*) (All Units cm^{-1}/atm; Percentage Difference in Brackets)

Transition								
J'	Ka'	Kc'	J"	Ka"	Kc"	γ^a	γ^b	γ^c
25	1	24	26	1	25	0.054 ± 0.002	0.0541 (-0.2)	0.04991 (7.6)
23	8	15	24	8	16	0.057 ± 0.005	0.0556 (2.5)	0.04935 (13.4)
20	11	10	21	11	11	0.057 ± 0.005	0.0514 (9.8)	0.05043 (11.5)
24	5	20	25	5	21	0.057 ± 0.002	0.0514 (9.8)	0.04952 (13.1)
23	7	16	24	7	17	0.058 ± 0.002	0.0534 (7.9)	0.04947 (14.7)
24	4	21	25	4	22	0.056 ± 0.002	0.0511 (8.8)	0.04958 (11.5)
25	0	25	26	0	26	0.053 ± 0.002	0.0508 (4.2)	0.04862 (8.3)
24	3	22	25	3	23	0.056 ± 0.002	0.0518 (7.5)	0.04974 (11.2)
23	6	17	24	6	18	0.062 ± 0.005	0.0523 (15.6)	0.05045 (18.6)

a. Reference 9
b. This work, QFT-ID
c. This work, ATC-ID

In addition to the N_2-broadening, the work of Meunier *et al.* contains results for O_2- and air-broadening as well. We present a comparison of the calculations with experiment in Table V and Figure 5 for O_2 as the perturbing gas, and in Table VI and Figure 6 for air-broadening: Meunier *et al.'s* results are accurate to 8.8% for O_2- and for air-broadening; although error bars were not given, the accuracy can be estimated to be slightly greater than 5%. For O_2-broadening the AAPD was 7.3% for the QFT-ID results and 12% for the ATC-ID results. Studying Fig. 5 we see the

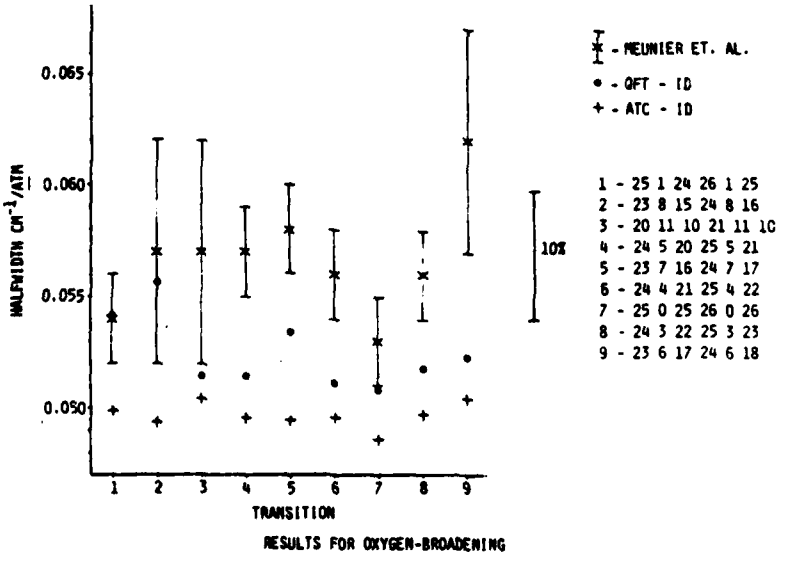

FIG. 5. Comparison of experimental O_2-broadened halfwidths [Ref. (9)] with ATC-ID and QFT-ID results for nine $\nu_1 + \nu_3$ transitions of ozone. Halfwidths are in units of cm^{-1}/atm. The rotational state quantum numbers are listed at the right along with an indication of a 10% error bar as a visual guide.

TABLE VI

Comparison of QFT and ATC (with Improved Dynamics) Calculations with the Experimental Air-Broadened Results of Meunier *et al.* (*8*) (All Units cm^{-1}/atm; Percentage Difference in Brackets)

Transition								
J'	Ka'	Kc'	J"	Ka"	Kc"	γ_{air}[a]	γ[b]	γ[c]
25	1	24	26	1	25	0.0675	0.0678 (-0.4)	0.06375 (5.6)
23	8	15	24	8	16	0.067	0.0656 (2.1)	0.06087 (9.1)
20	11	10	21	11	11	0.067	0.0645 (3.7)	0.05759 (14.0)
24	5	20	25	5	21	0.066	0.0652 (1.2)	0.06189 (6.2)
23	7	16	24	7	17	0.0645	0.0651 (-0.9)	0.06116 (5.2)
24	4	21	25	4	22	0.064	0.0658 (-2.8)	0.06222 (2.8)
25	0	25	26	0	26	0.063	0.0644 (-2.2)	0.05779 (8.3)
24	3	22	25	3	23	0.066	0.0664 (-0.6)	0.06285 (4.8)
23	6	17	24	6	18	0.0675	0.0649 (3.9)	0.06169 (8.6)

a. Reference 9
b. This work, QFT-ID
c. This work, ATC-ID

comparison of theory and experiment is not as good as the results for N_2-broadening. This is not surprising considering the nature of the O_2-broadening calculations (due to the very small quadrupole moment of O_2 close collisions occur and the perturbation calculations are suspect); however, we feel the QFT-ID results are satisfactory. Figure 6 shows the close agreement between experiment and the QFT-ID calculations, 2.0% AAPD with the maximum difference being 3.9%. The velocity-averaged ATC-ID results, although much improved over the classical path ATC results, have a 7.2% AAPD with several transitions showing large discrepancies.

From the calculations we find the QFT-ID method to give better agreement with experiment than the velocity-averaged ATC-ID method. The QFT-ID calculations are also simpler to carry out since an explicit velocity average has already been

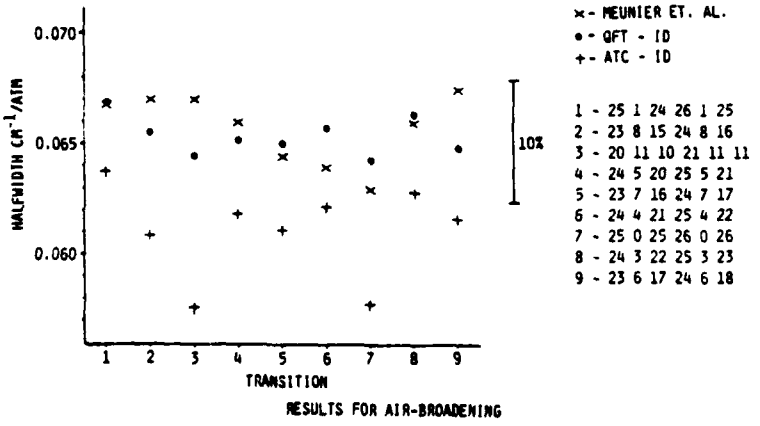

FIG. 6. Comparison of experimental air-broadened halfwidths [Ref. (*9*)] with ATC-ID and QFT-ID results for nine $\nu_1 + \nu_3$ transitions of ozone. Halfwidths are in units of cm^{-1}/atm. The rotational state quantum numbers are listed at the right along with an indication of a 10% error bar as a visual guide.

TABLE VII

QFT-ID Results for 127 ν_3 Transitions of Ozone. [Presented Are the Halfwidths (in Units of cm^{-1}/atm) for N_2-, O_2-, and Air-Broadening and, Whenever Possible, the Corresponding Experimental Value from Refs. (*8*) and (*9*)]

TRANSITION						HALFWIDTH (cm^{-1}/atm)					
						NITROGEN		OXYGEN		AIR	
J"	K_a"	K_c"	J'	K_a'	K_c'	QFT-ID	EXP	QFT-ID	EXP	QFT-ID	EXP
23	6	17	24	6	18	0.06828	0.070	0.05233	0.062	0.06493	0.0675
23	7	16	24	7	17	0.06821	0.067	0.05241	0.058	0.06510	0.0645
23	8	15	24	8	16	0.06825	0.071	0.05564	0.057	0.06560	0.067
24	4	21	25	4	22	0.06973	0.067	0.05111	0.056	0.06582	0.064
24	5	20	25	5	21	0.06890	0.069	0.05141	0.057	0.06522	0.066
25	0	25	26	0	26	0.06806	0.066	0.05082	0.053	0.06444	0.062
25	1	24	26	1	25	0.07137	0.072	0.05412	0.054	0.06775	0.0675
20	11	10	21	11	11	0.06803	0.071	0.05135	0.057	0.06453	0.067
24	3	22	25	3	23	0.07029	0.070	0.05181	0.056	0.06641	0.066
27	5	22	28	5	23	0.06927	0.06750	0.05147		0.06553	
28	1	28	29	1	29	0.06730	0.07330	0.05048		0.06377	
27	3	24	28	3	25	0.07228	0.09000	0.05210		0.06804	
27	0	27	28	0	28	0.06734	0.07780	0.05007		0.06371	
24	7	18	25	7	19	0.06821	0.07690	0.05406		0.06524	
26	2	25	27	2	26	0.06910	0.09180	0.05150		0.06536	
25	5	20	26	5	21	0.06901	0.07240	0.05144		0.06532	
25	3	22	26	3	23	0.07212	0.08380	0.05204		0.06790	
25	2	23	26	2	24	0.07309	0.07140	0.05245		0.06876	
23	7	16	24	7	17	0.06821	0.07840	0.05241		0.06510	
24	3	22	25	3	23	0.07029	0.07520	0.05181		0.06641	
22	7	16	23	7	17	0.06822	0.08470	0.05244		0.06511	
24	1	24	25	1	25	0.06855	0.08160	0.05106		0.06488	
22	6	17	23	6	18	0.06822	0.07660	0.05242		0.06490	
23	2	21	24	2	22	0.07252	0.07650	0.05259		0.06912	
22	5	18	23	5	19	0.06864	0.07830	0.05140		0.06502	
23	1	22	24	1	23	0.07238	0.07850	0.05384		0.06849	
23	0	23	24	0	24	0.06893	0.07190	0.05176		0.06533	
21	6	15	22	6	16	0.06818	0.06920	0.05254		0.06490	
22	3	20	23	3	21	0.07046	0.07890	0.05208		0.06660	
18	9	10	19	9	11	0.06870	0.06350	0.05627		0.06609	
21	3	18	22	3	19	0.07153	0.09220	0.05196		0.06742	
21	2	19	22	2	20	0.07382	0.08090	0.05282		0.06941	
19	7	12	20	7	13	0.06832	0.07080	0.05390		0.06529	
20	5	16	21	5	17	0.06843	0.09420	0.05135		0.06484	
21	1	20	22	1	21	0.07336	0.07980	0.05394		0.06928	
21	0	21	22	0	22	0.06997	0.07260	0.05157		0.06610	
17	9	8	18	9	9	0.06881	0.05620	0.05674		0.06627	
20	4	17	21	4	18	0.06930	0.07880	0.05147		0.06556	
19	6	13	20	6	14	0.06814	0.07430	0.05219		0.06479	
20	3	18	21	3	19	0.07054	0.09170	0.05245		0.06674	
20	2	19	21	2	20	0.07091	0.08280	0.05267		0.06708	
20	1	20	21	1	21	0.07016	0.08450	0.05155		0.06625	
19	4	15	20	4	16	0.06919	0.09570	0.05140		0.06546	
18	6	13	19	6	14	0.06815	0.08400	0.05201		0.06476	
19	3	16	20	3	17	0.07120	0.08970	0.05216		0.06720	
19	0	19	20	0	20	0.07116	0.07960	0.05169		0.06707	
18	4	15	19	4	16	0.06906	0.08160	0.05177		0.06543	
17	6	11	18	6	12	0.06818	0.09470	0.05195		0.06477	
18	3	16	19	3	17	0.07055	0.07660	0.05286		0.06683	
17	5	12	18	5	13	0.06821	0.08080	0.05146		0.06469	
18	2	17	19	2	18	0.07149	0.08150	0.05320		0.06765	
16	6	11	17	6	12	0.06822	0.08280	0.05191		0.06479	
17	3	14	18	3	15	0.07088	0.07580	0.05249		0.06702	
17	0	17	18	0	18	0.07249	0.08150	0.05225		0.06824	
16	4	13	17	4	14	0.06884	0.07570	0.05209		0.06532	
16	3	14	17	3	15	0.07048	0.07240	0.05327		0.06687	
16	2	15	17	2	16	0.07201	0.07680	0.05372		0.06817	
13	8	5	14	8	6	0.06922	0.07290	0.05679		0.06661	
16	1	16	17	1	17	0.07205	0.07990	0.05202		0.06784	
15	4	11	16	4	12	0.06876	0.07520	0.05206		0.06525	
15	3	12	16	3	13	0.07061	0.08910	0.05293		0.06689	
15	2	13	16	2	14	0.07297	0.07100	0.05278		0.06973	
15	0	15	16	0	16	0.07390	0.07990	0.05371		0.06966	
14	4	11	15	4	12	0.06868	0.09300	0.05235		0.06525	

TABLE VII—*Continued*

TRANSITION						HALFWIDTH (cm^{-1}/atm)					
						NITROGEN		OXYGEN		AIR	
J"	$K"_a$	$K"_c$	J'	K'_a	K'_c	QFT-ID	EXP	QFT-ID	EXP	QFT-ID	EXP
14	3	12	15	3	13	0.07036	0.09390	0.05358		0.06684	
12	7	6	13	7	7	0.06904	0.08570	0.05402		0.06588	
14	1	14	15	1	15	0.07303	0.06400	0.05230		0.06868	
13	4	9	14	4	10	0.06864	0.07360	0.05230		0.06521	
12	6	7	13	6	8	0.06859	0.07870	0.05219		0.06515	
13	3	10	14	3	11	0.07038	0.08220	0.05334		0.06680	
13	2	11	14	2	12	0.07383	0.07390	0.05404		0.06968	
13	0	13	14	0	14	0.07532	0.07640	0.05402		0.07085	
12	4	9	13	4	10	0.06860	0.07990	0.05248		0.06522	
12	3	10	13	3	11	0.07022	0.08290	0.05373		0.06677	
11	5	6	12	5	7	0.06825	0.07750	0.05157		0.06483	
11	0	11	12	0	12	0.07667	0.08330	0.05551		0.07223	
10	1	10	11	1	11	0.07489	0.08280	0.05293		0.07028	
9	4	5	10	4	6	0.06871	0.07920	0.05245		0.06529	
6	5	2	7	5	3	0.06867	0.09920	0.05188		0.06515	
7	2	5	8	2	6	0.07363	0.08060	0.05452		0.06962	
11	6	5	11	6	6	0.06879	0.07670	0.05286		0.06545	
7	6	1	7	6	2	0.06866	0.06630	0.05181		0.06512	
6	6	1	6	6	0	0.06761	0.07930	0.05382		0.06472	
4	4	1	4	4	0	0.06797	0.07160	0.05159		0.06453	
5	3	2	5	3	3	0.07039	0.07240	0.05343		0.06683	
3	0	3	2	0	2	0.08051	0.07270	0.05639		0.07545	
3	1	2	2	1	1	0.07877	0.07290	0.05624		0.07404	
6	1	6	5	1	5	0.07675	0.08550	0.05377		0.07192	
6	2	5	5	2	4	0.07368	0.09890	0.05446		0.06964	
7	2	5	6	2	4	0.07368	0.07230	0.05444		0.06964	
10	7	4	9	7	3	0.06923	0.07180	0.05422		0.06608	
7	0	7	6	0	6	0.07933	0.07130	0.05604		0.07444	
8	4	5	7	4	4	0.06888	0.07830	0.05252		0.06544	
7	1	6	6	1	5	0.07814	0.08540	0.05589		0.07247	
10	5	6	9	5	5	0.06858	0.09450	0.05168		0.06503	
9	3	6	8	3	5	0.07017	0.08390	0.05353		0.06667	
9	2	7	8	2	6	0.07362	0.08360	0.05482		0.06967	
10	4	7	9	4	6	0.06869	0.09200	0.05249		0.06529	
13	7	6	12	7	5	0.06904	0.06910	0.05402		0.06588	
11	4	7	10	4	6	0.06865	0.08680	0.05244		0.06524	
12	2	11	11	2	10	0.07297	0.07120	0.05497		0.06919	
13	4	9	12	4	8	0.06861	0.07340	0.05238		0.06520	
18	9	10	17	9	9	0.06881	0.09590	0.05674		0.06627	
13	0	13	12	0	12	0.07601	0.08470	0.05462		0.07152	
19	9	10	18	9	9	0.06870	0.07010	0.05627		0.06609	
14	4	11	13	4	10	0.06863	0.07550	0.05243		0.06522	
13	2	11	12	2	10	0.07376	0.07820	0.05415		0.06964	
13	1	12	12	1	11	0.07677	0.07700	0.05537		0.07228	
22	10	13	21	10	12	0.06830	0.05430	0.05244		0.06518	
15	4	11	14	4	10	0.06869	0.07170	0.05220		0.06523	
19	8	11	18	8	10	0.06863	0.06760	0.05600		0.06598	
16	5	12	15	5	11	0.06817	0.07750	0.05150		0.06467	
15	0	15	14	0	14	0.07461	0.07930	0.05351		0.07018	
16	1	16	15	1	15	0.07254	0.06930	0.05216		0.06826	
20	8	13	19	8	12	0.06854	0.06880	0.05587		0.06588	
17	2	15	16	2	14	0.07402	0.07620	0.05364		0.06974	
21	6	15	20	6	14	0.06815	0.08010	0.05261		0.06489	
22	1	22	21	1	21	0.06973	0.08280	0.05144		0.06589	
22	2	21	21	2	20	0.07061	0.07100	0.05240		0.06679	
26	1	26	25	1	25	0.06820	0.07520	0.05093		0.06457	
28	1	28	27	1	27	0.06758	0.07730	0.05064		0.06402	
23	2	21	22	2	20	0.07369	0.07620	0.05269		0.06928	
26	3	24	25	3	23	0.07019	0.06290	0.05170		0.06630	
28	5	24	27	5	23	0.06930	0.07150	0.05150		0.06556	
27	4	23	26	4	22	0.07003	0.06990	0.05109		0.06605	
28	2	27	27	2	26	0.06881	0.07440	0.05150		0.06517	
25	2	23	24	2	22	0.07332	0.08980	0.05251		0.06895	

performed; in the ATC-ID method, calculations must be done for a set of velocity values (we employ a seven-point quadrature). Thus, the QFT-ID calculation is faster by a factor of seven and gives better agreement with experiment.

Table VII lists our final calculations based on the QFT-ID method for the 127 transitions studied; presented are the halfwidths for N_2-, O_2-, and air-broadening and, whenever possible, the corresponding experimental value. All results are from quantum Fourier transform theory with dynamics correct to first order in time, QFT-ID. A final parameter derived from this study is the ratio of air-broadening to N_2-broadening; the usefulness of this parameter arises from the method in which air-broadened results are usually generated, i.e., N_2-broadened results are calculated and then scaled to air-broadened values. This method saves the time necessary to calculate O_2-broadened results. From the calculations for the 127 transitions, we find a very constant air/N_2 ratio, with an average of 0.95 and a standard deviation of 0.0056. This compares well with Meunier *et al.'s* value of 0.94.

We conclude this paper by stating that the use of QFT theory with improved collision dynamics yields collision-broadened halfwidths for ozone that are in good agreement with experimental measurements. Although the calculations take about five times longer than the straight-path methods, they are still feasible ($\sim$7 sec per transition on a CDC Cyber 170-750 computer). It is anticipated, in the near future, to have generated halfwidths and shifts for more than 4500 ozone transitions: the halfwidths will be added to the AFGL Main Gas Compilation (*32*).

ACKNOWLEDGMENTS

We acknowledge the following colleagues for stimulating discussions and for their encouragement L. S. Rothman, S. A. Clough, and R. H. Tipping. This work was supported by the Air Force Office of Scientific Research through AFGL Task 2310G1.

RECEIVED: July 24, 1984

REFERENCES

1. M. ARDON, "Oxygen," Ch. 3, Benjamin, New York, 1965.
2. R. H. HUGHES, *J. Chem. Phys.* **21**, 959–960 (1953); R. TRAMBARULO, N. S. GHOSH, C. A. BURRUS, AND W. GORDY, *J. Chem. Phys.* **21**, 851–855 (1953).
3. M. LICHTENSTEIN, J. J. GALLAGHER, AND S. A. CLOUGH, *J. Mol. Spectrosc.* **40**, 10–26 (1971); S. A. CLOUGH, Air Force Geophysics Laboratory, private communication (1983).
4. K. M. MACK AND J. S. MUENTER, *J. Chem. Phys.* **66**, 5278–5283 (1977); W. L. MEERTS, S. STOLTE, AND A. DYMANUS, *Chem. Phys.* **19**, 467–472 (1977).
5. M. A. H. SMITH AND L. L. GORDLEY, *J. Quant. Spectrosc. Radiat. Transfer* **29**, 413–418 (1983).
6. J. M. HOELL, C. N. HARWARD, C. H. BAIR, AND B. S. WILLIAMS (Private communication).
7. S. LUNDQVIST, J. MARGOLIS, AND J. REID, *Appl. Opt.* **21**, 3109–3113 (1982).
8. J. MARGOLIS, *J. Quant. Spectrosc. Radiat. Transfer* **29**, 539–542 (1983).
9. C. MEUNIER, P. MARCHÉ, AND A. BARBE, *J. Mol. Spectrosc.* **95**, 271–275 (1982).
10. G. YAMAMOTO AND T. AOKI, *J. Quant. Spectrosc. Radiat. Transfer* **12**, 227–241 (1972).
11. G. D. T. TEJWANI AND E. S. YEUNG, *J. Chem. Phys.* **63**, 1513–1517 (1975).
12. J.-Y. MANDIN, J.-M. FLAUD, AND C. CAMY-PEYRET, Laboratoire de Physique Moléculaire et d'Optique Atmosphérique, CNRS, Orsay, France, private communications.
13. P. W. ANDERSON, *Phys. Rev.* **76**, 647–661 (1949); **80**, 511–513 (1950); C. J. TSAO AND B. CURNUTTE, JR., *J. Quant. Spectrosc. Radiat. Transfer* **2**, 41–91 (1962).
14. R. W. DAVIES, *Phys. Rev. A* **12**, 927–946 (1975).

15. R. H. TIPPING, Thesis, Department of Physics, The Pennsylvania State University, 1969.
16. R. H. TIPPING AND R. M. HERMAN, *J. Quant. Spectrosc. Radiat. Transfer* **10**, 881–896 (1970).
17. R. H. TIPPING AND R. M. HERMAN, *J. Quant. Spectrosc. Radiat. Transfer* **10**, 897–908 (1970).
18. J. BONAMY, L. BONAMY, AND D. ROBERT, *J. Chem. Phys.* **67**, 4441–4453 (1977).
19. M. BERARD AND P. LALLEMAND, *J. Quant. Spectrosc. Radiat. Transfer* **19**, 387–396 (1978).
20. J. I. GERSTEN, *Phys. Rev. A* **4**, 98–108 (1970).
21. G. BACHET, *J. Quant. Spectrosc. Radiat. Transfer* **14**, 1277–1283 (1974); R. M. HERMAN, *Phys. Rev.* **132**, 262 (1963); *J. Quant. Spectrosc. Radiat. Transfer* **3**, 449 (1963).
22. D. ROBERT, M. GIRAUD, AND L. GALATRY, *J. Chem. Phys.* **51**, 2192–2205 (1969).
23. E. PIOLLET-MARIEL, C BOULET, AND A. LEVY, *Mol. Phys.* **33**, 255–258 (1977); P. ISNARD, C. BOOLET, D. ROBERT, AND L. GALATRY, *Mol. Phys.* **33**, 259–280 (1977).
24. R. P. LEAVITT, *J. Chem. Phys.* **73**, 5432–5450 (1980).
25. R. W. DAVIES AND B. A. OLI, *J. Quant. Spectrosc. Radiat. Transfer* **20**, 95–120 (1978).
26. A. GOLDMAN, Physics Department, University of Denver, and A. BARBE, Laboratoire de Physique Moléculaire, Universite de Reims, France, private communications.
27. R. W. DAVIES, R. H. TIPPING, AND S. A. CLOUGH, *Phys. Rev. A* **26**, 3378–3394 (1982).
28. R. W. DAVIES (unpublished).
29. J.-Y. MANDIN, J.-M. FLAUD, AND C. CAMY-PEYRET, *J. Quant. Spectrosc. Radiat. Transfer* **23**, 351–370 (1980).
30. A. STACE AND J. MURRELL, *J. Chem. Phys.* **68**, 3028 (1978).
31. J. O. HIRSCHFELDER, C. F. CURTISS, AND R. B. BIRD, "Molecular Theory of Gases and Liquids," Wiley, New York, 1954.
32. L. S. ROTHMAN, R. R. GAMACHE, A. BARBE, A. GOLDMAN, J. R. GILLIS, L. R. BROWN, R. A. TOTH, J.-M. FLAUD, AND C. CAMY-PEYRET, *Appl. Opt.* **22**, 2247–2256 (1983).
33. D. KORFF AND R. P. LEAVITT, *Phys. Lett. A* **53**, 351 (1975); D. ROBERT AND J. BONAMY, *J. Phys. (Paris)* **40**, 923 (1979); R. P. LEAVITT AND D. KORFF, *J. Chem. Phys.* **74**, 2180–2188 (1981).
34. D. E. STOGRYN AND A. P. STOGRYN, *Mol. Phys.* **11**, 371–393 (1966); D. E. STOGRYN (Private communication).
35. R. S. BERRY, S. A. RICE, AND J. ROSS, "Physical Chemistry," p. 775, Wiley, New York, 1980.

B6.

Theoretical N_2-broadened halfwidths of $^{16}O_3$

Robert R. Gamache and Laurence S. Rothman

Halfwidth and pressure-induced line shifts for ozone perturbed by nitrogen have been calculated using the quantum Fourier transform theory with improved dynamics (QFT-ID). All unique rotational transitions from $J = 1$ to 35 present on the AFGL main gas atlas (4852 transitions) have been considered. The halfwidth as a function of J, K_a, and transition type is considered for the first time over a full range of these quanta. Comparison with experiment shows the QFT-ID results for the halfwidth to be accurate to 5–10%. No corresponding measurements of the line shift have been made, hence the accuracy of the line shift is unknown; they can be used, however, for predicting trends.

I. Introduction

The use of molecular spectroscopy in the microwave and IR regions to study and monitor the atmosphere has proved to be one of the most practical and sensitive of methodologies. The results of such studies are very important in determining the background for target detection systems, chemical cycles of the atmosphere, concentration-altitude profiles, and climatic cycles. To obtain data from this method one must understand the absorption and emission spectrum of molecular constituents of the atmosphere. This can be done through high resolution simulation, e.g., AFGL's FASCODE program,[1] if a catalog of spectral parameters exists for the molecule in question. There is such a catalog for the seven most IR-active molecules of the terrestrial atmosphere[2] and for twenty-one trace gas constituents of the atmosphere.[3] Several other catalogs exist for molecules important to astrophysical and planetary studies.[4,5] To generate atmospheric synthetic spectra, at least four basic parameters are necessary: σ the resonant frequency, S the intensity, α the halfwidth, and E'' the lower state energy of the transition. While much of these data come from laboratory or field measurements, ultimately the parameters must be calculated due to the vast number of data needed, especially for long-path atmospheric simulations.

To understand atmospheric spectra for the study of trace gases, the main infrared-active absorbers must be well understood. In this work we are concerned with the molecule ozone which has a very rich spectrum and is known to play an important role in air chemical cycles, temperature regulation of the lower atmosphere and climate, and must be well determined in order to extract information on trace atmospheric constituents in the far IR.[6] For ozone much work has been done in determining the positions and intensities of transitions[7–14]; however, the halfwidths of the transitions have not been as extensively studied. Several experimental measurement programs have been performed,[8–14] although they amount to less than 200 transitions. Some theoretical calculations have been performed for collisional broadening of ozone.[15–18] In the work of Yamamoto and Aoki,[15] the emphasis was on investigating the relative contribution of the quadrupole–quadrupole interaction to the dipole–quadrupole interaction. In Ref. 16 the quadrupole moment tensor values were from an *ab initio* calculation.[19] Although the value of q, the magnitude of the quadrupole moment $q^2 = \theta_{zz}^2 + \frac{1}{3}(\theta_{yy} - \theta_{xx})^2$, used in this study does not differ significantly from recent measured values,[20] the individual components differ considerably. Reference 15 has demonstrated that the values of the components themselves affect the calculation of the halfwidth. The third study[17] considered only ten lines; the recent quadrupole component constants[20] were used but the calculations were done using the conventional Anderson-Tsao-Curnutte (ATC) theory[21] which has been shown to produce results much too low.[17,18,22] The last of these studies[18] used approximate trajectories to better represent actual trajectories and the quantum Fourier transform (QFT) method[23] with improved molecular constants. These QFT-ID (improved dynamics) calculations were compared with 127 experimentally measured halfwidths and the results agree to within 10%.

Here we present results for 4852 transitions of ozone broadened by N_2 calculated by the QFT-ID method.

Robert Gamache is with University of Lowell, Center for Atmospheric Research, 450 Aiken Street, Lowell, Massachusetts 01854, and Laurence Rothman is with U.S. Air Force Geophysics Laboratory, Optical Physics Division, Hanscom Air Force Base, Massachusetts 01731.

Received 19 December 1984.

QFT theory has been chosen over the standard ATC theory since it has provided better agreement with experiment[18] and explicitly includes velocity averaging in its formulation which results in a great reduction in computation time. The transitions studied considered J'' and J', lower and upper rotational quantum numbers, up to 35. Using the ratio of air-broadened to nitrogen-broadened halfwidths reported in Ref. 18 which was determined from transitions up to $J = 28$, air-broadened values were generated for all transitions with $J',J'' \leq 35$ that were present on the AFGL atlas.[2] (Transitions of higher J use extrapolated average values of the halfwidth.)

The pressure-induced shift was also computed for each transition. However, because of the lack of experimental measurement they are not discussed here. Because of the large number of transitions studied, the tables are not reproduced in this paper but are available from the authors, and the corresponding air-broadened values ($0.95\gamma_{N_2}$) will be present in the next version of the AFGL atlas.

II. Theory

The theory discussed here is an extension of the model first proposed by Tipping and Herman.[24] The method has been discussed by Berard and Lallemand[25] and similar methods based on Ref. 21 can be found in the literature.[18,26] The method considers an isotropic potential that can be treated by classical mechanics as well as the usual anisotropic potential treated by second-order perturbation theory. By assuming an isotropic potential one can replace the classical parameters b,v by the distance of closest approach r_c and the relative velocity at this point v_c resulting in dynamics that are correct to first order in time. This is shown in Fig. 1 where the classical path trajectory labeled b and v (solid straight line) is related to the first-order-in-time trajectory labeled r_c and v_c (dashed straight line) by the actual trajectory (solid curved line) determined from a potential. A full description of the method applied to ozone with N_2 and O_2 as perturbing gases can be found in Ref. 18; here we summarize the method.

Within the framework of the QFT-ID theory the collision-broadened halfwidth in cm^{-1}/atm for a transition $i \rightarrow f$ is given by a factor times the real part of a perturbation operator P_{if}, i.e.,

$$\gamma_{i\rightarrow f} = \frac{1}{2\pi c}\,\mathrm{Re}[P_{if}(\omega)], \tag{1}$$

where c is the velocity of light. The effect of collisions is obtained by averaging over angular orientations of the molecules, integrating over impact parameters, and averaging over the relative velocity using the Maxwell-Boltzmann velocity distribution function. This gives

$$P_{if} = n\bar{v}\int_0^\infty 2\pi b S(r_c,v_c)\,db, \tag{2}$$

where n is the number density of the perturbers, $\bar{v}$ is the mean relative thermal velocity, $(8kT/\pi\mu)^{1/2}$, μ is the reduced mass, and $S(r_c,v_c)$ is the interruption function

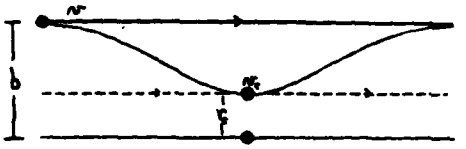

Fig. 1. Comparison of classical path, first-order-in-time, and actual trajectories.

dependent on the first-order-in-time trajectories labeled r_c and v_c. We note here that in QFT theory a proper velocity average of the halfwidth is done analytically resulting in the mean thermal velocity in Eq. (2). Thus unlike the perturbation operator in ATC theory (see Ref. 18), the velocity averaging has explicitly been done. The interruption function we obtain here is of the same form as that obtained in the ATC or QFT theory except r_c replaces b and v_c replaces v. Thus the tabulations of interruption functions found in the literature[27–29] can be used.

To evaluate the integral in Eq. (2) the first-order-in-time trajectory parameters r_c and v_c must be related to the classical path trajectories b and v. Evoking conservation of momentum gives

$$bv = r_c v_c, \tag{3}$$

and from conservation of energy one arrives at

$$\left(\frac{b}{r_c}\right)^2 = 1 - \frac{\phi(r)}{\frac{1}{2}\mu v^2}, \tag{4}$$

where $\phi(r)$ is the isotropic potential describing the trajectories. Here as in all other works[18,24–26] using this method, a Lennard-Jones potential is employed:

$$\phi(r) = 4\epsilon\left[\left(\frac{\sigma}{r}\right)^6 - \left(\frac{\sigma}{r}\right)^{12}\right]. \tag{5}$$

With the parameters b, v, r_c, and v_c related, the integral in Eq. (2) can be evaluated. This is done by the usual cutoff approach, i.e., the point (b_0) at which $S(r_c,v_c) = 1$ is obtained and the integral can be written

$$\int_0^\infty 2\pi b S(r_c,v_c)\,db = \pi b_0^2 + \int_{b_0}^\infty 2\pi b S(r_c,v_c)\,db. \tag{6}$$

Because the interruption function depends on r_c and v_c (i.e., the potential), the integral from b_0 to ∞ was not done by resonance function tabulation as it is in the conventional ATC and QFT methods. Here the integrals in Eq. (6) were calculated numerically to evaluate the perturbation operator and hence the halfwidth.

III. Results

We have performed calculations via the QFT-ID theory for ozone with nitrogen as the perturbing gas. In these calculations the dipole (O_3)–quadrupole (N_2) interaction (d–q) and the quadrupole (O_3)–quadrupole (N_2) interaction (q–q) have been considered. Vibrational dependence was taken into account for A- and B-type levels by using Hamiltonian constants for the ν_3 state and the ground state of ozone. The molecular constants used in the calculations are given in Table I and in all cases are reproducible and confirmed by

Table I. Molecular Constants and Parameters Used in the Calculations

Molecule/parameter	Value	Reference
Ozone		
Dipole moment	0.53087×10^{-18} esu cm^2	20,34
Quadrupole moments		
θ_{aa}	$-1.4(2) \times 10^{-26}$ esu cm^2	20
θ_{bb}	$-0.7(2) \times 10^{-26}$ esu cm^2	20
θ_{cc}	$2.1(3) \times 10^{-26}$ esu cm^2	20
Hamiltonian constants	See Ref. 35	35
Nitrogen		
Quadrupole moment	-1.4 ± 0.1 esu cm^2	36
Rotational constant b_e	2.010 cm^{-1}	37
Systems		
O_3–N_2		
Reduced mass	2.9375×10^{-23} g	
Lennard-Jones parameters		
ϵ	181.5 cm^{-1}	This work
σ	3.11×10^{-8} cm	This work
Other		
Temperature	296 K	This work
QFT scaling parameter α	2.99	This work

several studies (see references in Table I). In all calculations, the d–q and q–q interactions arising from the Anderson $S_{2\text{middle}}$ term were also included. For the QFT theory, as in ATC theory, the numerical coefficients for the middle term are just twice those given in Ref. 30 for the outer terms. The asymmetric quadrupole moment of O_3 was included using precisely the same formalism as developed by Yamamoto and Aoki,[15] and our definition of quadrupole moment components (as given in Table I) is identical to theirs.

In all calculations the temperature was fixed at 296 K. The QFT scaling parameter α was adjusted to give the best fit to the theoretical halfwidth of three transitions ($5_{3\,2}$—$5_{3\,3}$, $12_{2\,11}$—$11_{2\,10}$, $28_{5\,24}$—$27_{5\,23}$) computed using the ATC method, including velocity averaging. The choice of these transitions was such that they represented a good range of J and that proper velocity averaged ATC results were available from an earlier study (see Ref. 18, Table III). The inclusion of more transitions will not change α significantly. Since QFT already contains the average over velocity, adjusting α by theory must use velocity averaged ATC results and not the usual mean thermal velocity results. The advantage of the above method of fixing α is that there is no experimental bias in the QFT results.

The Lennard-Jones parameters for the calculations were derived by taking literature values for the oxygen atom[31] and for the nitrogen molecule.[32] Using a pairwise additive scheme[32] for the three oxygen atoms of ozone and the perturbing molecule N_2, we constructed the potential by averaging over angular orientations of the ozone molecule. This generated the values of σ and ϵ for the O_3–N_2 system found in Table I.

It should be noted that the Lennard-Jones parameters ϵ and σ were adjusted without any attempt at matching experiment; in fact all parameters were determined before halfwidth calculations were undertaken.

Calculations were done for all unique rotational transitions of ozone from $J'' = 1$ to 35 present in the AFGL atlas. Given the relationship between P and R transitions, namely,

$$\gamma[R(\Delta K_a,\Delta K_c)] = \gamma[P(-\Delta K_a,-\Delta K_c)], \quad (7)$$

all P transitions were put into R-type and only unique ones retained. This produced a list of 4852 transitions for which the nitrogen-broadened halfwidth and pressure-induced shifts were calculated. Although an exact relationship like Eq. (7) does not hold for the shift, the shift of the individual levels was calculated and the corresponding shifts for P transitions can be computed from the final results. Because of the absence of experimental line shift measurements for ozone we limit our discussion to the calculated halfwidths.

IV. Discussion

Before discussing the results, the accuracy of the QFT-ID calculation will be presented. Fortunately for N_2 broadening a fair number of experimental measurements[9–11,14] which cover a wide range of J are available for comparison. The QFT-ID results are compared to experiment in Table II. In general the agreement is close to or within experimental error.

Table II. Comparison of QFT-ID Calculations with Experiment for N_2 Broadening of Ozone at 296 K [a]

Experimental reference	Average experimental percent error	Percent difference compared with QFT-ID calculations
Lundqvist *et al.*[9]	5.0	8.7
Meunier *et al.*[10]	2.7	2.3
Margolis[11]	10.0	8.4
Connor and Radford[14]	4.0	6.2

[a] Comparison is based on transitions with $J'',J' < 35$, i.e., the upper limit of the present calculations.

Considering the higher accuracy results[9,10,14] only, the average percent error is ~5%. To obtain the accuracy of the calculated halfwidths, we take the weighted average of the results of the comparison given by

$$E = \frac{\sum_i \Delta_i n_i / E_{expi}}{\sum_i n_i / E_{expi}}, \quad (8)$$

where Δ_i is the absolute percent difference between experiment and theory for result i, n_i is the number of results of error E_{expi}, and E_{expi} is the experimental error for the ith result. The use of the absolute percent difference gives a larger value of E. However, we believe it is more meaningful than a percent difference which cancels some of the error. This analysis gives 7.0% as the average accuracy of the QFT-ID results for the halfwidth of N_2 broadening of ozone.

The first question we address from these calculations is whether the halfwidths are dependent on the type of transition, A-type or B-type. This is questioned because the two bands have different selection rules and transition probabilities and some experiments[8,9] have suggested different average values of the halfwidth for each band. This was also concluded in the theoretical work of Tejwani and Yeung.[16] The results from experiment were determined by a relatively small number of measurements which were not representative of a full range of J and K_a. The average halfwidth was evaluated from the calculations performed here: the 2855 A-type lines studied give $\bar{\gamma}_A = 0.0680$ cm^{-1}/atm and the 1730 B-type lines studied give $\bar{\gamma}_B = 0.0678$ cm^{-1}/atm. These calculations considered a wide range of J'' (1–35) and a full range of K_a; the results indicate the average halfwidth is independent of the type of transition. This is further demonstrated in the following discussion.

The calculations show the halfwidth is dependent on the rotational quantum numbers of the upper and lower states (vibrational dependence is small[18]) ranging from a maximum of 0.081 cm^{-1}/atm to a low of 0.059 cm^{-1}/atm, representing a fluctuation of ~32%. Averaging the halfwidth on J'' only gives the usual γ vs J'' dependence as shown in Fig. 2. If one analyzes the data more rigorously the situation is not so simple: with the large number of transitions studied, the different types of transition ($\Delta J, \Delta K_a$) give many variables that can be used as coordinates to look for trends. As a first step the data were separated into Q and R transitions. This still allows many possible connecting states from a given initial state. A further separation was achieved by considering transitions with different ΔK_a (e.g., 0,1,2, . . .) to give groups of halfwidths labeled by transition type, Q or R, and the ΔK_a for the transition. This yields four main groups to study, Q transitions $\Delta K_a = 0,1$ and R transitions $\Delta K_a = 0,1$. To analyze the data, 3-D plots were produced with the halfwidth (Z axis) vs J'' (X axis) vs K_a'' (Y axis). (Note from here on we drop the double prime superscript on the lower state quantum numbers.) To better view the structure the final plots were done with the x-y axis rotated to a viewing angle of 225° with the x-z axis only tilted 15°

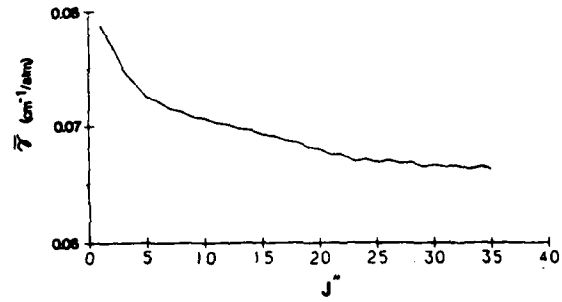

Fig. 2. N_2-broadened halfwidth of O_3 averaged as a function of J''.

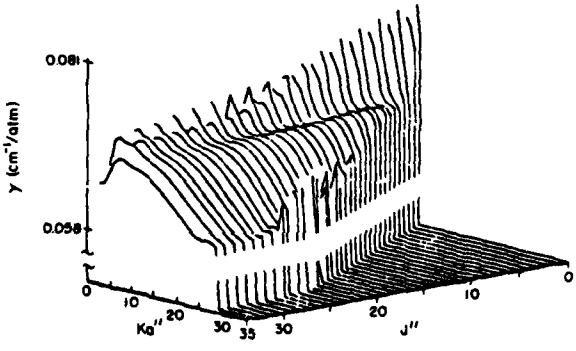

R-branch, $|\Delta Ka| = 1$

Fig. 3. Halfwidth vs J'' vs K_a'' for R transitions with $\Delta K_a = 0$.

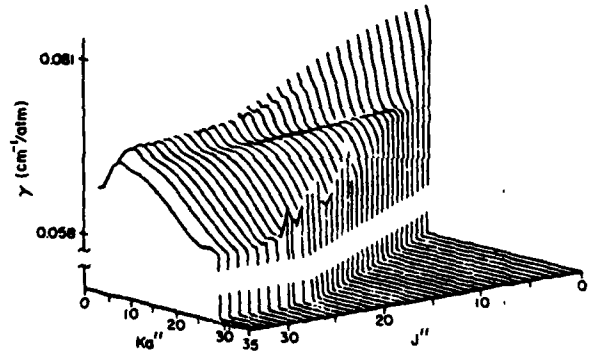

R-branch $|\Delta Ka| = 0$

Fig. 4. Halfwidth vs J'' vs K_a'' for R transitions with $\Delta K_a = 1$.

toward the viewer. Due to the similarity of the plots we present the results for the $R(\Delta K_a = 0)$ and the $R(\Delta K_a = 1)$ groups shown in Figs. 3 and 4, respectively. Note that Fig. 3 corresponds to A-type transitions and Fig. 4 to B-type transitions. The similar features observed in these plots confirm that the halfwidth is independent of transition type.

A surprising structure observed in Figs. 3 and 4 is the oscillation in the value of the halfwidth as a function of K_a for a particular J. With increasing K_a the halfwidth decreases at first after which it rises quickly and then decreases again out to $K_a = J$. These oscillations may be due to the resonances in the energy levels that occur

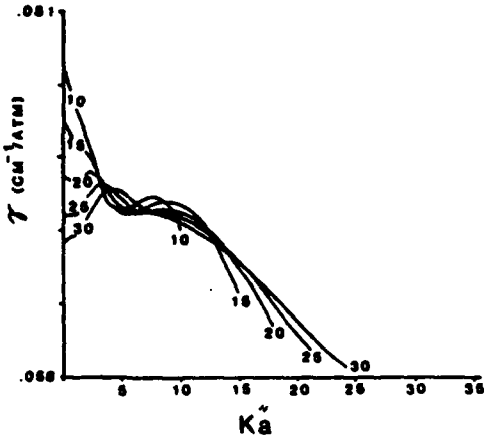

Fig. 5. Halfwidth vs K_a'' for particular values of J''.

with K_a for ozone. This may also be an artifact produced by the resulting Hamiltonian constants that are used to produce the eigenvectors and eigenvalues used in the calculations. The question of this unusual structure could be addressed by experimental study of the problem. The oscillating structure is further demonstrated in Fig. 5 where the halfwidth vs K_a is shown for $J = 10,15,20,25,30$.

The results of these calculations indicate that a constant or J-averaged halfwidth is not appropriate for studying the properties of ozone. For example, Smith and Gordley[33] have shown that, for ozone, inaccurate collision-broadened halfwidths can lead to significant errors in retrieved profiles for broadband radiometric data or for isolated strong transitions in high-resolution spectra. The results show a variation of 32% in the calculated values with respect to the average value 0.068 cm^{-1}/atm and clearly any work dependent on the halfwidths of ozone should take advantage of these new values.

V. Summary

Halfwidths for all unique rotational transitions of ozone have been calculated for N_2 broadening using the QFT-ID method. Air-broadened halfwidths have been obtained by scaling the N_2-broadened values by 0.95 as recommended by Ref. 18 contributing 1% uncertainty. For the AFGL atlas vibrational dependence is not considered; this contributed 1% on an average for 127 lines that were studied[18] with some of the lines being 4% different. The accuracy of the resulting halfwidths in the AFGL atlas is from 7 to 10%. These halfwidths will be present in the next version of the AFGL atlas.

References

1. S. A. Clough, F. X. Kneizys, L. S. Rothman, and W. O. Gallery, Proc. Soc. Photo-Opt. Instrum. Eng. 277, 152 (1981).
2. L. S. Rothman *et al.*, "AFGL Atmospheric Absorption Line Parameters Compilation: 1982 Edition," Appl. Opt. 22, 2247 (1983).
3. L. S. Rothman *et al.*, "AFGL Trace Gas Compilation: 1982 Version," Appl. Opt. 22, 1616 (1983).
4. R. L. Poynter and H. M. Pickett, "Submillimeter, Millimeter and Microwave Spectral Line Catalogue," JPL Publication 80-23, Revision 2 (JPL, California Institute of Technology, Pasadena, 1984).
5. N. Husson, A. Chedin, N. A. Scott, I. Cohen-Hallaleh, and A. Berroir, "La Banque de Données GEISA Mise à Jour 3," Laboratoire de Météorologie Dynamique *Note* 116 (1982).
6. H. Oelhaf, A. Leupolt, and H. Fischer, "Discrepancies Between Balloon-Borne IR Atmospheric Spectra and Corresponding Synthetic Spectra Calculated Line by Line Around 825 cm^{-1}," Appl. Opt. 22, 647 (1983).
7. A. Goldman, J. R. Gillis, D. G. Murcray, A. Barbe, and C. Secroun, J. Mol. Spectrosc. 96, 279 (1982); D. J. McCaa and J. H. Shaw, J. Mol. Spectrosc. 25, 374 (1968); A. Goldman *et al.*, "Atlas of Stratospheric IR Absorption Spectra," Appl. Opt. 21, 1163 (1982); A. Barbe, C. Secroun, P. Jouve, A. Goldman, and D. G. Murcray, J. Mol. Spectrosc. 86, 286 (1981); A. Barbe, U. Reims, A. Goldman, U. Denver and J. S. Margolis, JPL; private communication; J.-M. Flaud, C. Camy-Peyret, and L. S. Rothman, "Improved Ozone Line Parameters in the 10- and 4.8-μm Regions," Appl. Opt. 19, 655 (1980); C. Secroun, A. Barbe, P. Jouve, P. Arcas, and E. Arié, J. Mol. Spectrosc. 85, 8 (1981); A. Barbe, C. Secroun, P. Jouve, C. Camy-Peyret, and J.-M. Flaud, J. Mol. Spectrosc. 75, 103 (1979).
8. J. M. Hoell, C. N. Harward, C. H. Bair, and B. S. Williams, Opt. Eng. 21, 548 (1982).
9. S. Lundqvist, J. S. Margolis, and J. Reid, "Measurements of Pressure-Broadening Coefficients of NO and O_3 Using a Computerized Tunable Diode Laser Spectrometer," Appl. Opt. 21, 3109 (1982).
10. C. Meunier, P. Marché, and A. Barbe, J. Mol. Spectrosc. 95, 271 (1982).
11. J. Margolis, J. Quant. Spectrosc. Radiat. Transfer 29, 539 (1983).
12. N. Monnanteuil and J. M. Colmont, J. Quant. Spectrosc. Radiat. Transfer 29, 131 (1983).
13. J. M. Colmont and N. Monnanteuil, J. Mol. Spectrosc. 104, 122 (1984).
14. B. J. Connor and H. E. Radford, Center for Astrophysics, Harvard College Observatory; private communications (1984).
15. G. Yamamoto and T. Aoki, J. Quant. Spectrosc. Radiat. Transfer 12, 227 (1972).
16. G. D. T. Tejwani and E. S. Young, J. Chem. Phys. 63, 1513 (1975).
17. J.-Y. Mandin, J.-M. Flaud, and C. Camy-Peyret, CNRS, Campus d'Orsay; private communications (1983).
18. R. R. Gamache and R. W. Davies, J. Mol. Spectrosc. 109, 283 (1985).
19. S. Rothenberg and H. F. Schaefer III, Mol. Phys. 21, 317 (1971).
20. K. M. Mack and J. S. Muenter, J. Chem. Phys. 66, 5278 (1977); W. L. Meerts, S. Stolte, and A. Dymanus, Chem. Phys. 19, 467 (1977).
21. P. W. Anderson, Phys. Rev. 76, 647 (1949); Phys. Rev. 80, 511 (1950); C. J. Tsao and B. Curnutte, Jr., J. Quant. Spectrosc. Radiat. Transfer 2, 41 (1962).
22. R. R. Gamache, R. W. Davies, and L. S. Rothman, in *Proceedings, Thirty-Eighth Symposium on Molecular Spectroscopy* (Ohio State University, Columbus, Ohio), (1983), paper ME13.
23. R. W. Davies, Phys. Rev. A 12, 927 (1975).
24. R. W. Tipping, Thesis, Department of Physics, Pennsylvania State University (1969); R. H. Tipping and R. M. Herman, J. Quant. Spectrosc. Radiat. Transfer 10, 881 (1970); J. Quant. Spectrosc. Radiat. Transfer 10, 897 (1970).
25. M. Berard and P. Lallemand, J. Quant. Spectrosc. Radiat. Transfer 19, 387 (1978).
26. J. Bonamy, L. Bonamy, and D. Robert, J. Chem. Phys. 67, 4441

(1977).
27. D. Robert, M. Giraud, and L. Galatry, J. Chem. Phys. 51, 2192 (1969).
28. E. Piolett-Mariel, C. Boulet, and A. Levy, Mol. Phys. 33, 255 (1977); P. Ianard, C. Boulet, D. Robert, and L. Galatry, Mol. Phys. 33, 259 (1977)
29. R. P. Leavitt, J. Chem. Phys. 73, 5432 (1980).
30. R. W. Davies, R. H. Tipping, and S. A. Clough, Phys. Rev. A 26, 3378 (1982).
31. A. Stace and J. Murrell, J. Chem. Phys. 68, 3028 (1978).
32. J. O. Hirschfelder, C. F. Curtiss, and R. B. Bird, *Molecular Theory of Gases and Liquids* (Wiley, New York, 1954).
33. M. A. H. Smith and L. L. Gordley, J. Quant. Spectrosc. Radiat. Transfer 29, 413 (1983).
34. M. Lichtenstein, J. J. Gallagher, and S. A. Clough, J. Mol. Spectrosc. 40, 10 (1971); S. A. Clough, Air Force Geophysics Laboratory; private communication (1983).
35. A. Goldman, Physics Department, U. Denver, and A. Barbe, Laboratoire de Physique Moléculaire, U. Reims, France; private communications.
36. D. E. Stogryn and A. P. Stogryn, Mol. Phys. 11, 371 (1966); D. E. Stogryn, Mount St. Mary's College, Los Angeles; private communication (1983).
37. R. S. Berry, S. A. Rice, and J. Ross, *Physical Chemistry* (Wiley, New York, 1980), Chap. 21, p. 775.

Meetings Calendar continued from page 1643

1985
July

10–13 Hazards of Light Int. Symp., Manchester *U. of Manchester, R. Gregory, School of Medicine, Oxford Rd., Manchester M13 9PT, U.K.*

14–18 27th Rocky Mountain Conf., Denver *F. Lichte, U.S. Geological Survey, Box 25046, MS 928, DFC, Denver, Colo. 80225*

15–19 Laser Safety course, Wash., D.C. *Eng. Tech., Inc., P.O. Box 8859, Waco, Tex. 76714*

15–19 Principles of Microcomputers & Microprocessors course, Ann Arbor *Eng. Summer Conf., 200 Chrysler Ctr., N. Campus, U. of Mich., Ann Arbor, Mich. 48109*

15–19 Infrared Spectroscopy: Instrumentation, Polymer Spectra, Sample Handling, & Computer Assisted Spectroscopy course, Brunswick *D. Mayo, Chem. Dept., Bowdoin Coll., Brunswick, Me. 04011*

15–19 Finite Elements in Mechanical & Structural Design A: Linear Static Analysis course, Ann Arbor *Eng. Summer Confs., 200 Chrysler Ctr., N. Campus, U. of Mich., Ann Arbor, Mich. 48109*

15–19 Optical System Design course, Rochester *E. Snyder, Inst. of Optics, U. of Rochester, Rochester, N.Y. 14627*

15–26 Contemporary Optics course, Rochester *E. Snyder, Inst. of Optics, U. of Rochester, Rochester, N.Y. 14627*

22–26 Finite Elements in Mechanical & Structural Design B: Dynamic & Nonlinear Analysis course, Ann Arbor *Eng. Summer Confs., 200 Chrysler Ctr., N. Campus, U. of Mich., Ann Arbor, Mich. 48109*

22–26 Applied Laser Tooling Int. course, Vigo *M. Perez-Amor, E.T.S. Ing. Industriales, Vigo, Spain*

22–26 Guided-Wave Optical Systems course, Rochester *E. Snyder, Inst. of Optics, U. of Rochester, Rochester, N.Y. 14627*

22–26 Applied Molecular Spectroscopy course, Tempe *J. Fuchs, Chem. Dept., Ariz. State U., Tempe, Ariz. 85287*

23–25 Optical Fiber Measurements course, Aspen *K. Zimmerman, Off. of Conf. Services, U. of Colo., Boulder, Colo. 80303*

24–30 14th Int. Conf. on Physics of Electronics & Atomic Collisions, Palo Alto *SRI Int., 333 Ravenswood Ave., Menlo Park, Calif. 94025*

24–31 ICPEAC XIV, Stanford *D. Lorents, SRI Int., Chem. Phys. Lab., Menlo Park, Calif. 94025*

25–28 2nd Int. Symp. on The Stability & Preservation of Photographic Images, Ontario *D. Schultze, SPSE, 7003 Kilworth La., Springfield, Va. 22151*

29–2 Aug. Optical Propagation, Detection, & Communication course, Cambridge *Dir. of Summer Sessions, Rm. E19-356, MIT, Cambridge, Mass. 02139*

continued on page 1681

END

FILMED

1-86

DTIC